UPSCALING THE ESTIMATED FOREST CARBON STOCK FROM VHR SATELLITE IMAGE AND AIRBORNE LIDAR TO RAPIDEYE SATELLITE IMAGE

PEMA WANGDA
February, 2012

SUPERVISORS:
Dr. Y. Hussin
Mr. Ir. Kees Bronsveld

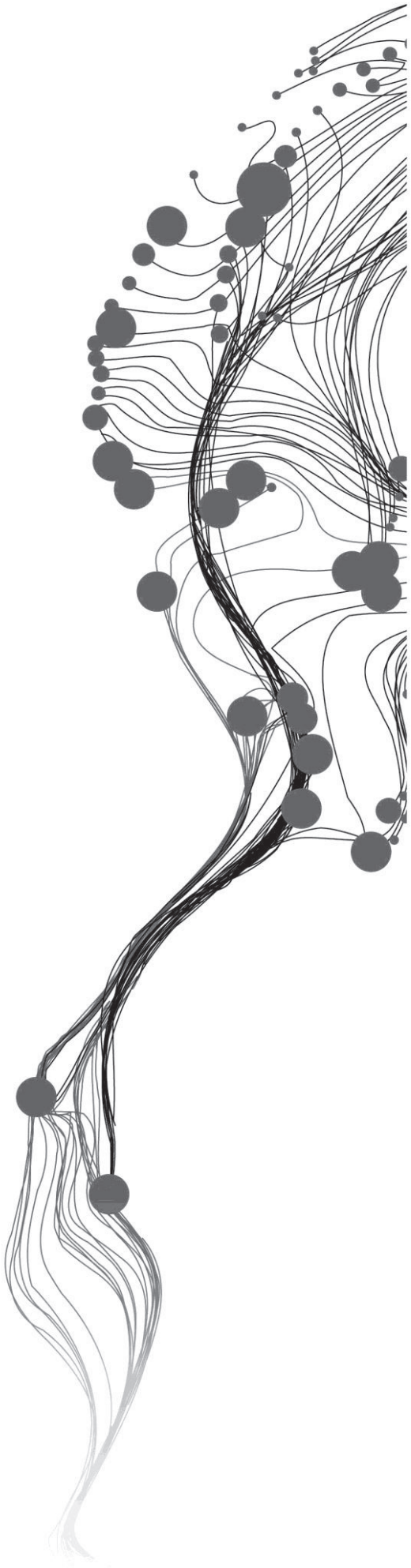

UPSCALING THE ESTIMATED FOREST CARBON STOCK FROM VHR SATELLITE IMAGE AND AIRBORNE LIDAR TO RAPIDEYE SATELLITE IMAGE

PEMA WANGDA

Enschede, The Netherlands, February, 2012

Thesis submitted to the Faculty of Geo-Information Science and Earth Observation of the University of Twente in partial fulfilment of the requirements for the degree of Master of Science in Geo-information Science and Earth Observation.
Specialization: Natural Resources Management

SUPERVISORS:
Dr. Y. Hussin
Mr.Ir. Kees Bronsveld

THESIS ASSESSMENT BOARD:
Chair: Dr. A. Voinov
External Examiner: Dr. T. Kauranne – (Arbonaut Oy Ltd & Department of Mathematics and Physics – Lappeenranta University of Technology, Finland

ABSTRACT

Estimating forest carbon stock is of paramount importance to assess the mitigation effects of forests on global warming and climate change. The drive for robust, accurate and cost-effective methods for carbon stock estimation over large areas is ever great with the launch of carbon crediting mechanisms in the developing countries such as UN-REDD. Traditional ground based measurement requires abundant manpower, resources, cost and time. Remote sensing based technologies aptly answer the need of time in enhancing the successful implementation of such programs. The integration of VHR satellite imagery and the LiDAR (Light Detection and Ranging) provide opportunities to estimate carbon with improved accuracy. However, high costs and low spatial extent of such data prohibit carbon estimation at a larger scale. The objectives of this study were to model and estimate forest carbon by integration of VHR satellite imagery and LiDAR, and upscale the carbon stock to a larger area using relatively coarser satellite imagery.

The study used the 0.5m spatial resolution VHR GeoEye image and airborne LiDAR data for individual tree crown segmentation. CHM developed from LiDAR data explained about 75 % of the variance in field measured height. Individual tree crown segmentation through the region growing approach resulted in an accuracy of 74% using the 1:1 correspondence method and 70% using the D goodness measure approach. Using allometric equation, the aboveground carbon was calculated based on the field measured DBH and tree height. Log transformed multiplicative regression models were developed to establish relationships between the field based carbon and the CPA and tree height derived from the segmented objects. The significance of the models were tested using F-test and were found to be statistically significant at 95 % confidence level. The developed models for *Shorea robusta* and Other tree species explained about 86 % and 78 % of the variances in carbon stock respectively.

The carbon stock derived from the combined VHR imagery and airborne LiDAR data were up-scaled to a relatively coarser 5m spatial resolution RapidEye imagery. Up-scaling was carried out by aggregating the carbon in each 5m pixel of the RapidEye image. Regression models were developed to establish the relationship between carbon and the spectral reflectance of RapidEye variables (NDVI, Red Edge NDVI, PC1 and the single bands of red edge and NIR). Weak relationships were observed between the carbon and the spectral reflectance of the RapidEye image. All the models resulted in low R^2 (NDVI=0.10, RedEdge NDVI= 0.12, PC1=0.18, red edge band = 0.14 and NIR=0.11).

In general, the methodology developed in this study established the usefulness of integrating the VHR satellite imagery and airborne LiDAR data for modelling and estimating carbon stock. Similarly, the methodology for up-scaling developed in this study can be used to up-scale the carbon stock from small areas to larger areas. However, further research is needed to explore the possibility of using cross-polarized L-band (i.e. ALOS Pal-SAR) and medium resolution satellite imageries with middle infrared bands for up-scaling the carbon stock to a landscape level.

Key words: Aboveground carbon stock, Region growing, LiDAR, Crown projection area, Canopy height model, Up-scaling, Spectral reflectance

ACKNOWLEDGEMENTS

This thesis would not have been possible without the support of several organizations and individuals who directly or indirectly extended their assistance and guidance during the entire period from the preparation to the completion of this study.

My heartfelt gratitude goes to my first supervisor, Dr. Y. Hussin for his unreserved guidance, support and encouragement throughout the entire research period. It was a privilege as well as pleasure to work under his dynamic supervision. I also take this opportunity to thank my second supervisor Mr. Ir. Kees Bronsveld for his constructive comments and suggestions. I would also like to thank Dr. A. Voinov for his constructive comments during the proposal and mid-term presentation.

I am grateful to all NRM staff for providing me a good learning environment at ITC. Dr. Michael Weir, Course Director of NRM deserves special thanks for his genuine concern for the welfare of all NRM students and his cooperation during the last 18 months.

Support from Mr. Basanta Gautam (Arbonaut Limited) and Mr. Khamarrul Azahari Razak (PhD candidate at ITC) during the initial crucial period of the research is highly appreciated. I also thank Mr. Hammad Gilani (ICIMOD), Mr. Himlal Shrestha (ICIMOD) and Mr. Eak Bahadur Rana (ICIMOD) for facilitating the field work efficiently. Thanks also go to Mr. Rana B.K from ANSAB for providing the GPS and Vertex hypsometer and Mr. Purna Magar for his helping hand during the fieldwork campaign.

I would like to thank International Centre for Integrated Mountain Development (ICIMOD) and Forest Resource Assessment (FRA), Nepal for providing data and necessary support for this research. Support from Asia Network for Sustainable Agriculture and Bio-resources (ANSAB), Federation of Community Forest Users' Nepal (FECOFUN), Arbonaut of Finland is also appreciated.

My sincere thanks goes to all fieldwork mates Yogendra, Nguyet, Sajana, Lopez, Purity, Tsikai, Constantine and Sola for the cheerful and hardship times during the fieldwork. Thanks are also due to Mr. Nguyen Quang and Mr. Chandra Ghimire (PhD candidates) for their assistance during the final phase of my study. Gratitude also goes to all my Bhutanese friends (Arun, Ugyen, Kesang, Jigme, Karma, Chogyal) for making me feel homely amidst stressful moments. Thanks to Vinod, Duc and Enock for sharing their valuable experiences. To all NRM colleagues and friends from various parts of the globe for making the life at ITC a truly international experience and for sharing wonderful as well as hardship times during the entire course of the study.

I would also like to express my gratification to Nuffic for providing the scholarship and the Royal Government of Bhutan for granting the permission to pursue my studies.

My deepest gratitude goes to my mother, uncle Karma and rest of my family and friends back home who were always with me showering their wishes and support. Finally, I thank my wife Jigme and our daughter Yetsho for their encouragement and support to achieve this endeavor.

Pema Wangda
12th February 2012
Enschede

DEDICATED TO MY LATE FATHER

TABLE OF CONTENTS

LIST OF FIGURES

LIST OF TABLES

LIST OF ACRONYMS

AGB	Above Ground Biomass
CF	Community Forests
CFUGs	Community Forest User Groups
CHM	Canopy Height Model
CPA	Crown Projection Area
DBH	Diameter at Breast Height
DEM	Digital Elevation Model
DN	Digital Numbers
DSM	Digital Surface Model
FAO	Food and Agricultural Organization
FRA	Forest Resource Assessment
GHGs	Green House Gases
ICIMOD	International Centre for Integrated Mountain Development
IPCC	Intergovernmental Panel on Climate Change
LiDAR	Light Detection and Ranging
MSS	Multispectral Data
NDVI	Normalized Difference Vegetation Index
NIR	Near Infra Red
REDD	Reduced Emission from Deforestation and Forest Degradation
RMSE	Root Mean Square Error
UNFCCC	United Nations Framework Convention on Climate Change
VI	Vegetation Indices
VIF	Variance Inflation Factor
VHR	Very High Resolution

1. INTRODUCTION

1.1. Background

Carbon dioxide (CO_2) together with other greenhouse gases (GHGs) plays an important role in the Earth's climate. GHGs act as insulator or blanket to keep the earth warm by absorbing long-wave infrared radiations, so that is favourable to life. However, climate change caused by increase in CO_2 concentration and other GHGs in the atmosphere is a worldwide concern. CO_2 in the atmosphere is increasing by 1.4 ppm per year and this increase will contribute to the increase in temperature by 1.8°C to 4°C by the end of the century (IPCC, 2007). The United Nations Framework Convention on Climate Change (UNFCCC) requires all Parties to the Convention commit themselves to develop, periodically update, publish, and make available to the Conference of Parties (COP) their national inventories of emissions by sources and removals by sinks of all GHGs using comparable methods (UNFCCC, 2009). Thus, carbon sequestration is a key topic in all climate change discussions.

Forests play a crucial role in climate change adaptation and mitigation because forests are one of the largest carbon pools on earth. As both carbon sources and sinks, forests have the potential to form an important component in efforts to combat global climate change. According to the Food and Agriculture Organization of the UN (FAO, 2010), the world's total forest area is presently estimated at 4 billion hectares corresponding to 31 percent of the total land area. The world's forests store more than 650 billion tons of carbon, 44 percent in the biomass, 11 percent in dead wood and litter, and 45 percent in the soil (FAO, 2010).

The Intergovernmental Panel on Climate Change (IPCC) has identified deforestation and forest degradation in developing countries as a major cause of GHG emissions (IPCC, 2007). Deforestation and forest degradation accounts for nearly 20 percent of global GHG emission, more than the entire global transport sector and second only to energy sector (UNEP, 2010). The rate of deforestation and loss of forest is alarmingly high at an estimated loss of 13 million hectares per year during the last decade. Most of the forest loss continues to take place in the countries and areas in the tropical regions (FAO, 2010).

In 2008, the United Nations Framework Convention on Climate Change (UNFCCC) launched an initiative known as "Reducing Emission from Deforestation and Forest Degradation" (REDD), whereby developing countries would be offered incentives to reduce emission from deforestation and increase carbon sequestration (UN-REDD, 2008). By stimulating sustainable forest management practices in the existing forests as well as increasing the forest areas, it is envisaged that REDD can increase the forest carbon stock and contribute significantly towards mitigation of global climate change.

Nepal is signatory to UNFCCC and also a member country of the UN-REDD programme. Nepal's forest area estimated at about 5.8 million hectares covering 40% of the country's land (Dhital, 2009). The success of community forestry as a major forest management practice in Nepal offers significant potential to conserve forest and at the same time, reap benefits from international carbon crediting mechanisms such as UN-REDD or Clean Development Mechanism (CDM) of the Kyoto Protocol (Dhakal & Raut, 2010). However, the UN-REDD member countries are required to develop cost effective, robust and compatible methods for estimation of carbon stock in the country as a readiness requirement for the implementation of REDD (UN-REDD, 2010).

1.2. Application of tools and techniques for biomass and carbon estimation

The principal element in the estimation of carbon stock in a forest is the measurement of forest biomass which includes both aboveground and belowground living mass, dead wood and litter. The most accurate way to quantify the aboveground biomass (AGB) in the forest is to cut down all trees per unit area, dry them and weigh the biomass (Gibbs et al., 2007). Although, the field based method of harvesting and weighing is very accurate, it is time consuming, labour intensive and destructive method (Brown, 2002; Gibbs, et al., 2007; Lu, 2006). Using allometric equations and modelling, the field measurements of diameter at breast height (DBH) independently or in combination with tree height can be converted to AGB and carbon stock estimates (Gibbs, et al., 2007). However, this method is also laborious and is not practical for application in large and inaccessible forest areas.

Remote sensing technologies offer alternatives to the conventional forestry inventory methods and it can be an essential tool in the estimation of AGB and carbon stock. Remote sensing techniques in combination with ground based measurements have been widely used to estimate forest biomass in a cost effective and faster method than traditional inventory methods with an acceptable degree of accuracy (Gibbs, et al., 2007). Several studies have been carried out to estimate forest biomass by the using different methods and different sensors (Asner, 2009; Johansen et al., 2007; Leckie et al., 2003; Muukkonen & Heiskanen, 2007; Zheng et al., 2004). The use of coarse resolution optical RS imageries such as NOAA-AVHRR, MODIS, etc, for biomass estimation is limited due to occurrence of mixed pixels and inconsistent accuracy at regional or local scale (Lu, 2006; Patenaude et al., 2005). However, coarse resolution imageries still remains useful and produce consistent results at global scale (Gibbs, et al., 2007). Despite the usefulness of moderate resolution optical RS imageries (10-30 m spatial resolution) such as Landsat, ASTER, etc, for many applications, including AGB estimation at local and regional scale (Lu, 2006), it is confronted with the problem of mixed pixels (Muukkonen & Heiskanen, 2007) and data saturation in complex biophysical environments (Lu, 2006). However, the launch of Very High Resolution (VHR) satellites such as IKONOS, QuickBird, GeoEye and Worldview in recent years, provide new opportunities to estimate forest biomass and carbon stock with improved accuracy. The VHR satellite imageries have been used in many studies to extract bio-physical parameters of vegetation such as the use of QuickBird (Gonzalez et al., 2010; Leboeuf et al., 2007), IKONOS (Song et al., 2010), GeoEye (Tsendbazar, 2011) and Worldview (Baral, 2011).

Frequent cloud cover, haze and smoke conditions in the atmosphere control the acquisition of high quality remotely sensed data by optical sensors particularly in tropical landscape. These limitations can be overcome by using Radar (Radio Detection and Ranging) technology that observes under all weather conditions and also during day and night (Gibbs, et al., 2007; Rosenqvist et al., 2003). Radar uses microwave energy and captures the backscatter from the object. Radar wavelengths penetrate the vegetation and provide direct sensitivity to the vegetation structure and biomass (Patenaude, et al., 2005). Nevertheless, the use of Radar for quantifying forest carbon stock is limited to relatively homogeneous or young forest because the radar backscatter tends to saturate at certain biomass levels (Le Toan et al., 2004; Lu, 2006; Patenaude, et al., 2005). Also, the use of Radar for biomass estimation is not efficient in hilly or mountainous areas due to increased error (Gibbs, et al., 2007; Le Toan, et al., 2004).

The application of optical remote sensing for forest biomass estimation is also limited to produce only 2-dimensional images and it cannot represent the 3-dimensional spatial features of forests (Gibbs, et al., 2007; Omasa et al., 2003). Airborne Light Detection and Ranging (LiDAR) has established as a standard technology for high spatial three dimensional topographic data acquisition in recent years. In contrast to the optical remote sensing, LiDAR is able to penetrate the vegetation canopy through the gaps between leaves and branches till the ground surface (Jochem et al., 2011). Also, LiDAR has certain characteristics, such as high sampling intensity, direct measurement of heights, precise geo-location and automated

processing for deriving forest biomass (Popescu, 2007). Thus, the LiDAR data can represent full 3-dimensional structure of the forest canopy and has been adopted by many studies for AGB quantification (Lefsky et al., 1999; Patenaude et al., 2004; Popescu, 2007; Popescu et al., 2004). Moreover, LiDAR offers substantial improvement over other sensors in the accuracy of its prediction of forest attributes (Gonzalez, et al., 2010; Lefsky et al., 2001; Sexton et al., 2009). Evaluating several sensors for prediction of forest structural attributes of Douglas-fir forest in United States, Lefsky et al (2001) reported that LiDAR performed better than other sensors such as single date Landsat TM and multi-temporal Landsat TM and Airborne Data Acquisition and Registration (ADAR), a high spatial resolution sensor.

1.3. Research conceptual framework

Accurate estimation of carbon stock in forests is important because forests are one of the largest carbon sinks on earth. The estimation of above ground biomass (AGB) is essential to estimate the total carbon pools in the forest (Brown, 2002; Gasparri et al., 2010). AGB is defined as the total amount of aboveground oven dry mass of a tree, which is expressed in tons per unit area (Brown, 2002). AGB can be directly converted to the total carbon content that is stored in a forest by a conversion co-efficient, which is usually about 0.47 of the AGB (Dong et al., 2003; Gibbs, et al., 2007). Remote sensing has been a valuable source of information for mapping and monitoring forest resources for the past few decades and has the potential to acquire forest biomass estimation with greater coverage at lower cost (Ke & Quackenbush, 2011a; Lu, 2006).

Accurate measurements of forest carbon is difficult to obtain without the precise measurements of biomass (Singh et al., 2011). The use of allometric regression model is a crucial step in estimating biomass (Brown et al., 1989) and allometry generally relates measurable independent variables like diameter at breast height (DBH) and height to biomass (Basuki et al., 2009; Singh, et al., 2011). The field measurements of forest biophysical parameters such as DBH and height facilitates forest biomass estimation with improved accuracy (Brown, 2002). DBH is an important predictive variable among the biophysical parameters of tree (Leboeuf, et al., 2007) which explains more than 95% variation in biomass (Gibbs, et al., 2007). The CPA is strongly related to other parameters such as DBH, tree height and biomass (Hemery et al., 2005; Shimano, 1997; Song, et al., 2010). The relationship between CPA, height and DBH can be extended to model and estimate aboveground biomass and carbon.

The increasing availability of VHR satellite images and LiDAR data provide opportunities to interpret forests at an individual tree level. The VHR satellite images can be used to recognize, identify and delineate individual tree crown (Gougeon & Leckie, 2006). However, VHR satellite imageries favours a shift in the image analysis paradigm from pixel based approach towards object based approach (Blaschke et al., 2006). This is because the spectral response of individual pixels in VHR imageries no longer represents the characteristics of a target of interest (e.g., forest stand, tree canopy) (Ke et al., 2010). Object Based Image Analysis (OBIA) allows extraction of meaningful objects during image segmentation and offers various advantage of using spectral characteristics, texture, size, shape, compactness, context information with adjacent image objects, etc, during classification (Liu et al., 2006). OBIA and image segmentation techniques have been used in many studies (Chubey et al., 2006; Conchedda et al., 2008; Johansen, et al., 2007). For instance, Johansen, et al.,(2007) applying OBIA technique to map vegetation structural classes using QuickBird image obtained an overall accuracy of 79% and Conchedda, et al., (2008) obtained an overall land cover classification accuracy of 86% using SPOT XS data.

A wide variety of individual tree crown detection and delineation algorithms based on high spatial resolution optical imagery have been developed. Individual tree detection and delineation algorithms are not only limited to optical imagery but can be extended to the combined high spatial resolution imagery and LiDAR (Ke & Quackenbush, 2011a; Kim et al., 2010). Some commonly used tree detection and

delineation algorithms include 1) valley following (Gougeon & Leckie, 2006), 2) region growing (Culvenor, 2002), 3) watershed segmentation (Wang et al., 2004) and 4) marker controlled watershed segmentation (Chen et al., 2006). Comparing the first three automatic tree detection and delineation methods, Ke & Quackenbush (2011a) found out that region growing algorithm produced higher accuracy than either valley following or watershed segmentation algorithms. Similarly, Tsendbazar (2011) also reported that region growing method resulted in higher accuracy than the valley following algorithm. Region growing approach assumes that the centre of the tree crown is brighter than the edge of the tree crown (Culvenor, 2002). Detecting the brightest pixel of the crown gives a possibility to locate the tree crown centre, and growing a region from the crown centre based on illumination image helps to delineate individual tree crowns (Ke & Quackenbush, 2011a).

With the increasing availability of VHR satellite images and commercial Airborne Laser Scanners over the last few years, an integration of optical imagery and airborne LiDAR is envisaged to estimate forest AGB and carbon with an improved accuracy. Several studies have combined LiDAR and multispectral optical images for estimation of forest biophysical attributes and obtained more accurate estimates than using either LiDAR or optical images independently (Holmgren et al., 2008; Ke, et al., 2010; Leckie, et al., 2003; Popescu, et al., 2004). For instance, Holmgren et al., (2008) reported an increase in overall classification accuracy of individual trees by 8% when VHR imagery was fused with LiDAR. Similarly, Ke, et al., (2010) found that the integration of QuickBird imagery and LiDAR improved the forest classification accuracy (kappa=91.6%). LiDAR provides rich information on the vertical structure of forests such as tree height, canopy height, canopy closure and density (Hollaus et al., 2007; Lefsky, et al., 2001), but does not provide information to distinguish between tree species and health attributes (Popescu, et al., 2004). Similarly, the VHR imagery offers opportunity to isolate individual trees and also differentiate the species but does not provide direct three-dimensional information such as tree height and crown height (Kim, et al., 2010). Therefore, a great potential exists for combination of VHR optical imagery and LiDAR for the extraction of forest structural parameters for AGB and carbon estimation with higher accuracy than either optical imagery or LiDAR independently. Moreover, the need for data integration between optical images and LiDAR has been recommended by several previous studies (Baltsavias, 1999; Leckie, et al., 2003; Tsendbazar, 2011; Wulder et al., 2007).

The VHR satellite images and LiDAR provides accurate AGB and carbon estimates than the medium or coarse resolution images (Gibbs, et al., 2007; Lu, 2006). However, drawbacks such as the need for large data storage, longer time for image processing and data analysis and high cost limits its application at a regional or national scale (Lu, 2006). Moreover, information on global carbon budget and fluxes are required at various spatial and temporal scales (Gibbs, et al., 2007). Alternatively, inexpensive microsatellites such as RapidEye (swath width 77 km) with daily revisit time has the potential to develop continuous global maps in a cost effective way (Kramer & Cracknell, 2008). In this context, RapidEye (5 meters spatial resolution) represents a relatively coarser resolution image than VHR GeoEye image but such images may offer best option in developing countries. It is because the cost for image purchase may influence the application of VHR images for forest monitoring purposes in large areas. Therefore, there is a need to develop a methodology to upscale the carbon derived from the integration of VHR image and LiDAR data over small areas to a regional level by using relatively coarser satellite images.

Many studies have demonstrated that vegetation indices such as normalized difference vegetation index (NDVI), perpendicular vegetation index (PVI), simple ratios (SR) and spectral vegetation index (SVI) obtained from satellite data as well as the individual bands of an image are useful predictors of biomass in forests through regression modeling (Lu et al., 2004; Roy & Ravan, 1996; Zheng, et al., 2004). In order to up-scale the AGB or carbon estimates to a regional level, vegetation indices and linearly transformed

images derived from satellite images and the individual bands can be linked to the AGB or carbon estimates (Lu, et al., 2004; Zheng, et al., 2004).

1.4. Problem Statement

Significant developments have been made in the estimation of forest AGB and carbon based on field measurement and remote sensing based approaches over the years. Although, the integration of VHR satellite imagery and LiDAR data for estimation of AGB and carbon is promising, the VHR satellite images and LiDAR data are very expensive compared to medium and coarse resolution satellite images. High cost and low spatial extent of the VHR satellite images (e.g. GeoEye) and LiDAR data are still a limitation for carbon estimation and mapping at regional scale. Also, the acquisition of data from such sensors cannot be performed routinely with high temporal frequency (Hudak et al., 2002). However, the accurate AGB and carbon estimates from VHR satellite imagery and LiDAR over smaller areas can be utilized as a reference data for estimating AGB and carbon for larger areas using a medium resolution satellite images (Asner, 2009; Gautam et al., 2010). Therefore, there is a need to develop techniques which are capable of combining the accurate carbon estimates derived from the combined VHR image and LiDAR data to relatively coarser resolution satellite images such as RapidEye. Successful development of such an approach can use the carbon estimates over limited areas and upscale it to coarser images for larger areas.

1.5. Research objectives

The overall objective of this study is to model and estimate aboveground carbon by integration of VHR GeoEye satellite image and airborne LiDAR data over a limited area and; up-scale and investigate the relationship between forest carbon stock and the spectral reflectance of RapidEye satellite image.

The specific objectives:

1. To assess the ability of combined VHR GeoEye satellite imagery and airborne LiDAR data for delineating individual tree crowns.
2. To determine the relationship between CPA, height and aboveground carbon in the study area.
3. To estimate and validate carbon stock using CPA and height from combined VHR satellite image and airborne LiDAR data in the study area.
4. To upscale the carbon stock map and investigate its relationship with the spectral reflectance of RapidEye image.

1.6. Research Questions and Hypothesis

Specific Objectives	Research Questions	Research Hypothesis
1	How accurately can the tree crowns be segmented from the combined VHR GeoEye satellite image and LiDAR data?	Individual tree crown can be segmented with a reasonable accuracy (≥75%)
2	What is the relationship between CPA, height and carbon in the study area?	There is a significant relationship between CPA, height and carbon.
3	How accurately can the aboveground carbon stock be estimated using CPA and height from VHR satellite image and LiDAR data?	Aboveground carbon can be estimated with a reasonable accuracy
4	a. How the estimated carbon from VHR satellite image and LiDAR data can be up-scaled to the RapidEye image of 5m resolution?	
	b. What/how strong is the relationship between up-scaled carbon stock and the spectral reflectance of RapidEye image?	There is a significant relationship between the up-scaled carbon stock and the spectral reflectance of RapidEye image.

1.7. Thesis outline

Chapter 1
The general background of the research and the research conceptual framework for the application of VHR imagery and LiDAR data for modelling and estimation of aboveground carbon stock are discussed. Issues on the up-scaling are also discussed. Research problem and objectives follows thereafter.

Chapter 2
The description of study area in terms of its geographic location, climatic conditions and vegetation characteristics are covered.

Chapter 3
This chapter discusses the materials and methods used in this research to achieve the research objectives.

Chapter 4
Results of the carbon estimates including the tree crown delineation approaches and regression modelling are described. Results on up-scaling and the relationship between the carbon and the spectral reflectance of RapidEye satellite image are also described.

Chapter 5
Discussion of the results obtained in this study. It includes estimation of tree heights from the LiDAR data, image segmentation, classification of tree species, regression modelling, mapping of carbon, up-scaling and the relationship between carbon stock and the spectral reflectance of RapidEye image.

Chapter 6
Conclusions with reference to the research objectives and questions are drawn in this chapter. Recommendations from this study are also included.

2. DESCRIPTION OF THE STUDY AREA

2.1. Geographic location

The study area is located in Ludhikhola watershed, which lies in Gorkha District of the Western Development Region of Nepal. The Ludhikhola watershed area is situated in the southern part of Gorkha district, located between 27°55'02"-27°59'43"N latitude and 84°33'23"- 84°40'41"E longitude (Figure 2.1). The total area of the watershed is 5750 hectares, out of which 4869 hectares is forest area, 632 hectares is agriculture land and the rest is barren, grassland and natural water bodies. There are 31 Community Forest User Groups (CFUGs) managing an area of 1888 hectares of forests as Community Forests (CF).

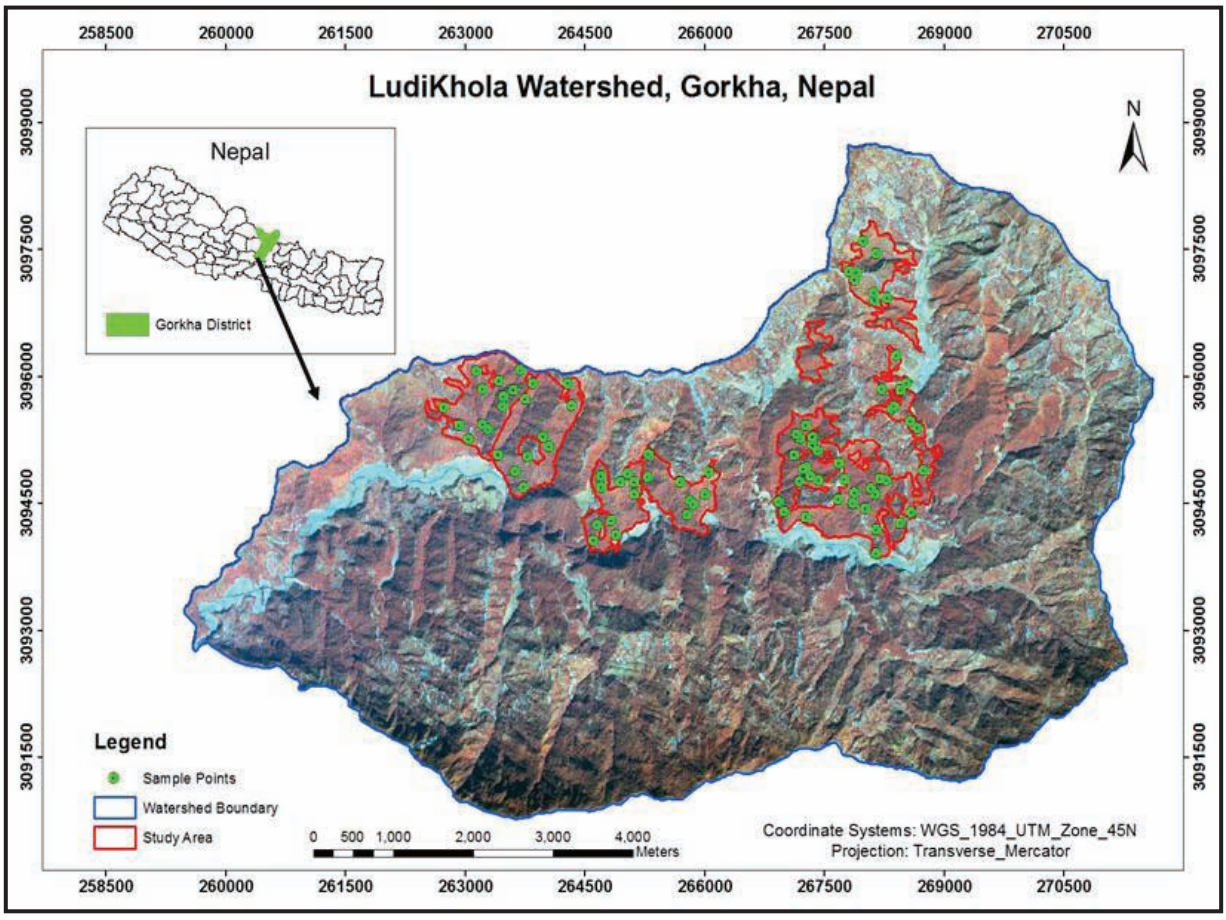

Figure 2.1: Map of the Ludhikhola watershed with an inset of 5 Community Forests

2.2. Topography and Demography

Ludikhola watershed represents the hill physiographic region with elevation ranging from 318 m to 1714 m above mean sea level. The Ludhikhola watershed falls in the mid-hill region of Nepal and lies in the middle mountain ecological zone. About 61% of the area consist of steep slope terrain (e.g. 30-60%) while the remaining 39% include flat lands and gentle slopes of less than 30%. This watershed is inhabited by socially ethnic and diverse communities of *Magar, Gurung, Tamang, Dalit, Brahmin* and *Chhetri.*

2.3. Climate

The climate of the study area varies from sub-tropical at lower altitudes to temperate at higher altitudes. The area has four main season namely autumn, monsoon, summer and winter with an average daily temperature of 14.5°C. The average temperature recorded in 2001-2006 was 23.10°C whereas between 1978 -1982, the temperature recorded was 21.6 °C. The average annual rainfall ranges from 1,972 to 2000 mm and the rainy season lasts from June to September (ICIMOD, 2010).

2.4. Vegetation

The area represents a typical sub-tropical forest that was exposed to high deforestation, and recently has been conserved through community forest management. The area is characterized by an altitudinal variation and has upper tropical to sub-tropical lower forests. The forest comprises of mixed forest with *Shorea robusta* (Sal*)* as the dominant tree species and is most commonly found in the southern aspects and lower altitudes of northern aspects. In the upper parts of northern aspects, the dominant species are *Schima wallichii* (Schima) and *Castanopsis indica* (Chestnut) followed by few other associated species like *Rhus wallichii* (Ceasar weed)*, Mangifera indica* (Mango), *Ficus racemosa* (Fig), *Terminalia bellirica* (Belliric Myrobalan), *Syzygium cumini* (Black plum)*, Lyonia ovalifolia* (Oval leaved Lyonia)*, Lagerstromia parviflora* (Myrtle).

2.5. Land Cover Classes

There are five land cover types in the Ludhikhola watershed which is presented in Table 2.1. Two different types of forests are classified as Open Broadleaved Forest and Open Broadleaved Forest.

Table 2.1: Land Cover types in Ludikhola watershed; Source (ICIMOD, 2010)

Land Cover Class	Area (Hectares)	% of Area
Close Broadleaved Forest	3837	67.34
Open Broadleaved Forest	996	17.31
Agriculture Areas/Built-up Areas	632	10.99
Bare Soil	241	4.19
Natural water bodies	9	0.17

2.6. Criteria for study area selection

Ludhikhola watershed is one of the pilot sites under the REDD project as it represents the middle part of Nepal and comprises of different forest types and species. Out of the 31 CFUGs in the watershed areas, only 5 CFUGs were selected for the following reasons.

a. The selected CFUGs were comparatively accessible than other remaining CFUGs.
b. The availability of satellite images from ICIMOD and FRA, Nepal facilitated the study.
c. The altitudinal variations were also taken into account and the altitude in the selected CFUGs ranges from 470 -1050m
d. The processing capability of eCognition software has a limitation for segmenting large areas.

3. DESCRIPTION OF METHOD AND DATA USED

3.1. Dataset and Materials used

3.1.1. Satellite Imageries

GeoEye1 data

GeoEye1 satellite was launched on broad a United Launch Alliance (ULA) Delta III launch vehicle on 6th September 2008 in the United States. GeoEye1 has the highest resolution of any commercial optical imaging system and collect images with a ground resolution of 0.41-meters and 1.65-meters resolution in the panchromatic and multispectral modes respectively. While the satellite collects imagery at 0.41-meters, GeoEye's operating license from the U.S. Government requires re-sampling the imagery to 0.5-meter for all customers not explicitly granted a waiver by the U.S. Government. GeoEye1 has the distinction of offering exceptional geo-location accuracy, where the customers can map natural and man-made features to better than five meters of their actual location on the surface of the Earth without ground control points.

GeoEye1 image acquired on 2nd November 2009 with the following specification listed in Table 3.1 was used in this study. The Ortho-rectification was carried out by ICIMOD, Kathmandu, Nepal.

Table 3.1: GeoEye1 satellite image characteristics

Sensor Name	Geo-Eye1
Spatial resolution	Panchromatic: 0.5m Multispectral: 2m
Dynamic view	11 bits
Spectral range	Panchromatic: 450 - 800nm Blue: 450 - 510nm Green: 510 - 580nm Red: 655 - 690nm Near Infrared: 780 - 920nm
Orbit height	684 kilometers
Orbit type	Sun-synchronous
Swath width	15.2 km
Projection	UTM 45 N
Datum	WGS84
Nominal collection azimuth	315.3 degree
Nominal collection elevation	64.6 degree
Sun angle azimuth	163.65 degree
Sun angle elevation	46.0 degree
Image Acquisition time	05:12 GMT, 10:57 AM (Kathmandu)

RapidEye Data

RapidEye was launched by DNEPR-1 Rocket on 29th August 2008 in Kazakhstan. The RapidEye constellations consist of five satellites and have a unique ability to acquire high-resolution, large-area image data on a daily basis. RapidEye's satellites include the red-edge band, which is sensitive to changes in chlorophyll content. RapidEye satellite image acquired on 22th April 2011 with the following specification was used in this study. The characteristics of the RapidEye image is shown in Table 3 .2.

Table 3.2: RapidEye satellite image characteristics

Sensor Name	RapidEye
Spatial resolution	Ground sampling distance(Nadir): 6.5 m Pixel size (Ortho-rectified) : 5 m
Dynamic view	Up to 12 bit
Spectral range	Blue: 440 - 510 nm Green: 520 - 590 nm Red: 630 - 685 nm Red Edge: 690 - 730 nm Near Infrared: 760 - 850 nm
Orbit height	630 kilometers
Orbit type	Sun-synchronous
Swath width	77 km
Revisit time	Daily (Off-nadir) / 5.5 days (at nadir)
Projection	UTM 45 N
Datum	WGS84
Image Acquisition time	05:55 GMT, 11:40 AM (Kathmandu)

3.1.2. LiDAR data

The LiDAR data for this study was acquired by Arbonaut Limited, Finland during the period 16th March 2011 to 2nd April 2011 using a Leica ALS-40 (Airborne Laser Scanner) sensor with an aerial platform. The data was collected for Forest Resource Assessment (FRA) Project under the Ministry of Forest and Soil Conservation, Nepal. The laser scanner instrument was mounted abroad a 9N-AIW helicopter, which flew at an altitude of 2200m above ground level. The mean point densities within the study area are 0.8 points per m^2. The original dataset covered the entire Terai Arc Landscape (TAL) and two ICIMOD's biomass sites of Nepal. The LiDAR data used in this study is from ICIMOD's biomass site of Ludhikhola watershed in Gorkha district. Additional information about the used LiDAR sensor is listed in Table 3.3.

Table 3.3: LiDAR data characteristics

Date Flown	20110316 / 20110328 / 20110401 / 20110402
Times of collection (UTC)	02:45 – 08:20 / 03:46 – 05:00 / 04:01 – 05:45 / 03:31 – 05:30
Date Processed	20110530
Projection /Datum	UTM WGS84
Files format	ASPRS LAS
Flying speed	80 knots
Sensor pulse rate	52.9 khz
Sensor Scan speed	20.4 lines/second
Nominal outgoing pulse density @ground level	Average: 0.8 points per square meter
Sun position	>20 degrees
Swath @ ground level	1601.47 m
Point spacing	max 1.88 m across, max 2.02 m down
Sidelap/Side overlap	60%/30%
Vertical accuracy	45 cm
Horizontal accuracy	45 cm

3.1.3. Other ancillary data

Topographic maps of Ludhikhola watershed at 1:25000 scale (Source: Survey Department of Government of Nepal). The watershed area and CFUGs boundary shape files of the study area were provided by ICIMOD.

3.1.4. Field equipments

Various field equipments were used during the field work campaign in the period from 20th September 2011 to 20th October 2011. The equipments and the purpose of its use are shown in Table 3.4.

Table 3.4: List of field equipments used

Field Equipments	**Purpose/Usage**
iPAQ and GPS	Navigation
Suunto compass	Orientation
Häglof Vertex Hypsometer	Tree height measurement
Diameter tape (3m)	DBH measurement
Measuring tape (30m)	Length measurement
Spherical Densiometer	Crown cover measurement
Suunto clinometers	Slope measurement
Field data tally sheets	Record field data

3.1.5. Software

Table 3.5 shows a list of software used for data preparation, processing and analysis to facilitate this research.

Table 3.5: List of software(s) used

Software	**Purpose**
ArcGIS version 10	GIS utilities and analysis
eCognition Developer 8	Object Based Image Analysis
ERDAS Imagine 2011	Image processing
LASTools	Visualising, processing and interpretation of LiDAR data
Quick Terrain Modeler (Trial Version 7.4)	
ENVI 4.8	Image processing
Microsoft Office suite	Writing, presenting, analysing, etc.
SPSS & R	Statistical Analysis

3.2. Methods

The overall method consists of two major parts namely 1). Modelling and estimating the carbon stock from the integration of VHR satellite imagery and LiDAR data; and 2). Up-scaling the carbon stock and analysing the relationship between the carbon stock and spectral reflectance of RapidEye image through regression modelling. The methodology (Part 1) for the modelling and estimation of carbon stock from the integration of VHR GeoEye satellite imagery and LiDAR data is presented as a schematic flowchart in Figure 3.1.

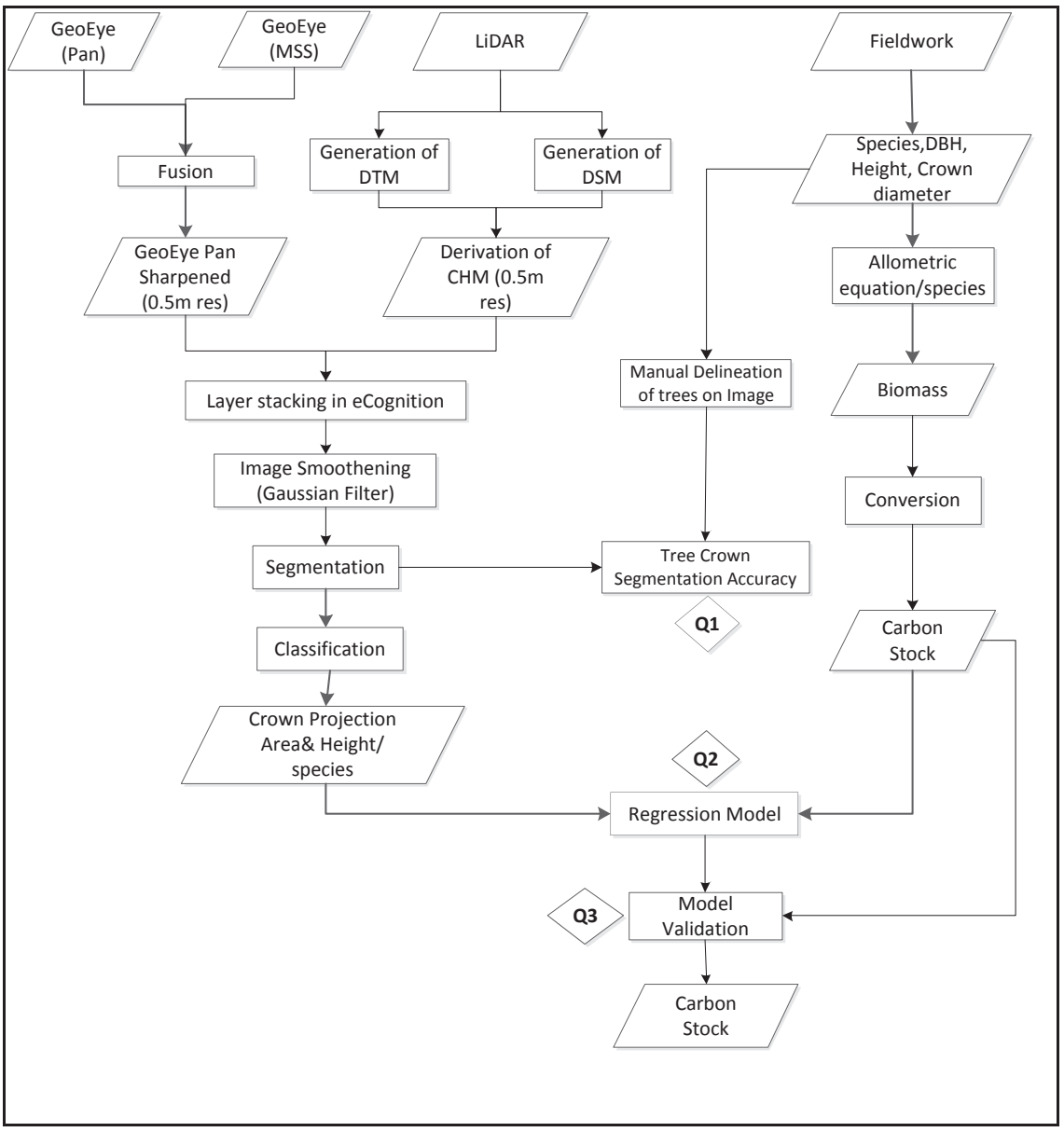

Figure 3.1: The Methodological Flowchart for aboveground carbon estimation

The methodology (Part 2) for the up-scaling and analysing the relationship between the carbon stock and the spectral reflectance of the RapidEye image is presented as a schematic flowchart in Figure 3.2.

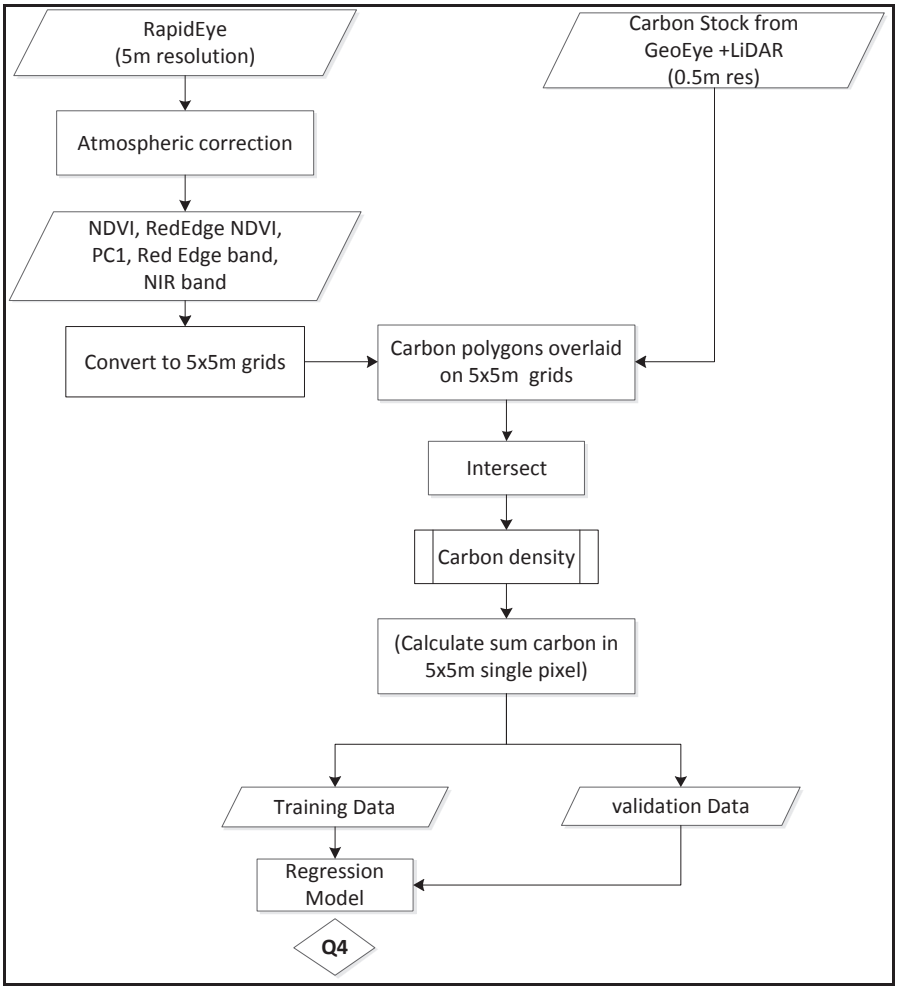

Figure 3.2: The Methodological Flowchart for Up-scaling

3.3. Pre-fieldwork

3.3.1. Pre-processing of optical data

Pre-processing the raw data also called as image restoration and rectification is usually carried out prior to data analysis. The pre-processing corrects for any distortion due to the characteristics of the imaging system and imaging conditions. These procedures include radiometric correction to correct for uneven sensor response over the whole image and geometric correction to correct for geometric distortion due to Earth's rotation and other imaging conditions. Furthermore, if accurate geographical location of an area on the image needs to be known, ground control points (GCP's) are used to register the image to a precise map known as geo-referencing.

The GeoEye image provided by ICIMOD, Nepal was already pre-processed and geo-referenced to WGS 84 UTM Zone 45N projection system. The RapidEye image provided by FRA Project, Nepal was also geo-referenced to WGS 84 UTM Zone 45N projection system. Parts of three separate RapidEye image tiles covered the study area. Atmospheric correction to the RapidEye image was applied to each image tiles using the ATCOR2 module in ERDAS Imagine 2010. The metadata for ATCOR2 is provided in

Appendix 1. After the atmospheric correction, the images were mosiaced and then subset to the study area.

3.3.2. Image fusion

Image fusion refers to a technique of combining multiple images into composite images, so that the product contains more information than that of individual input images. In literature, several image fusion algorithms and techniques exist such as Intensity, Hue and Saturation (HIS), Principal Component Analysis (PCA), Brovey transform (BT), Multiplicative Transform (MT), High Pass Filter (HPF), etc.

The IHS colour transform separates a standard red, green and blue image into spatial (I) and spectral (H, S) information (Zhang, 2002). IHS transform a colour image composite from RGB space into IHS space, replaces the intensity component by a panchromatic image with a higher resolution. This is followed by reversely transforming the replaced component from IHS space back to the original space to obtain a fused image.

The High Pass Filter (HPF) resolution merge method involves a convolution of the high spatial resolution image using a high pass filter. The filtered high resolution image is then added to each multispectral band of the low spatial resolution image at the pixel level. The main advantage of the HPF over IHS method is they produce the same number of bands in the output as the original multispectral image. HPF resolution merge fusion was carried out in ERDAS Imagine 2010 using the GeoEye 0.5 meter panchromatic band and 2 meter multi-spectral bands of blue, green, red and near-infrared bands. The image fusion process resulted in pan-sharpened MSS image of 0.5 meter spatial resolution.

3.4. Fieldwork

3.4.1. Sampling Design

There are several methods to sample a particular forest. A stratified random sampling (SRS) approach was chosen as a sampling design for the field work data collection. The stratum was based on the CFUGs boundary. Stratification reduces the variation within the strata and increases the precision of the population estimate (Husch et al., 2003). Moreover, SRS offers advantages such as; it ensures better coverage of the population than simple random sampling and yields more accurate estimates of the population for a given sampling intensity (Maniatis & Mollicone, 2010). The number of sampling plots for the study area was determined using the formula given below;

Area of sampling (a) = Sampling Intensity (I) * Total area of Stratum (A)/100
Source: (DOF, 2004)

No. of plot (n) = Area of sampling (a)/ Area of one sample plot (p)

3.4.2. Locating the sample plots

With the aid of iPAQ, Garmin GPS and printed maps, the centre of the sample plots were located. However, the exact location of the plot centre varied between 3 – 5 meters from the true location due to weak signals received by iPAQ and GPS depending on the canopy cover and weather conditions. Plots were located on the imagery using identifiable reference points such as road crossings, footpath, open spaces, etc on the image and known distances and direction from these points.

3.4.3. Sampling Plots

Circular plots are preferred because it is easy for plot layout in the field requiring only a single dimension of radius to define perimeter (Husch, et al., 2003). Also the determination of trees inside the plot is less problematic than other shapes such as square plots. Circular plots with a radius of 12.62 meters (plot size = 500m^2) were established in the field. However, the radius of the plots varied after application of slope correction depending on the slope of the plot.

3.4.4. Data collection from field work

The fieldwork was carried out during the month of September and October, 2011. A total of 86 sampling plots were located. The specie of each individual tree was identified inside the sampling plot. Then DBH and tree height were measured for each tree inside the sampling plot. Crown diameter was measured for sample trees by averaging two cross directional measurements taken at north-south and west-east direction. The data was collected for trees with DBH of 10cm or more, since trees with DBH less than 10 cm are generally assumed to contribute little to the total biomass of forest (Brown, 2002). Sample trees were identified on the printed GeoEye image.

3.5. Post Fieldwork

Field data of the sampling plots in the study area were compiled and organized in Microsoft excel. Descriptive statistics were computed. Identified trees on the printed image in the field were manually delineated on screen by digitizing in ArcGIS 10. Crown diameter information of trees collected from the field aided in digitizing the identified individual tree crowns. To ensure consistency, a uniform map scale of 1: 300 was maintained throughout the manual delineation process. A total of 423 trees were manually delineated by on screen digitizing.

3.6. LiDAR data Processing

Pre-processed LiDAR data of the study area was provided by FRA, Nepal. Basic pre-processing of the raw LiDAR Data was carried out by Arbonaut Limited using Terrascan software. Filtering the point clouds into ground and non-ground returns is the core component of LiDAR data processing (Meng et al., 2010). This process enables the generation of a digital elevation model (DEM) and digital surface model (DSM) for further analysis such as deriving the tree height. The raw data (x, y, z coordinates) in las format were processed into DEM and DSM using the open source software LasTools. LasTools provides the tools required to generate DSMs and DTMs from raw or basically preprocessed LiDAR data. The processes for derivation of DEM, DSM and CHM are described in the following two sub-sections.

3.6.1. Generation of DEM and DSM

The most commonly used derivative of LiDAR data in forestry is the Canopy Height Model (CHM). Before deriving the CHM, the DEM and DSM were generated. Creating a raster dataset from the raw LiDAR data is a pre-requisite procedure for creation of DEM and DSM (Meng, et al., 2010). The DEM was created by filtering the last return LiDAR point clouds into ground points using the lasground function in LasTools. The filtered ground points were then interpolated by triangulated irregular network (TIN) method using the blast2dem function with a cell size of 0.5m. Similarly, the DSM was created by gridding the first return non ground LiDAR points using the lasgrid function with a cell size of 0.5m. The grid size of 0.5 meter was chosen for DEM and DSM to match the spatial resolution of the pan-sharpened MSS GeoEye image. The DEM and DSM are stored in a 2D raster image, where grayscale values represent the height values.

3.6.2. Derivation of CHM

The Canopy Height Model (CHM) is a LiDAR derived 3-D surface which provides vegetation height information above the ground level. The CHM was derived by subtracting the height value of the DEM at

each pixel from the height value of the DSM. A height difference between the DSM and DEM represents the absolute height of the trees (Ali et al., 2008; Kim, et al., 2010). Based on the maximum tree heights measured during the fieldwork, tree heights above 40 m were filtered out. CHM was also stored in a 2D raster image, where grayscale values represent the absolute tree height. The manually delineated tree crown polygons were overlaid on the CHM raster. The ground measured tree heights and its corresponding CHM raster value representing the tree heights from the CHM were extracted for validating the height. This process was carried out in ArcGIS 10.

3.7. Co-registration of satellite images and LiDAR derived CHM

Accurate co-registration between multiple datasets is extremely important in all image analysis tasks for precisely extracting information content from different datasets (Zitová & Flusser, 2003). It is because of their heterogeneity in terms of difference in sensors used, times of data collection, reference systems, etc. Co-registration usually involves integrating datasets from different sources to establish a correspondence among the features of interest. The most common strategy is to use the LiDAR data as the source of reference for image geo-referencing (Kim & Habib, 2009). However, it was difficult to identify distinct LiDAR features or points which can be recognized in the image. Therefore, an ortho-rectified aerial photo acquired during the same day and time as the acquisition of the LiDAR data was used as a reference image. The ortho-rectified pan-sharpened MSS GeoEye image was co-registered with the ortho-aerial photo using a total of 49 ground control points (GCP) in ERDAS Imagine 2010. An average RMSE of 1.9 m was obtained for the image to image co-registration. Similarly, the RapidEye image was also geo-rectified using the same ortho aerial photo. The operation was carried out in ERDAS Imagine 2010 Autosync program. A total of 64 tie points were automatically generated and a RMSE of 1.3 m was obtained.

3.8. Image filtering

Image filtering is an image enhancement technique for improving the visual interpretability of an image. Filtering produces more homogeneous image segments and reduces the amount of convolution in the final segmented objects (Mora et al., 2010). The filtering process enhances the distinction between image objects and the background by removing the image noise occurred during data acquisition (Ke & Quackenbush, 2011b). An average filter size of 3x3 pixels and 5x5 pixels were tried for the MSS Geoeye image. Since the filter size of 3x3 pixels window gave better visualization, a 3x3 pixel filter was applied to the MSS GeoEye image in ERDAS Imagine 2010.

3.9. Object Based Image Classification

The basic units for object based image classification are the image objects or the segments rather than the pixels as compared to traditional pixel based classification (Blaschke, 2010). In addition to the spectral information of an image, the object-based classification also uses other information such as shape, texture, and contextual relationships (Ke, et al., 2010). Image segmentation and image classification are two major steps in the object based image classification approach. Image segmentation and image classification are discussed in the following two sub-sections;

3.9.1. Image segmentation

The tree crown delineation was carried out by image segmentation in eCognition Developer 8.7. Segmentation basically means grouping of neighbouring pixels based on similarity criteria such as digital numbers, shape, texture, size, etc. Image segmentation in this thesis means separation of tree crowns from the background image as well as the separation between individual tree crowns. Two basic segmentation approaches available in eCognition are top-down approach which cuts objects into smaller pieces and bottom-up approach which merges smaller pieces into larger objects (Definiens, 2009b). Among many

image segmentation algorithms, region growing segmentation was chosen in this study because it has been proven to be effective for the more complex structure of naturally regenerating forests (Erikson, 2003; Ke & Quackenbush, 2011a; Larsen et al., 2011). Region growing exploits spatial information and guarantees forming closed connected region (Weihong et al., 2008). Moreover, this study will serve as a comparative study in the same area conducted by Shah (2011), where region growing approach for individual tree crown segmentation was employed using the GeoEye imagery only.

3.9.1.1. Region growing approach

Tree crown delineation using the region growing approach in eCognition Developer 8.7 was based on the co-registered pan-sharpened MSS GeoEye image and the CHM derived from LiDAR data. The region growing algorithm aggregate pixels starting with the seeds and grows into the neighbouring pixels until a certain threshold is reached (Blaschke, et al., 2006). The basic assumption of tree crown delineation using region growing approach is that the centre of a crown appears radiometrically brighter than the edge or boundary of the crown (Culvenor, 2002). Identification of local maxima and local minima throughout the image and clustering of crown pixels are three main processes in region growing (Culvenor, 2002). Choosing the seeds and the similarity criteria are important factors because the region growing starts from the seeds by comparing neighbouring pixels and growing them into regions that satisfy a chosen homogeneity criteria (Weihong, et al., 2008).

A filtered MSS pan-sharpened GeoEye image with four layers of (red, green, blue and NIR bands) and the LiDAR derived CHM layer were stacked in eCognition Developer 8.7 before segmentation. Gaussian filter of 3x3 pixel window size was applied to the LiDAR derived CHM layers before segmentation. The use of Gaussian filter was preferred over the median filter because the Gaussian filter preserves the edge features which aids in image segmentation (Wang, et al., 2004). The image smoothening also reduces noise caused by small branches and their shadow within one crown. Individual tree crowns were segmented in a sequence of steps which are discussed in the following sub-sections;

a. Chess board segmentation and masking of shadow and open areas
b. Finding the local maxima and local minima
c. Growing from the seed (treetop)
d. Watershed transformation to refine the shape of tree crowns
e. Smoothening of tree crown shape and removal of undesired objects

a. **Chessboard segmentation and masking of shadow and open areas**

The chessboard segmentation algorithm was applied to the stacked layer of pan-sharpened MSS GeoEye image and the CHM layer. The purpose of the chessboard segmentation is to partition the image into homogenous area prior to application of region growing process for individual tree crown delineation. Chessboard segmentation is a top-down segmentation process which cuts the scene or image objects into equal squares of a given size (Definiens, 2009b). Figure 3.3 shows the diagrammatic representation of the chessboard segmentation.

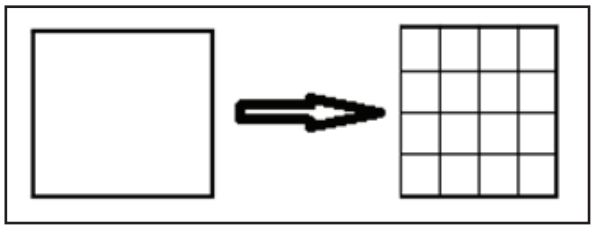

Figure 3.3: Diagrammatic representation of chessboard segmentation

Based on the processing capabilities of the eCogntion Developer 8.7 software, chessboard segmentation with an object size of 2x2 pixels was found to be appropriate for creating identical sized objects. Chessboard segmented objects with pre-defined mean brightness values based on the pan-sharpened MSS GeoEye image were used to assign the pixels to shadow and open area classes as indicated in Figure 3.3. The remaining objects were assigned to the trees class. The objective of this process was to separate trees from the background and other classes such as shadow and open areas. The mean layer values of CHM layer with a minimum threshold value of 2 m was used to separate trees from low lying and shrubby vegetation. In the shadowed region, objects above 2 meters were separated from the shadow and assigned to the trees class. The remaining pixels belonging to shadow and open areas were merged using the merge algorithm and were excluded from further analysis. Figure 3.4 shows the ruleset for assigning the chessboard segmented objects to different classes.

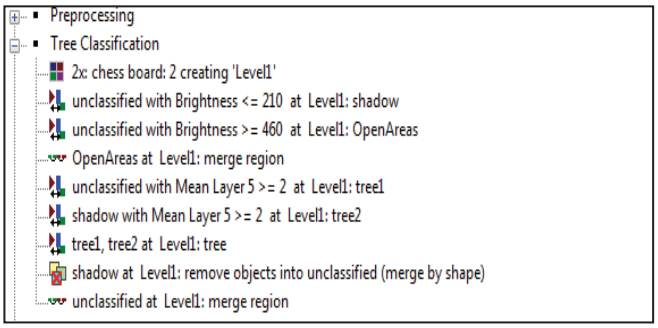

Figure 3.4: Process for shadow and open area masking

b. Finding the local maxima and local minima

The selection of seeds is a key step in the segmentation process because the segment result are sensitive to the selection of the initial growing points (Weihong, et al., 2008). Local maxima defines the position of seeds (i.e. top of the tree) which are used as a starting point for growing process (Culvenor, 2002). Careful selection of filter window size is important in seed selection, because smaller window size may assign large tree crown with more than one local maximum. Similarly, a large filter window size may fail to detect the local maxima of trees with small tree crowns. In this study, the local maxima were chosen based on the CHM layer with a filter window size of 4x4 pixels, as this kernel was appropriate considering the average crown diameter of 4 m measured during the field work. The local maxima were detected as treetops and were used as a seed to initiate a region growing based on threshold intensity within the image. Closely located seeds were merged to avoid over-segmentation by applying a merge region algorithm. On the other hand, the local minima defines the absolute boundaries of the tree crown during the growing process (Culvenor, 2002). Similar window filter size of 4x4 pixels was applied to locate the local minima throughout the image. A merge algorithm was applied to the local minima to form a network of tree crown boundaries. Figure 3.5 shows the ruleset for selecting the local maxima and local minima.

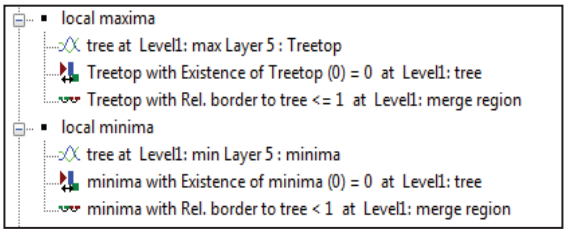

Figure 3.5: Finding the local maxima and local minima

c. Growing from the seed

The near infrared (NIR) band was selected as the illumination image for the region growing process because near infrared band is sensitive to vegetation. Seeded region growing was an iterative process started in the seed pixels (treetop). The growing of seeds (treetop) continued until a given threshold brightness value is reached and was also conditioned by encountering a local minima and encountering a previously defined tree crown. Figure 3.6 shows the criteria set for growing individual tree crowns.

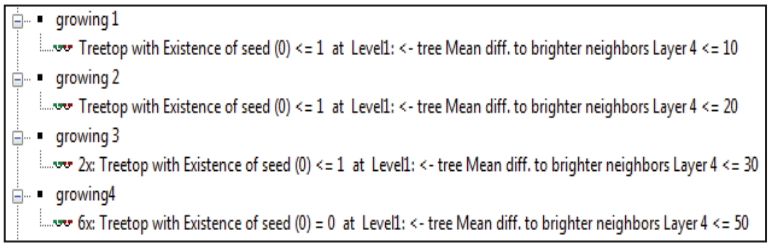

Figure 3.6: Growing from the seed

d. Smoothening the shape of tree crowns and removal of undesired objects

A watershed transformation was applied to separate large tree crowns into individual trees. Bigger sized tree crowns were separated by assigning a length factor parameter. The crown diameter information collected during the fieldwork was used to determine the length factor. A length factor of 14 pixels was used which is equivalent to a tree crown diameter of 7 meters. Further, a morphology operation was applied to smoothen the boundary of the object segments. Closed image object parameter was chosen and a circular mask of 8 pixels was applied to refine the shape of tree crowns. Closed image object adds surrounding pixels to an image object whereas the open image object removes isolated pixels from an image object (Definiens, 2009a). Tree crowns with asymmetrical shapes with a value of more than 0.8 were merged to form a single tree crown. Moreover, small objects with an area of less than 4 pixels were removed because these objects were too small to represent tree crowns. To give a final shape to the tree crown segments, objects with roundness values of more than 1.3 were removed. Figure 3.7 shows the smoothening process to refine the shape of tree crowns.

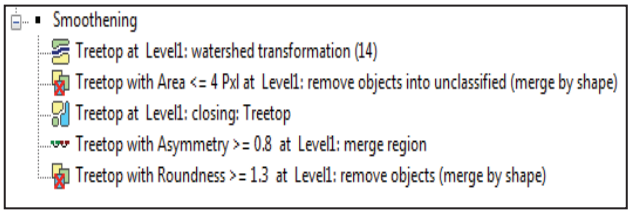

Figure 3.7: Smoothening process

3.9.1.2. Validation of Segmentation

Before the classification of species, validation of segments is important because the accuracy of the classification is partly depended on the representation of objects in the segmentation (Clinton et al., 2010). There are several methods to validate the accuracy of segmentation which can be broadly classified into goodness methods and discrepancy methods. In the goodness method, the segmentation results obtained by applying a segmentation algorithm are compared with reference segments (Zhang, 1996). The segmented individual tree crowns were assessed for quality with an goodness measure approach proposed by (Clinton, et al., 2010). The method takes into account the area and positional difference between reference objects and the segments. They have defined over segmentation and under segmentation as described in the following equations;

$$Over\ segmentation_{ij} = 1 - \frac{area(x_i \cap y_j)}{area(x_i)} \qquad \text{… Equation (i)}$$

$$Under\ segmentation_{ij} = 1 - \frac{area(x_i \cap y_j)}{area(y_j)} \qquad \text{…. Equation (ii)}$$

where, x_i and y_j are reference objects and corresponding objects respectively.

Over segmentation and under segmentation are in a range of 0 and 1, where a value of 0 in both the cases define a perfect segmentation with each segments matching the training objects accurately. Combining the over segmentation and under segmentation, the index D (goodness of fit) is interpreted as the "closeness" to an ideal segmentation result, in relation to a predefined reference set (Clinton, et al., 2010). The value of D ranges from 0 and 1 with 0 defining a perfect segmentation.

$$D = \sqrt{\frac{Over\ segmentation^2 + Under\ segmentation^2}{2}} \qquad \text{….Equation (iii)}$$

The tree crown segments were also validated using the 1:1 correspondence method between manually delineated individual tree crowns and the automatic segments derived from eCognition. One to one matching takes position, shape and size of an object into consideration and the objects were considered to be matched if the reference object and the segmented object overlaps by at least 50% (Zhan et al., 2005). The manually delineated individual tree crowns were superimposed on the automatic segments in 1:1 correspondence method. The individual tree crown segment was considered perfect match when there was an overlap of at-least 50% or more between the reference manually delineated individual tree crowns and automatic segments generated by eCognition.

3.9.2. Image Classification

After the image segmentation, each segment is a candidate object for classification. The segmented image objects were classified by the nearest neighbour classification in eCognition Developer 8. The nearest neighbour method computes the Euclidean distance from the observation to be classified to the nearest training sample observation and assigns it to that class. This method takes the spectral, spatial and contextual information necessary to interpret an image. eCognition supports a supervised classification technique to train and build up a knowledge base for the classification of image objects (Definiens, 2004). Features for classification in eCognition are computed based on image objects and not on single pixels. Height information from CHM and the mean brightness values from NIR band were selected in the feature space optimization to ensure classification of objects with similar height and spectral attributes. The maximum layer value of bands in the feature space represents the brighter pixel of tree crowns which enables separation of different classes (Gougeon & Leckie, 2006). The training dataset comprising of 70% of the identified trees on the image from the field work were used to train the sample tree species, while the remaining 30% was used for validating the classification result. The training dataset was used as a thematic layer to train the image objects for the classification of species.

In this study, only two broad classes are considered for classification because earlier study in the same area indicated a weak class separability among different tree species using transformed divergence method (Shah, 2011). The best separability class was found for *Shorea robusta* while the other co-dominant tree species such as *Schima wallichii, Rhus wallichi, Castanopsis indica* showed weak class separability. Therefore, the tree species were classified into two classes only namely *Shorea robusta* and Other tree species.

3.9.3. Accuracy Assessment

To evaluate the accuracy of the classification, an error matrix is a standard accuracy assessment procedure for image classification. An error matrix was generated and the producers and users accuracies were calculated for each class from the error matrix. A validation dataset comprising of 127 trees (96 *Shorea robusta* and 31 Other tree species) were used for classification accuracy assessment. The accuracy assessment of the classified image was carried out in ERDAS Imagine 2011.

3.10. Aboveground Biomass and carbon stock calculation

Aboveground biomass was calculated using allometric equation (Equation iv) with the field measured DBH and tree height. The application of appropriate allometric equation for biomass estimation is of crucial importance for reducing errors (Chave et al., 2005). However, species and site specific allometric equations were not available for the study area. The general allometric equation for moist mangrove forest stands developed by Chave et al., (2005) was used to calculate the AGB. The AGB was then converted to carbon stock using the conversion co-efficient of 0.47 as recommended by IPCC (2007).

$$AGB = 0.0509 * \rho D^2 H \quad \text{……Equation (iv)}$$

Where,
AGB = aboveground tree biomass [kg];
ρ = wood specific gravity [gcm^{-3}];
D = tree diameter at breast height (DBH) [cm]; and
H = tree height [m]

The same allometric equation was also used by ICIMOD for implementation of REDD Pilot Project in three watershed areas of Nepal and justifies its use due to non-availability of site and species specific allometric equation for the study area. The specific wood gravity for three tree species and all other tree species used for AGB calculation are presented in Table 3.6.

Table 3.6: Specific wood gravity of different tree species; Source (ICIMOD, 2010)

Rank1 tree species	Rank 2 tree species	Rank 3 tree species	All other species
Shorea robusta (0.88 gcm^{-3})	*Schima wallichii* (0.69 gcm^{-3})	*Castanopsis indica* (0.74 gcm^{-3})	Mean of Terai/lower slope mixed hardwood forest (0.72 gcm^{-3})

3.11. Regression Modeling

Regression modelling is commonly used for biomass estimation studies. The multiple regression analysis is the most common approach for development of AGB estimation models (Lu, 2006). It is used to model the relationship between a dependent variable and one or more independent variables. Individual tree crown segments which were correctly classified and that have 1:1 spatial correspondences with the referenced manually delineated individual trees were used to develop the regression models. The relationship between the dependent variable (aboveground carbon) as obtained from the allometric equation and the two independent variables (tree height obtained from CHM and the CPA from the segmented tree crowns) were investigated through log transformed regression models. Both the dependent variable (aboveground carbon) and the independent variables (height and CPA) were log transformed. The log transformation was carried out because, when the histograms of the variables were plotted, the trend showed a positively skewed distribution (See Appendix 5 & 6). Log transformation of

the variables are recommended when the variables typically shows skewed distribution which can be made symmetric by transforming the data (Keene, 1995). Moreover, preliminary analysis of the relationship through scatter plots between dependent variable (aboveground carbon) and the single independent variables (height and CPA) exhibited non-linear relationships. Log transformation is used in allometry specifically to uniformly depict relative variation between variables and is a non-linear transformation (Kerkhoff & Enquist, 2009). Therefore, a natural logarithmic transformation was applied to both the independent and dependent variables.

Prior to the developing the multiple regression models, a diagnostic test for multi-collinearity was conducted for the independent variables. In multiple regression modelling, highly correlated variables causes a problem for parameter estimation and the contribution of each variable is not reliable. The Variance Inflation Factor (VIF) is one of the indicators that measures how much variance of an estimated regression co-efficient is increased due to collinearity.

Validation of the model performance and accuracy assessment of the estimated carbon are important in carbon estimation process. Two most widely used methods for model validation are co-efficient of determination (R^2) for the models developed and the root mean square error (RMSE) (Lu, 2006). Co-efficient of determination (R^2) shows the percentage of variation in one variable that is associated with other variables. The strength and the significance of the models were validated using the partitioned 30% validation dataset. The following equation (v) was used to calculate the RMSE.

$$\mathrm{RMSE} = \sqrt{\frac{1}{n}\sum_{i=1}^{n}\left(X_{Oi} - X_{pi}\right)^2} \quad \ldots\ldots\ldots\ldots\ldots \text{ Equation (v)}$$

Where,
X_O = Observed carbon,
X_p = Predicted carbon,
n = number of observations

3.12. Relationship between carbon Stock with spectral reflectance of RapidEye Image

3.12.1. Derivation of variables from RapidEye image

A comparative analysis of the relationship between spectral responses and forest biophysical parameters such as aboveground carbon stock is needed to be explored for up-scaling the aboveground carbon derived from small areas to larger areas. Vegetation indices such as normalized difference vegetation index (NDVI) are often used for biomass/carbon estimation by using the red and near infrared wavelengths. The most commonly used vegetation indices is the NDVI (Lu, et al., 2004). The NDVI was extracted from RapidEye image using the equation (vi) in ENVI 4.8.

$$NDVI = \frac{(NIR - RED)}{(NIR + RED)} \ldots\ldots\ldots\ldots \text{ Equation (vi)}$$

Moreover, the RapidEye image has a red edge band which is sensitive to chlorophyll useful for detecting vegetation. Similarly, the Red Edge NDVI was also extracted from the RapidEye image using equation (vii) adapted from (Wu et al., 2009) in ENVI 4.8.

$$RedEdge\ NDVI = \frac{(NIR - RedEdge)}{(NIR + RedEdge} \ldots\ldots\ldots\ldots \text{Equation (vii)}$$

The Principal Component Analysis (PCA) was performed on the image in ENVI 4.8. PCA transforms an original image into a smaller dataset of uncorrelated variables which contains the maximum information from the original images. The first component (PC1) contains the most variance and each subsequent component contains less variance than the previous components (Wang, et al., 2004). Hence, the first principal component was chosen for this study to test the relationship between up-scaled carbon stock and the spectral reflectance of the RapidEye image.

Similarly, the red edge band and near infrared (NIR) bands were also used to test the relationship with the up-scaled carbon stock. Red edge and the NIR bands were chosen because these bands are sensitive to chlorophyll content in the vegetation (Wu, et al., 2009).

3.12.2. Up-scaling from reference carbon to RapidEye Image

Up-scaling also known as aggregation is a process of scaling up spatial data from a finer spatial resolution image to a coarser resolution image. The basic idea of the up-scaling process is to use a moderate or a relatively coarser resolution satellite image to estimate and map carbon stock at a landscape level. It is well known that the cost of VHR satellite images (e.g. GeoEye) and LiDAR data are very expensive and covers relatively small areas. Processing of such data requires longer time and several software packages and techniques. However, if a carbon estimate derived from the integration of VHR satellite image and the LiDAR data can be related to the data or product of image transformation (e.g. NDVI, RedEdge NDVI, PC1, red edge and NIR bands) from a moderate or relatively coarser satellite images, the cost and time for estimating carbon can be reduced significantly. Moreover, relatively coarser satellite images cover larger spatial extent and the development of such an approach will benefit the programs such as REDD for regional level carbon estimation and mapping in a cost effective way.

Up-scaling of carbon derived from the integration of VHR Geoeye image and LiDAR data to a relatively coarser RapidEye image (5m spatial resolution) was carried out in ArcGIS 10. The carbon polygons were overlaid on the NDVI, RedEdge NDVI, PC1 images and the red edge and NIR band images. All the raster images were converted into 5m x 5m grids representing the spatial resolution of RapidEye image and each 5mx5m grid contained its corresponding raster values. In both the carbon polygon and the grids, the densities of both values were calculated. The carbon polygon and the raster grids were intersected in ArcGIS10 followed by calculating the area of intersection. The new carbon values inside the intersected area were calculated within each grid. The sum of carbon in each 5 m pixel of the RapidEye and its corresponding raster values were extracted for further analysis. Since the dataset obtained was huge, a grid of 100mx100m was created over the study area and 10 grids were chosen randomly for further analysis. Data was partitioned into 70:30% as training and validation datasets respectively. Individual tree crowns as visualised in the VHR imagery and its corresponding tree crowns as visualized in RapidEye imagery is shown in Figure 3.8. An example of the carbon polygons superimposed on the NDVI image derived from 5 m RapidEye image for up-scaling is shown in Figure 3.9. The reddish colour represents areas with no vegetation and the black polygons represent the carbon from individual trees.

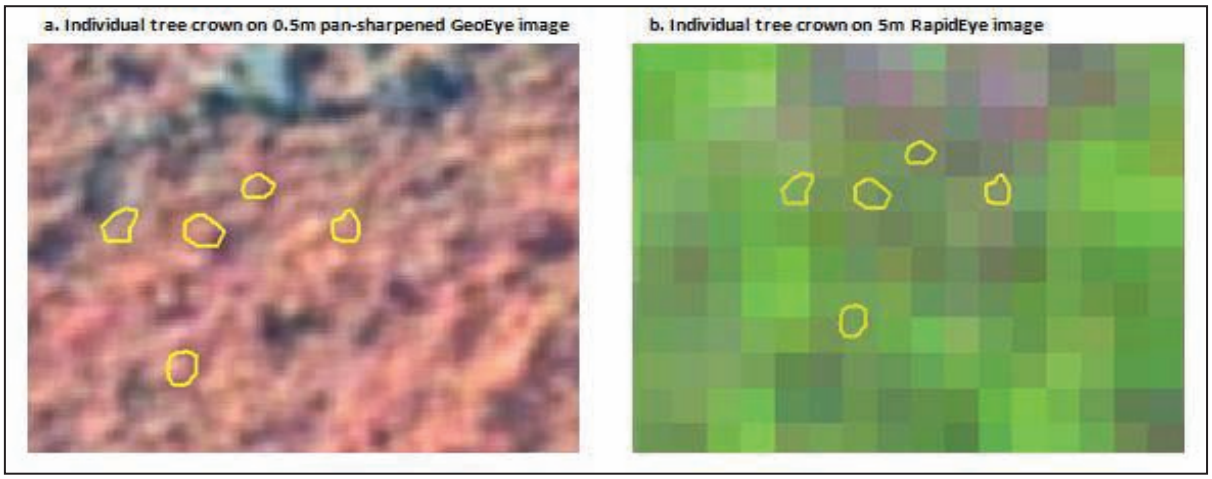

Figure 3.8: Visualization of individual tree crowns on GeoEye and RapidEye

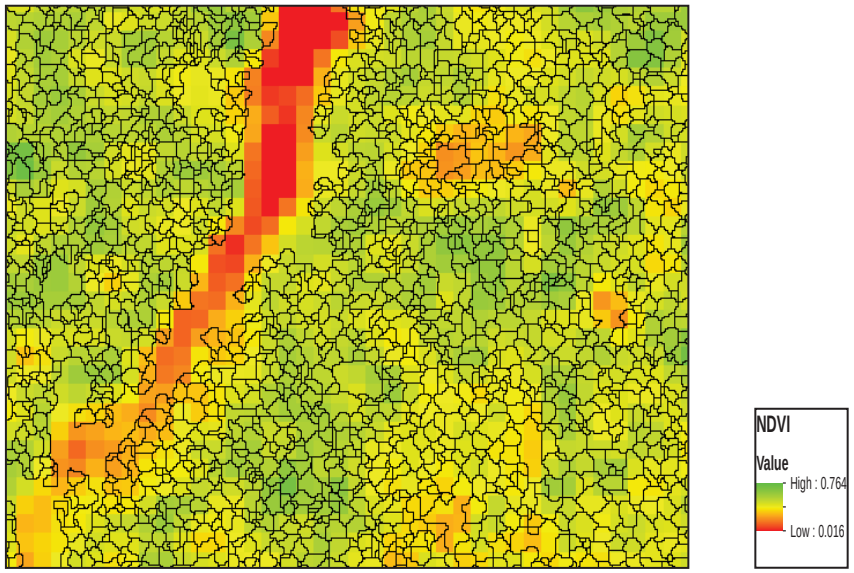

Figure 3.9: Carbon polygon superimposed on NDVI image

3.12.3. Regression modelling between Carbon and RapidEye variables

The relationship between up-scaled carbon stock and the spectral reflectance of RapidEye image through NDVI, Red Edge NDVI, PC1 and the single bands of red edge and near infrared (NIR) were assessed by regression modelling. The up-scaled carbon was used as a dependent variable and the derived vegetation indices, PC1, red edge band and the NIR band were used as single independent variables. The performance of the regression models were assessed by comparing the co-efficient of determination (R^2) for each independent variable. The co-efficient of determination measures the percentage of variation explained by the regression model.

4. RESULTS

4.1. Descriptive Statistics of the field data

Field inventory data comprising of DBH above 10 cm and tree height were recorded for 2793 tree in 86 plots of Ludhikhola watershed, Gorkha, Nepal. A total of 423 trees were identified on the image which was manually delineated on screen by digitizing in ArcGIS 2010. The descriptive statistics of the DBH, height and crown diameter for *Shorea robusta* and other tree species is presented in Table 4.1. The DBH of *Shorea robusta* and Other tree species have a mean of 17cm and 18 cm respectively. *Shorea robusta* and Other tree species have a mean height of 13m and 10m respectively. The mean crown diameter is 4m for *Shorea robusta* and 5m for other tree species.

Table 4.1: Descriptive statistics of *Shorea robusta* and Other tree species

	Shorea robusta				Other tree species			
Attributes	Mean	Min	Max	Std. Dev	Mean	Min	Max	Std. Dev
DBH (cm)	17	10	83	8.74	18	10	60	8.64
Height (m)	13	2	35	4.97	10	2	29	4.64
Crown Diameter (m)	4	0.5	13	1.46	5	1	15	2.01

DBH and tree heights measured in the field were analysed using box plot for *Shorea robusta, Schima wallichii, Rhus wallichii, Castanopsis indica* and other tree species. Species wise box plots of diameter at breast height (DBH) and height are shown below in Figure 4.1.

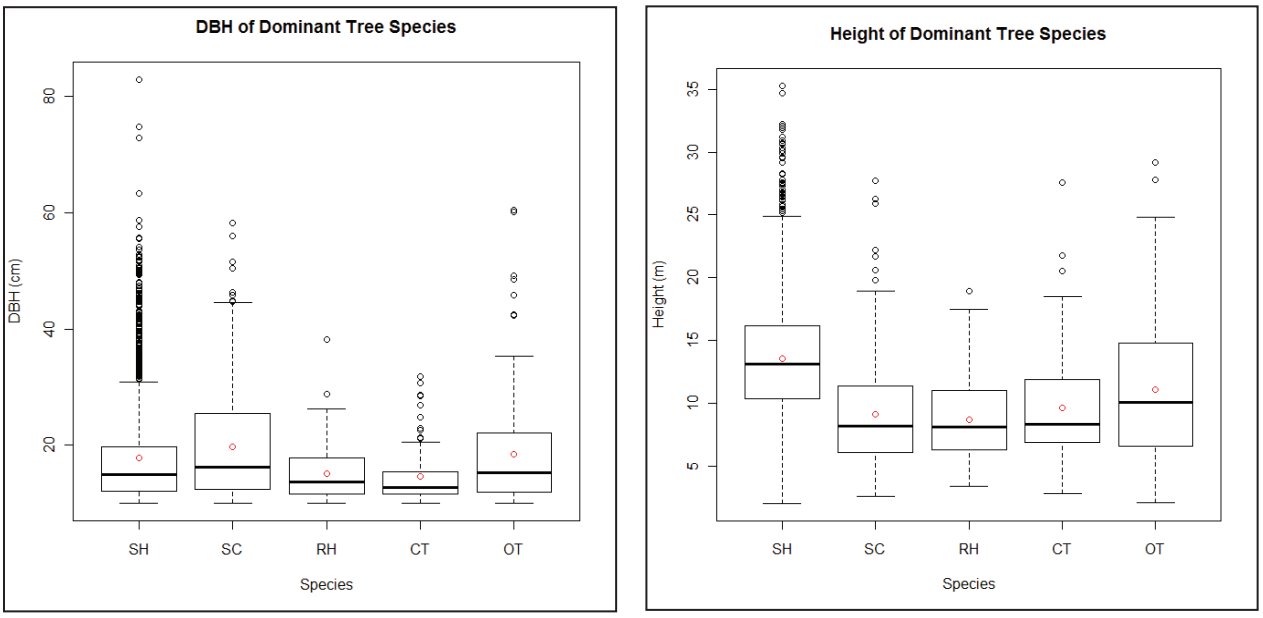

Figure 4.1: Box plots of the DBH and height of dominant tree species

SH=*Shorea robusta,* SC=*Schima wallichii,* RH=*Rhus wallichii,* CT=*Castanopsis indica,* OT=*Other tree species*)

Schima wallichii had the largest mean DBH and *Shorea robusta* had highest mean tree height. The box plot indicated that the tree species in the study area have high variability in terms of DBH and height. The maximum diameter and highest tree height were recorded for *Shorea robusta* at 83 cm and 35 m respectively.

A total of 27 different species were recorded in the study area (See Appendix 2). *Shorea robusta* is the dominant tree constituting about 74% of the tree species followed by *Schima wallichii* at 12%, *Rhus wallichii* and *Castanopsis indica* at 3 % each. *Terminalia alata* constituted about 2% of the tree species. *Pinus roxburghii* is also found at elevations above 700 meters above mean sea level in the watershed area, but only a single sample plot occurred in this study. Figure 4.2 shows the tree species distribution in the study area.

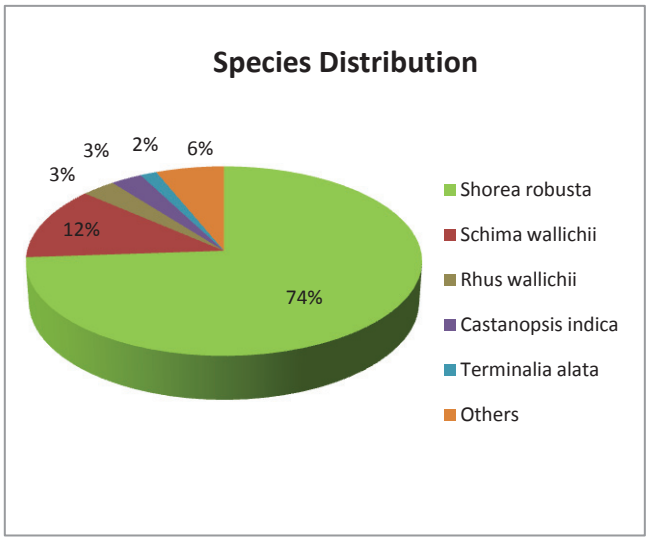

Figure 4.2: Tree species distribution in the study area

4.2. Derivation of CHM

A Canopy Height Model (CHM) was derived by subtracting the digital elevation model (DEM) from the digital surface model (DSM). The DEM and DSM for a part of the study area as visualized in Quick Terrain Modeler are shown in Figure 4.3.

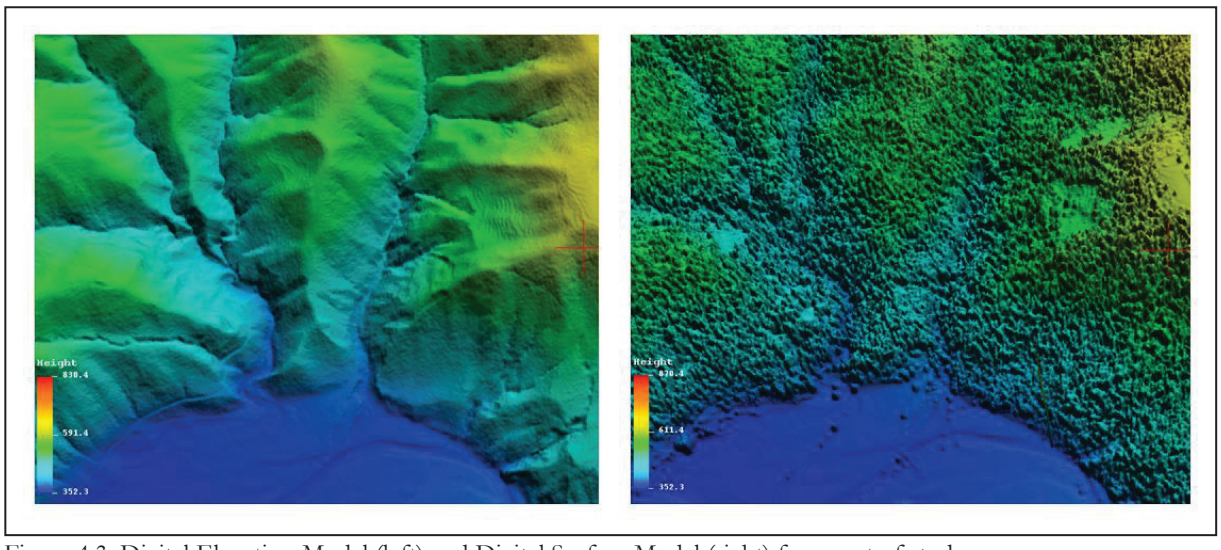

Figure 4.3: Digital Elevation Model (left) and Digital Surface Model (right) for a part of study area

The CHM with a spatial resolution of 0.5 m is a three dimensional surface that shows the vegetation height above the ground level. Figure 4.4 shows the subset of a three dimensional CHM with the individual tree crown apparent on the 3-D representation.

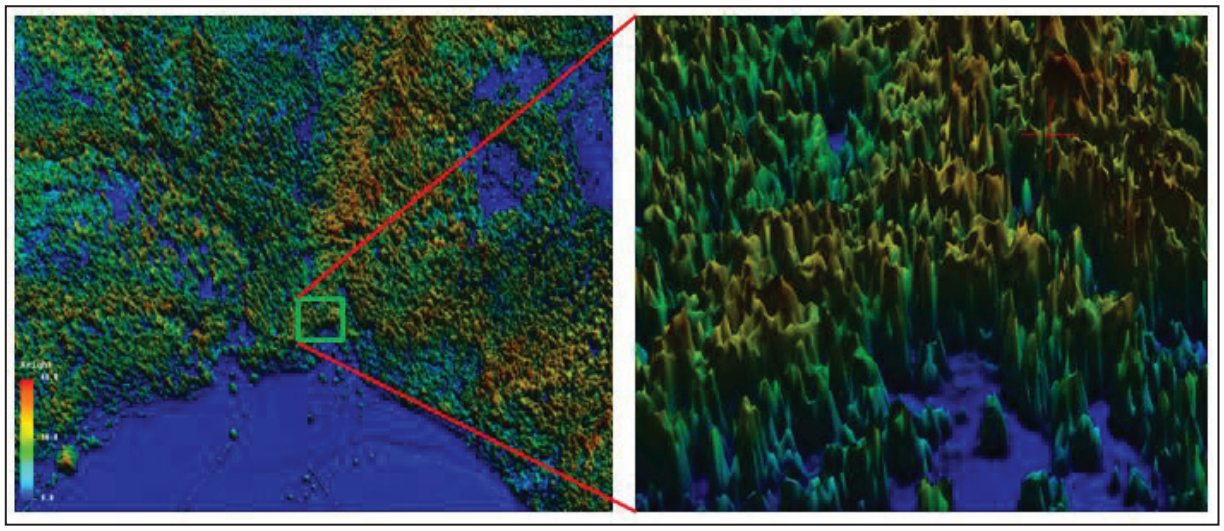

Figure 4.4: 3-D representation of the Canopy Height Model

The descriptive statistics of the field measured height and CHM estimated height is shown in Table 4.2.

Table 4.2: Descriptive statistics of the field height and CHM height in meters

Summary	Field Height	CHM Height
Mean	16.4	15.3
Standard Deviation	4.5	4.6
Minimum	6.1	5.2
Maximum	30.3	29.9
Observations	410	410

The field measured height as an independent variable was regressed against the CHM estimated height as a dependent variable. The co-efficient of determination (R^2) was 0.75 and the correlation coefficient was 0.86. A t-test was employed to test the relationship between the field height and the CHM height. The relationship was found to be statistically significant at 95 % confidence level (Appendix 4). Comparison between the field measured height and the LiDAR estimated height indicated that the LiDAR under predicted the actual tree heights measured in the field. There was an average underestimate of 1.1 m for the CHM tree height. The RMSE for the CHM predicted height obtained was 2.6 m with a RMSE percent of 16%. Figure 4.5 shows the scatter plot of field height and CHM height.

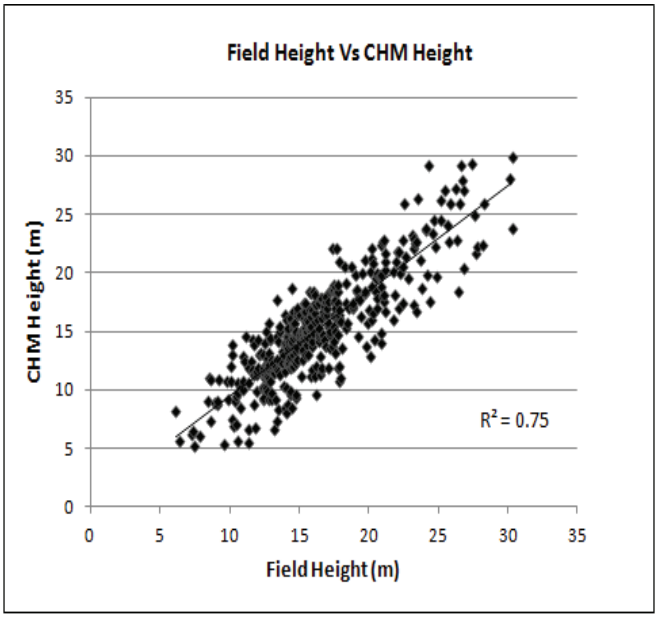

Figure 4.5: Scatter plot of the CHM derived height and Field measured height

4.3. Image Segmentation

Chessboard segmentation algorithm with 2x2 pixels was applied to the stacked layers of pan-sharpened MSS GeoEye image (0.5m spatial resolution) and CHM image (0.5m spatial resolution). The purpose of the chessboard segmentation was to partition the image into homogenous objects for individual tree crown delineation based on similar homogeneity conditions. Figure 4.6 shows a subset of a pan-sharpened image and a chessboard segmented image for further processing.

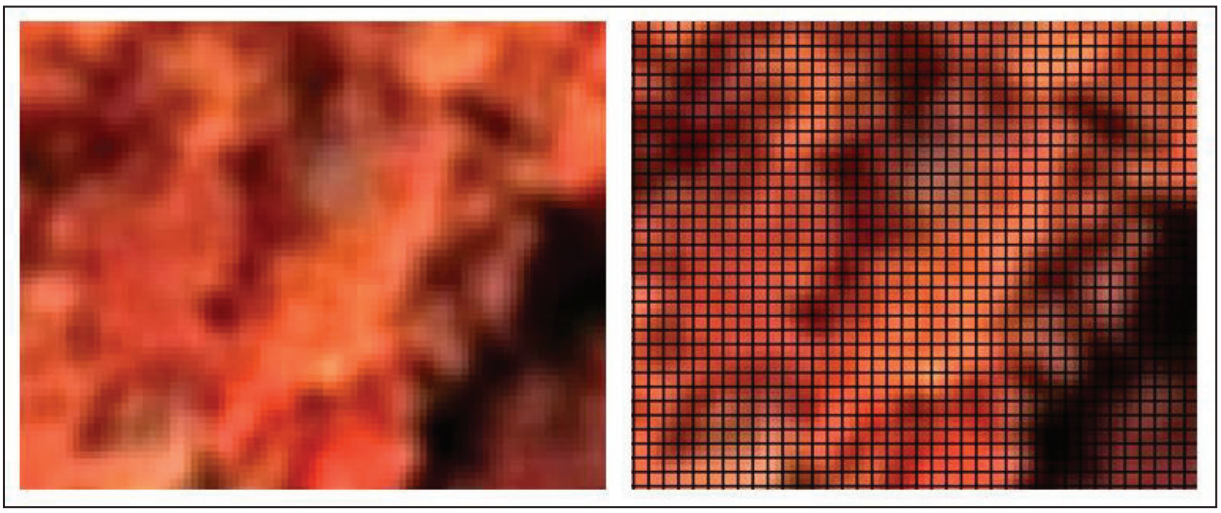

Figure 4.6: A subset of pan-sharpened image (left) and chessboard segmented image (right)

The implementation of the region growing algorithm on the combined pan-sharpened MSS GeoEye image and the CHM layer resulted in the delineation of closed objects. As indicated in the Figure 4.7, individual trees were segmented after masking the open areas and low lying vegetation. The green colour represents the trees after masking the open areas (cyan colour) and; the low lying and shrubby vegetation (reddish colour). Trees with heights above 2 meters are considered for individual tree crown delineation because the minimum tree height measured in the field was 2 m. Figure 4.8 shows the treetops detected by the find local maxima algorithm in region growing approach.

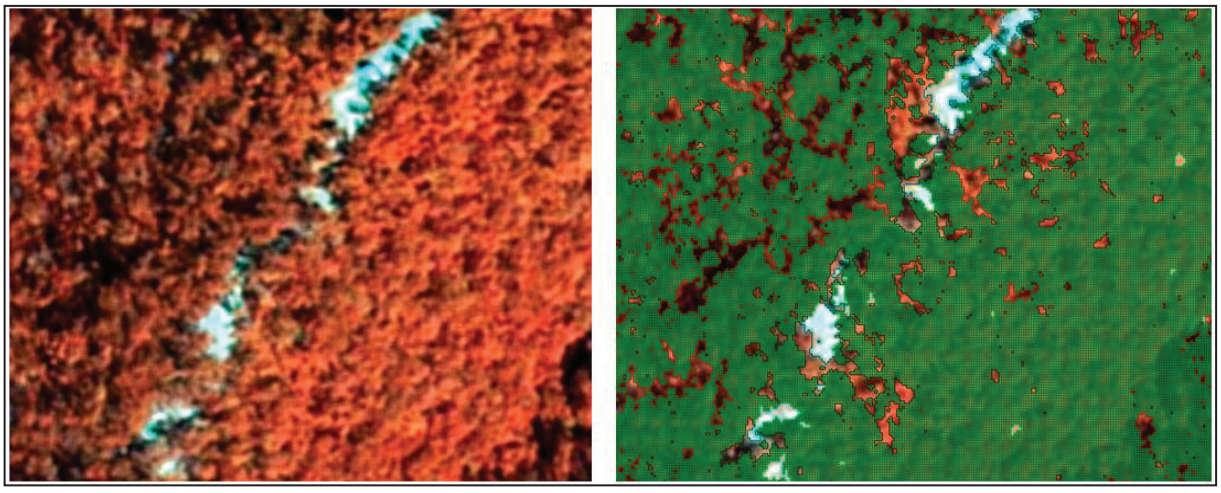

Figure 4.7: A subset of pan-sharpened image (left) and the masked open areas and low height vegetation (right)

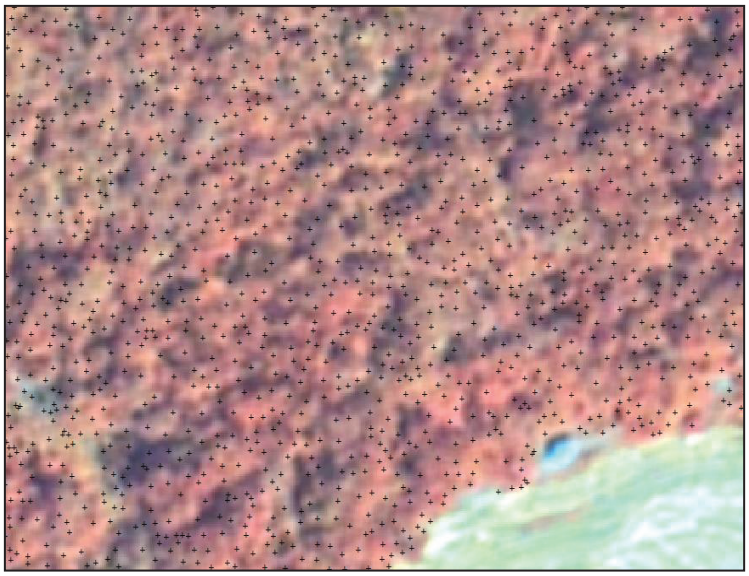

Figure 4.8: Detected local maxima on pan-sharpened GeoEye image

The accuracy assessment of the individual tree crown delineation was carried out using intersector tool. A total of 423 manually delineated reference tree crowns were used as training input against the automatic tree crown segments obtained from the region growing approach. Figure 4.9 shows a subset of the individual tree segments obtained from automatic delineation. An example of the manually delineated individual tree crowns superimposed on the automatic individual tree crowns for assessing the accuracy in 1:1 correspondence method in a part of the study area is shown in Figure 4.10.

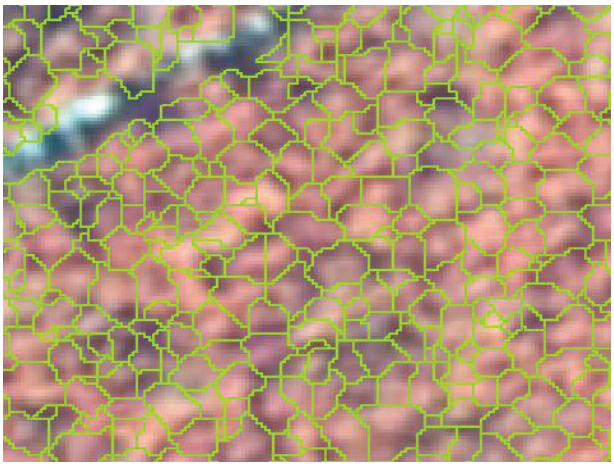

Figure 4.9: Individual tree crowns derived from eCognition

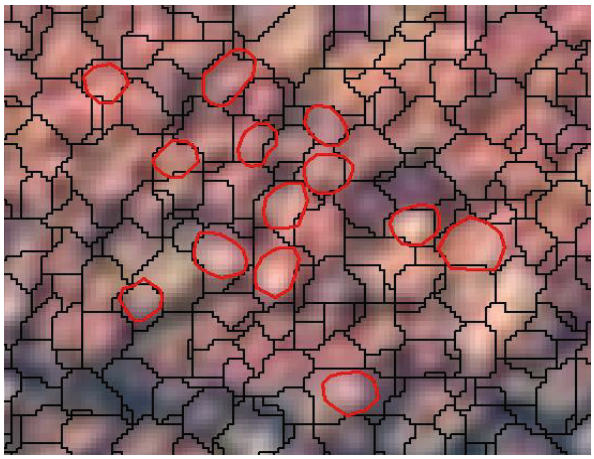

Figure 4.10: Manual delineated tree crowns (red colour) superimposed on the automatic segments (black colour)

The accuracy assessment report for the individual tree segments using the D goodness measure is given in Table 4.3.

Table 4.3: Accuracy assessment for the segmented tree crowns

Over Segmentation	0.18
Under Segmentation	0.39
D value	0.30
Overall Segmentation accuracy	70 %

The over-segmentation and under-segmentation were 0.18 and 0.39 respectively with an overall D value of 0.30. The D value of 0.30 explains an error of 30% in segmentation and thus the segmentation accuracy of is 70%.

The segmentation accuracy was also assessed by 1:1 correspondence method using the same dataset of 423 manually delineated tree crowns. The reference manually delineated tree crowns were considered perfectly matched if there was an area overlap of more than 50% with the automatic tree crowns segments. The result from the 1:1 correspondence for the segmentation accuracy is presented in Table 4.4. An overall segmentation accuracy of 74 % was obtained.

Table 4.4: One-to-one correspondence of manually delineated tree crowns and eCognition segmented tree crowns

Total number of matched tree crowns	Total reference tree crowns	Correctly segmented tree crowns
313	423	74 %

4.4. Classification of tree species

Individual tree segments were classified into two main classes namely *Shorea robusta* and Other tree species. A total of 296 trees were used for training the classifier and a total of 127 trees were used for assessing the classification accuracy. Accuracy assessment was carried out using the standard accuracy assessment procedure of an error matrix. Users and Producers accuracy were computed form the error matrix. The Users accuracy gives an indication on the reliability of the classified image as a predictive device relative to what species are on the ground. The Producers accuracy describes the accuracy by class, of the classification by the classification program. The accuracy matrix is given in Table 4.5.

Table 4.5: Accuracy matrix for the nearest neighbour classification

	Reference Data				
Class name	Shorea robusta	Other tree species	Total Classified	Error of Commission (%)	Users' accuracy (%)
Shorea robusta	92	19	111	17.1	82.9
Other tree species	4	12	16	25.0	75.0
Total	96	31	127		
Error of Omission (%)	4.2	61.2			
Producers' accuracy (%)	95.8	38.7			
Overall Accuracy = 81.8 %					

An overall accuracy of 81.8% was obtained from the nearest neighbourhood classification and a Kappa statistics value of 0.41 was obtained. The classification assessment report indicated that *Shorea robusta* was more correctly classified compared to the Other tree species with a producer's accuracy of 95.8% and user's accuracy of 82.9%. Figure 4.11 shows the classified map of the study area.

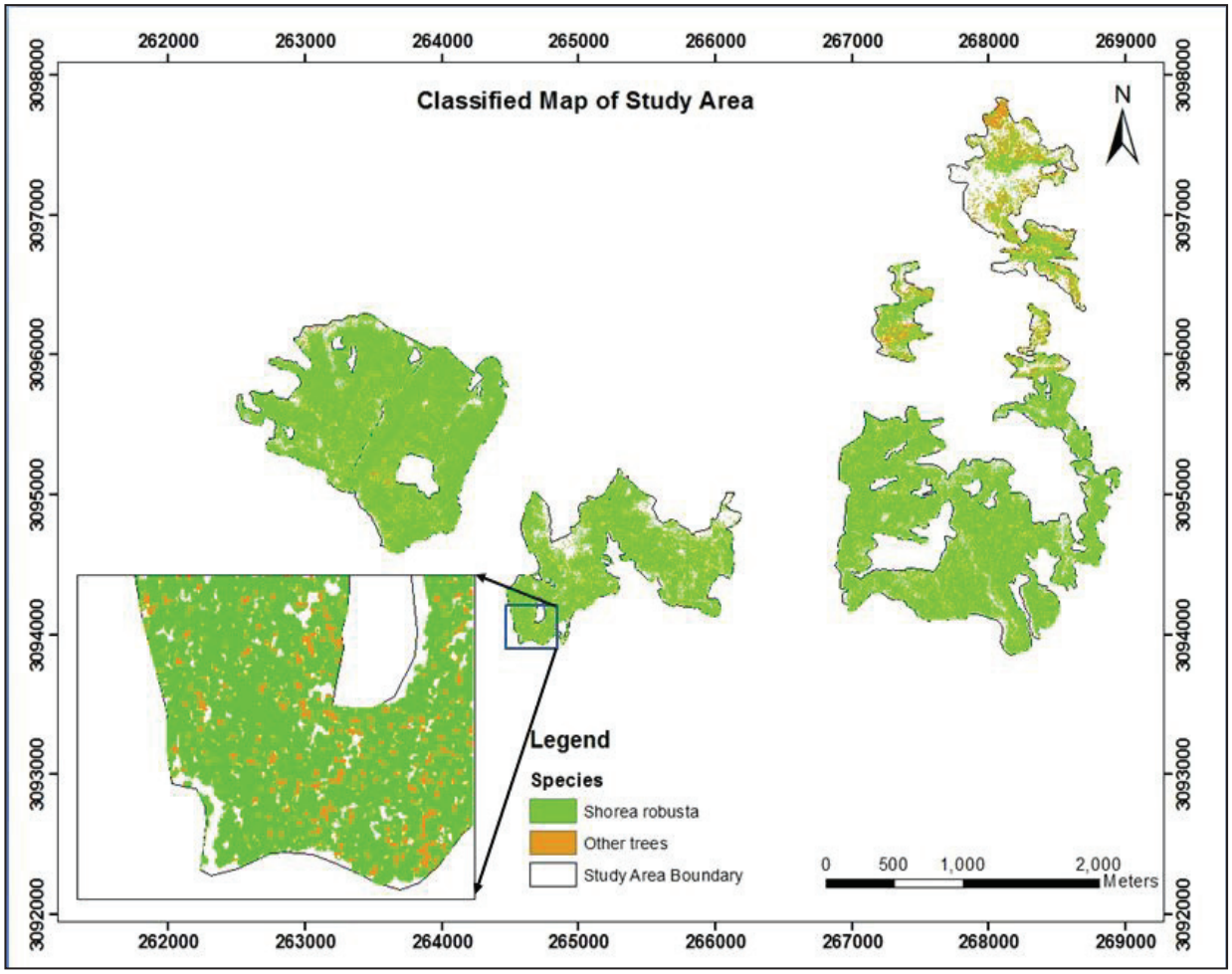

Figure 4.11: Tree species classification map of the study area

4.5. Regression Analysis

4.5.1. Descriptive statistics of variables used for modelling

A total of 230 trees (193 *Shorea robusta* and 37 Other tree species) were used for model development. These trees correspond to the total number of correctly classified trees and perfectly matched trees with 1:1 correspondence method. The maximum value of CHM within the segmented tree crown was assigned as the height of individual trees and the area of the segmented crown as the CPA. The descriptive statistics of the variables used for carbon stock modelling is shown in Table 4.6.

Table 4.6: Descriptive statistics of the variables used for regression modelling

	Shorea robusta			Other tree species		
	Height	CPA	Carbon	Height	CPA	Carbon
Mean	16.35	20.52	215.16	14.51	21.49	163.03
Standard Deviation	4.43	8.01	232.47	5.29	9.19	166.48
Minimum	5.36	5.46	26.01	5.69	4.47	11.96
Maximum	29.32	47.71	1102.2	28.87	43.23	858.94
Observation		193			37	

4.5.2. Relationship between height, CPA and aboveground Carbon of *Shorea robusta* and Other tree species

Relationship between CPA, Height and Carbon

As a preliminary analysis, scatter plots were plotted with carbon as a dependent variable and the single independent variables of CPA and CHM height for both *Shorea robusta* and Other tree species. The best of fit was obtained using a polynomial regression between the carbon, CPA and CHM height. Figure 4.12 shows the scatter plots of carbon as a dependent variable and the CPA and CHM height as a single independent variable for *Shorea robusta*. Figure 4.13 shows the scatter plots with the same variables for Other tree species.

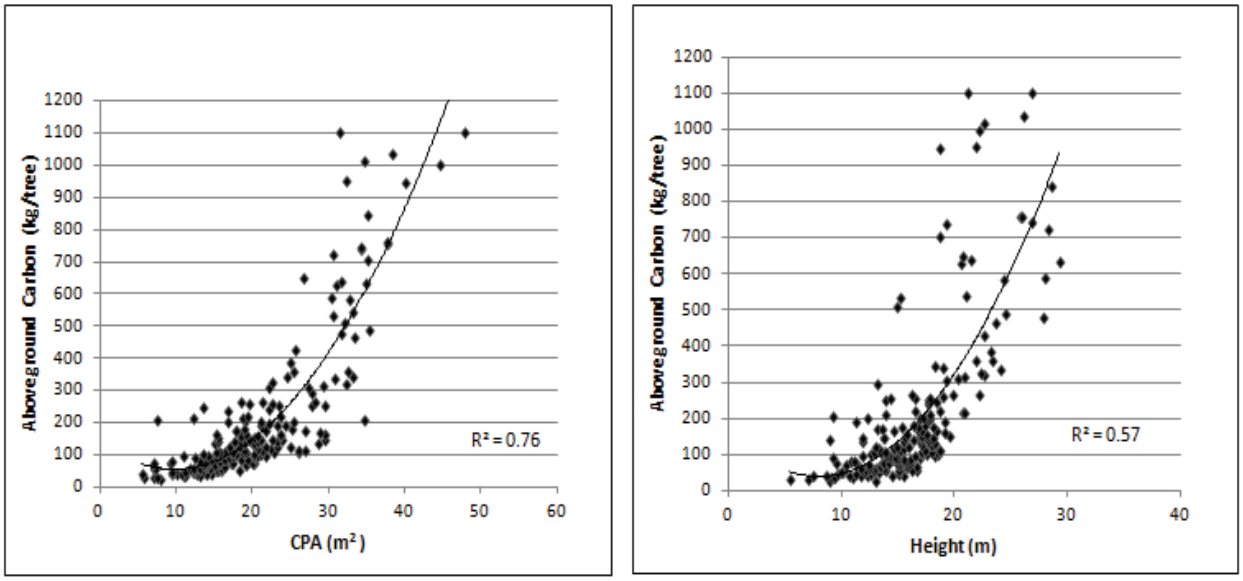

Figure 4.12: Scatter plots of carbon and the single independent variables for *Shorea robusta*

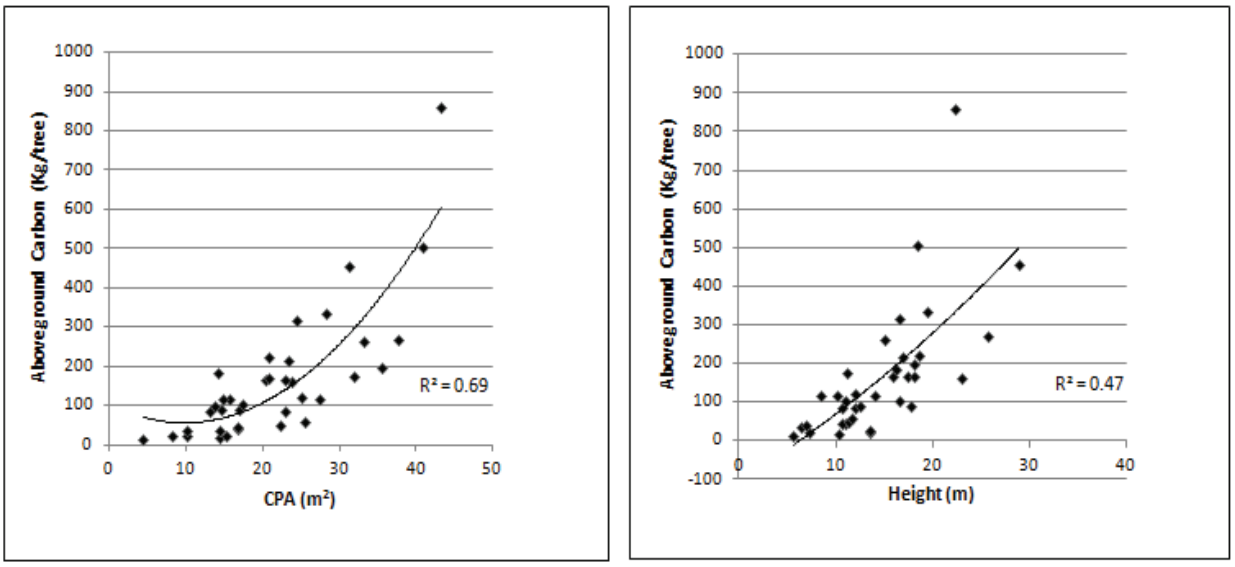

Figure 4.13: Scatter plots of carbon and the single independent variables for Other tree species

Prior to the multiple regression analysis, the Variance Inflation Factor (VIF) were calculated to check for multi-collinearity between the dependent variables for both *Shorea robusta* and Other tree species. The Variance Inflation Factor (VIF) calculated for the independent variables was 2.08 for *Shorea robusta* and 1.64 for Other tree species. In both cases, no multi-collinearity problem existed between the independent variables since the calculated VIFs were less than 10.

Multiple regression models using a natural logarithmic transformation were used to assess the relationship between carbon and the extracted tree variables (CPA and the CHM height) for both *Shorea robusta* and Other tree species. The log transformation was carried out to correct for non-linearity and heteroscedascity exhibited by the variables. The log transformed multiplicative model used in this study is shown in Equation (viii). The carbon predicted from the multiplicative log transformed models was back transformed to obtain carbon values in kg/tree.

$$\ln Y = \beta_0 + \beta_1 \ln X_1 + \beta_2 \ln X_2 \quad \text{.....Equation (viii)}$$

Where, Y: Aboveground carbon estimated from allometric equation
X_1: Height extracted from individual trees
X_2: CPA derived from automated tree segments
ln: Natural logarithm
β_0: Intercept
β_1, & β_2: Regression coefficients for X_1 and X_2

The results from the multiple regression models explaining the aboveground carbon using the CPA of individual trees and the tree height are shown in Table 4.7.

Table 4.7: Results from the multiple regression modelling

Shorea robusta	
Regression statistics	CPA & Height
Multiple R	0.86
R Square	0.74
Adjusted R Square	0.74
Stanard Error	0.44
Observations	193
Co-efficients	
Intercept	-1.70
Slope (Height)	1.10
Slope (CPA)	1.23
p-value	
Intercept	2.98E-07
Slope (Height)	4.61E-10
Slope (CPA)	1.22E-21

Other tree species	
Regression statistics	CPA & Height
Multiple R	0.87
R Square	0.76
Adjusted R Square	0.75
Standard Error	0.50
Observations	37
Co-efficients	
Intercept	-1.75
Slope (Height)	1.17
Slope (CPA)	1.12
p-value	
Intercept	0.007927
Slope (Height)	0.00022
Slope (CPA)	1.97E-05

The multiple regression models for *Shorea robusta* and Other tree species were tested using the F-test. The test revealed that the models were statistically significant at 95% confidence level. The results of the test of significance are shown in Appendix 7.

Model validation

The multiple regression models were validated using the 30% partitioned dataset. Two of the most common statistical measures (co-efficient of determination and RMSE) were used for model validation. Observed and predicted aboveground carbon from the multiple regression models using CPA and height as independent variables were plotted against each other. The models were validated using 85 trees (observations) in case of *Shorea robusta* and 19 trees (observations) for other tree species. The graphical representation of the results obtained from the model validation is shown in Figure 4.14.

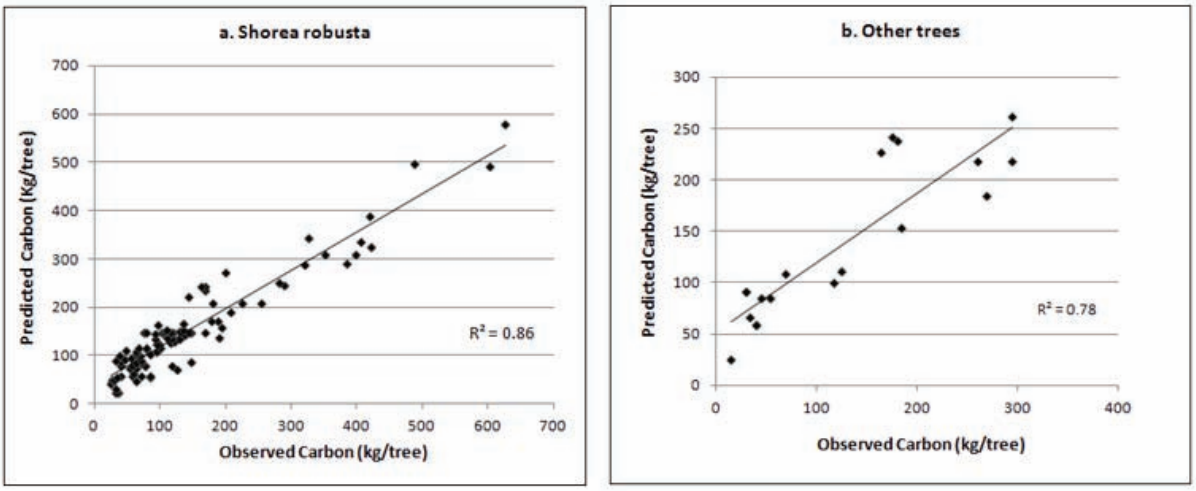

Figure 4.14:Scatter plots of observed and predicted carbon

The co-efficient of determination (R^2) between the observed carbon and the predicted carbon were 0.86 and 0.78 for *Shorea robusta* and Other tree species respectively. The co-efficient of determination (R^2) of 0.86 shows that 86% of the variability of the observed carbon in *Shorea robusta* was explained by the model. Similarly, 78 % of the variability of the observed carbon in Other tree species was explained by the model. The RMSE for *Shorea robusta* was 43 kg/tree with a RMSE percent of 32 % and for the Other tree species, a RMSE of 44 kg/tree with a RMSE percent of 34 % was obtained.

4.6. Carbon Stock Mapping of the study Area

Validated multiple regression models were used to estimate the aboveground carbon for *Shorea robusta* using the equation (ix) and for Other tree species using the equation (x). The individual tree crown segments classified as *Shorea robusta* and Other tree species through object based image classification and the multiple regression models described below were used to map the aboveground carbon in the study area.

ln Carbon = -1.70 + 1.10 * ln Height + 1.23 * ln CPA …….. Equation (ix)
ln Carbon = -1.75 + 1.17 * ln Height + 1.12 * ln CPA . . . . . Equation (x)

Where, ln: natural logarithm

The carbon stock map for the study area is presented in Figure 4.15. The carbon stock maps of each CFs are presented in Appendix 8.

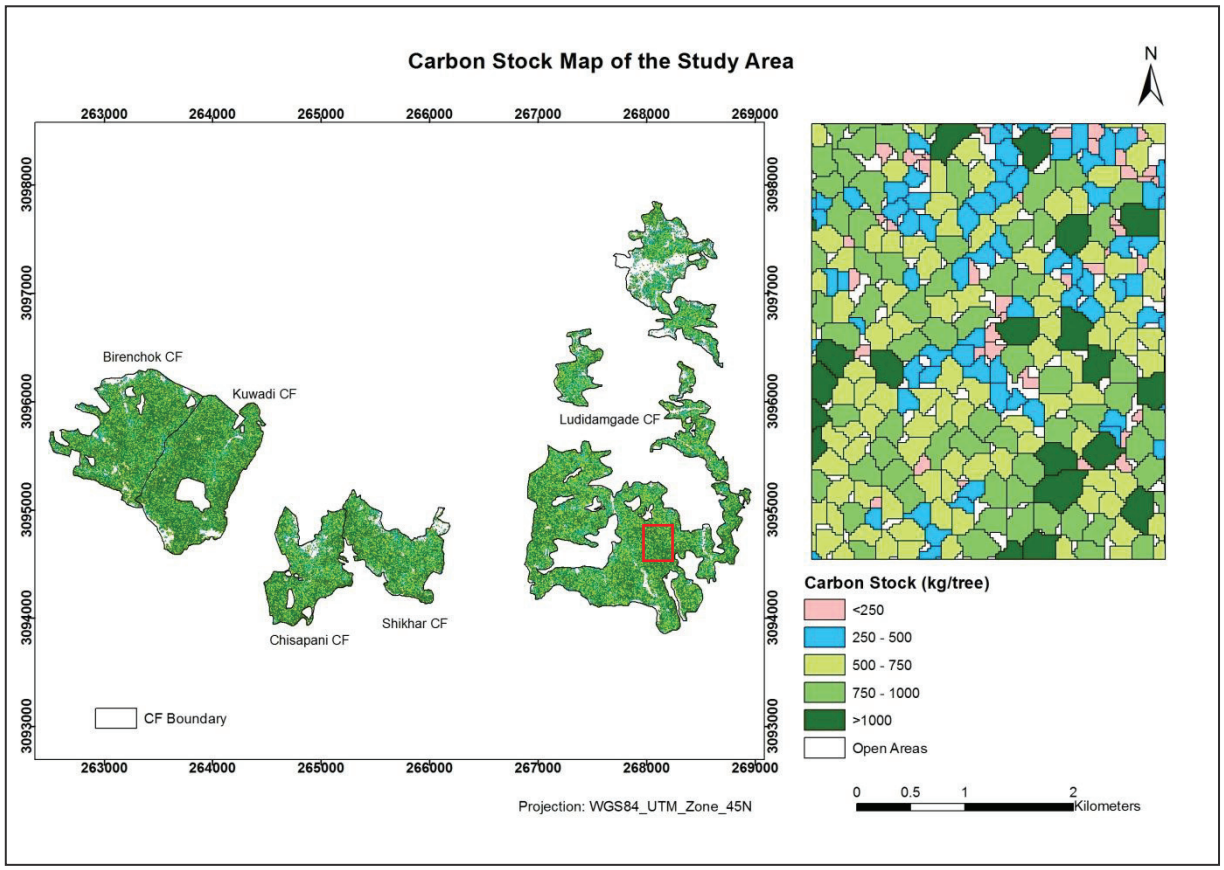

Figure 4.15: Carbon stock map of the study area

The total carbon stock estimated for the five Community Forests was 36010 MgC. The maximum carbon stock was found in Ludidamage CF with a total carbon stock of 14014 MgC and the lowest in Shikhar CF with a total carbon stock of 3543 MgC. The average carbon stock in the study area was estimated at 65 $MgCha^{-1}$. The CFUGs wise aboveground carbon stock is presented in Table 4.8.

Table 4.8: CFUG wise estimated carbon stock

Community Forests	*Shorea robusta* (MgC)	Other tree species (MgC)	Total Carbon (MgC)	CF Area (ha)	Per ha
Birenchok CF	5806	464	6270	84	75
Chisapani CF	3026	707	3733	50	74
Kuwadi CF	7705	745	8450	92	91
Ludidamgade CF	12033	1981	14014	271	51
Shikhar CF	3019	524	3543	51	70
Total	**31589**	**4421**	**36010**	**548**	
Per ha	**57**	**8**	**65**		

4.7. Up-scaling of carbon derived from intergration of VHR imagery and LiDAR data

Up-scaling is the process of aggregating pixels from a high spatial resolution image or map to a low spatial resolution image or map. The carbon derived from the integration of VHR GeoEye imagery and the LiDAR data (both 0.5m spatial resolution) was up-scaled by aggregating the total carbon to each 5m pixel of RapidEye image, which originally consist of 100 pixels of 0.5 m resolution GeoEye image. Figure 4.16 shows the carbon polygons obtained from the integration of VHR satellite imagery and LiDAR superimposed on GeoEye image and RapidEye image respectively.

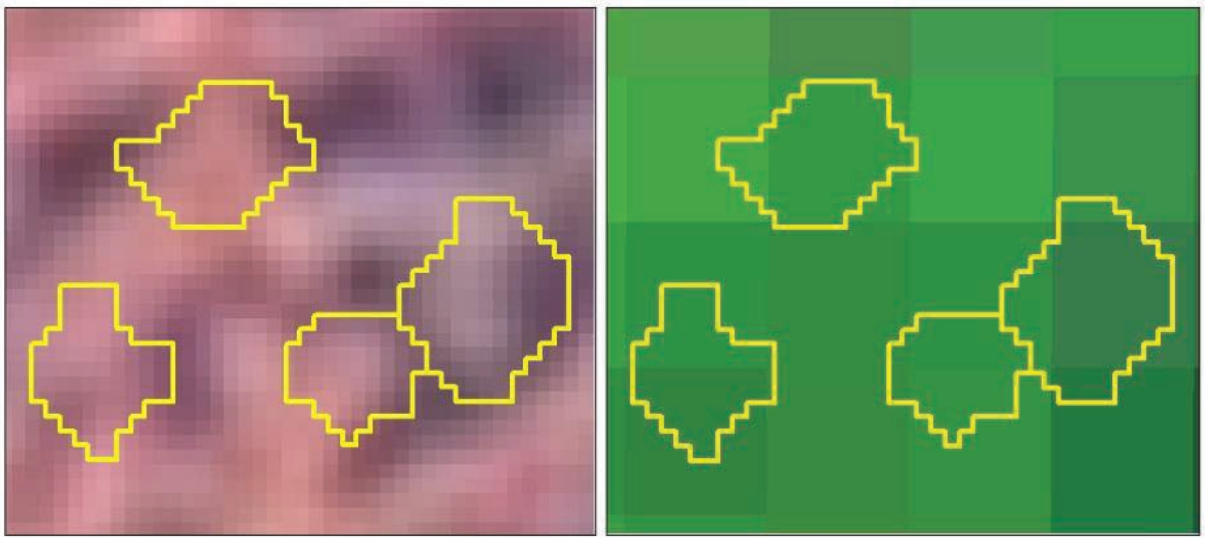

Figure 4.16: Individual tree crowns superimposed on 0.5 m GeoEye image (left) and on 5m RapidEye image (right)

The carbon in each pixel of the RapidEye image was aggregated by summing up the total carbon of the tree crowns as a whole or parts of tree crown falling within that particular 5x5m grid of the RapidEye image. The results obtained from up-scaling the carbon polygon in 5m pixel of RapidEye image is shown in Figure 4.17. Figure 4.17 c shows the aggregated total carbon in each 5x5m grid.

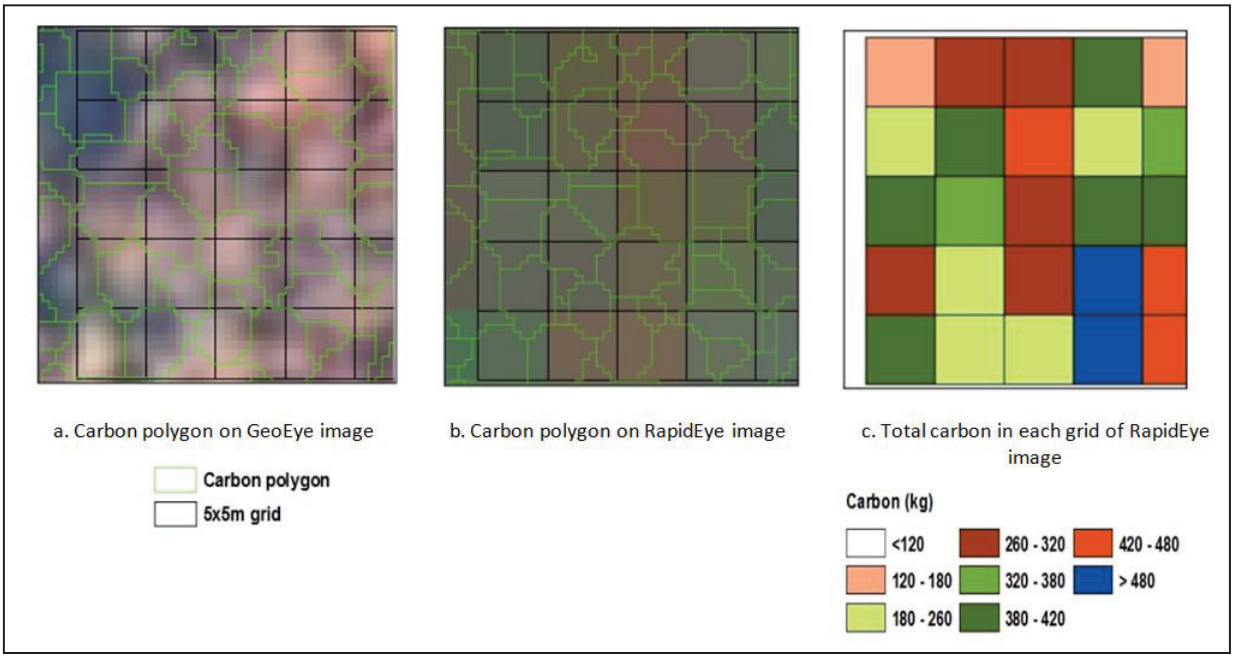

Figure 4.17: Up-scaling from GeoEye image to RapidEye image

4.8. Relationship between carbon and spectral reflectances of the RapidEye image

The descriptive statistics of the variables used to test the relationship between up-scaled carbon and the spectral reflectance of RapidEye imagery through regression modelling is presented in Table 4.9.

Table 4.9: Descriptive statistics of the variables used for modelling

	NDVI		Red Edge NDVI		PC1		Red Edge Band		NIR Band	
	NDVI	Carbon	REVI*	Carbon	PC1	Carbon	RE**	Carbon	NIR	Carbon
Mean	0.5	259.3	0.4	223.1	1324.2	258.5	5681.2	246.1	8220	256.6
Std Dev	0.04	110.8	0.04	95.9	463.9	110.3	371.0	111.2	444.1	250.3
Min	0.4	6.4	0.26	6.9	105	7.1	4688	6.3	6899	6.1
Max	0.7	568.1	0.50	580.8	2567	567.2	6667	534.9	9490	566.8
Counts	2126		2475		2094		2173		2152	

* REVI= Red edge vegetation index; **RE=Red edge

Linear regression models were used to study the relationship between the up-scaled carbon and the spectral reflectance of RapidEye imagery for up-scaling to larger scale using the 70% partitioned dataset. The results of the regression modelling using the sum carbon as dependent variable and its corresponding indices (NDVI, Red Edge NDVI and PC1) and the individual bands (Red Edge and NIR band) as the independent variables are shown in Table 4.10.

Table 4.10: Results from the regression modelling

Regression statistics	NDVI	RedEdge NDVI	PC1	RedEdge DN	NIR DN
Multiple R	0.329	0.356	0.418	0.379	0.335
R Square	0.108	0.127	0.175	0.144	0.112
Adjusted R Square	0.108	0.126	0.174	0.143	0.111
Standard Error	104.62	89.63	100.19	102.86	107.93
Observations	2126	2475	2094	2173	2128
Co-efficients					
Intercept	-183.426	-107.21	126.7473	892.17	959.69
Slope	815.2725	882.2938	0.099485	-0.11371	-0.08587
p-value					
Intercept	3.93E-11	1.01E-09	2.94E-75	5.98E-133	5.60E-101
Slope	5.07E-55	3.36E-75	1.57E-89	2.02E-75	3.01E-58

The regression models for NDVI, Red Edge NDVI, PC1, red edge band and the NIR bands were tested using the F-test. The test revealed that all the models were statistically significant at 95% confidence level. The results of the test of significance are shown in Appendix 9.

The co-efficient of determination (R^2) were low for all five models. Amongst the vegetation indices and PC1, the highest R^2 obtained was 0.18 for PC1 component and the least for NDVI with a R^2 of 0.10. For the individual bands, the R^2 obtained for red edge band and NIR band was 0.14 and 0.11 respectively. The variability of the aboveground carbon explained by the spectral data is very low. The scatter plots showing

the relationship between up-scaled carbon and the spectral reflectance of the RapidEye image are shown in Figure 4.18.

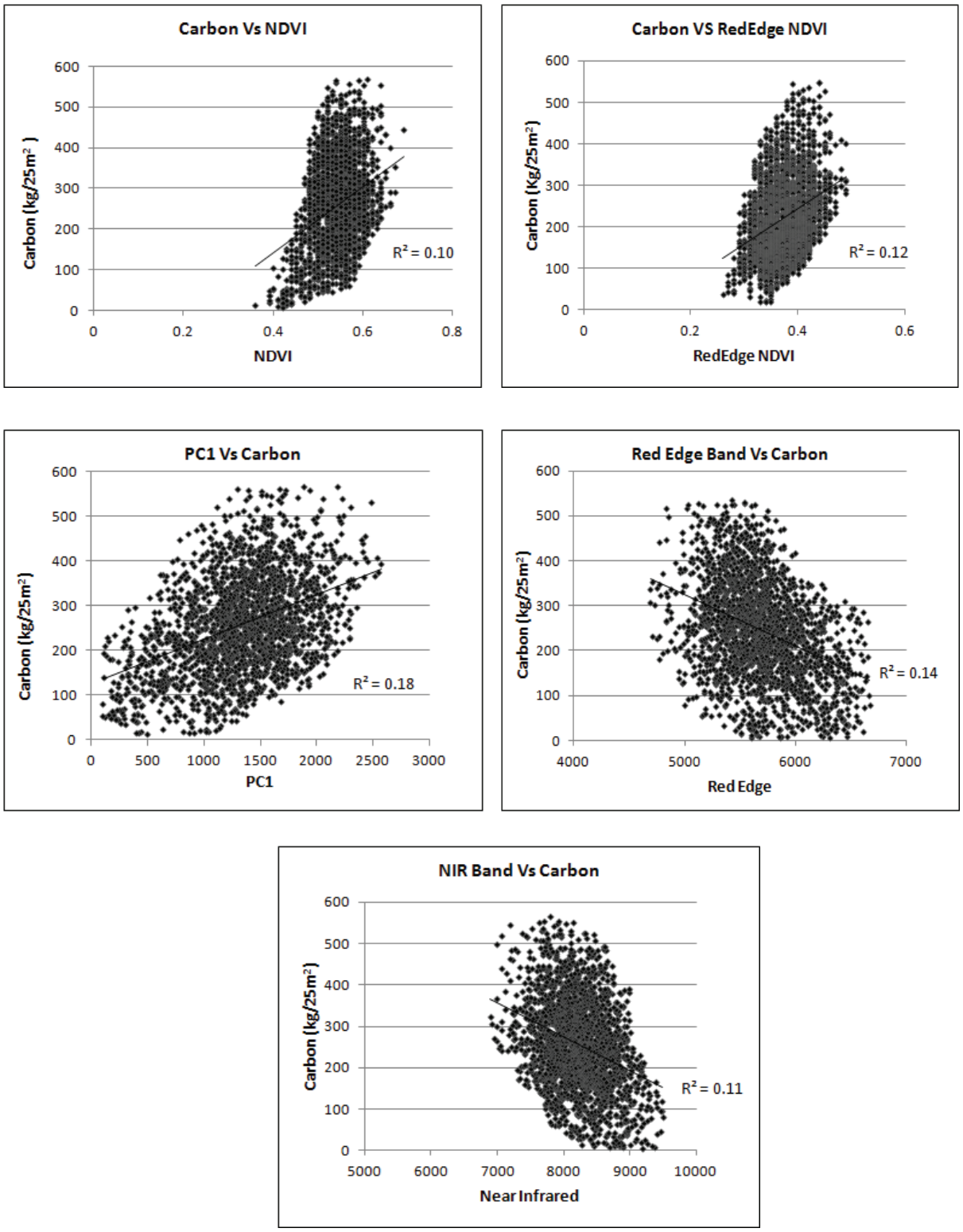

Figure 4.18: Scatter plot showing the relationship between carbon and RapidEye variables

Since all the developed models resulted in low co-efficient of determination ranging from 0.10 to 0.18, the validations of the models were not carried out. With weak relationship between the up-scaled carbon and the spectral reflectance of the RapidEye image, the up-scaling of carbon to 5m spatial resolution of RapidEye image for larger areas could not be carried out.

5. DISCUSSIONS

5.1. Derivation of CHM

The CHM was derived by subtracting the DEM from DSM. Comparison of the field measured height and the LiDAR estimated height showed a coefficient of determination (R^2) of 0.75. In general, the CHM estimated tree heights obtained in this study are in line with the findings of other studies. For instance, Kwak et al., (2007) reported that LiDAR predicted the tree heights with a R^2 of 0.74 and a RMSE of 1.32 m for *Quercus* species using LiDAR sampling density of 1.8 points/m^2. In this study, there was an average underestimation of the ground measured tree heights by 1.1 m with a RMSE of 2.6 m. As reported in other studies, under estimation of tree heights by the CHM is a common phenomenon when field measured heights are compared with the CHM predicted height (Heurich et al., 2004; Kwak, et al., 2007; Leckie, et al., 2003; Lim et al., 2003). Leckie et al., (2003) observed that the tree height of the automated segments obtained from CHM were consistently underestimated versus the ground reference heights with an average error of 1.3 m. Similar results of tree height under prediction by the CHM was also observed by Lim et al., (2003) when the maximum field measured height of the sample plots was regressed against the maximum LiDAR height in a mixed hardwood deciduous forest. Heurich et al.,(2004) reported an underestimation of CHM estimated height by 0.42 m with a RMSE of 1.41m in a deciduous forest stand. However, in this study the RMSE was slightly higher than reported in other studies.

Various reasons can be attributed to high RMSE such as the process of interpolating grid based DEM and gridding the DSM, co-registration error between the GeoEye and the CHM, the low point LiDAR sampling density, type of forests, etc. The LiDAR data was interpolated to a DEM in a raster format because the LiDAR provides point wise sampling data unlike the full coverage of an area as in optical imagery. The interpolation of LiDAR point clouds can introduce error into the DEM. It is because the average LiDAR point sampling density used in this study was 0.8 /m^2, but the distribution of LiDAR points were not homogeneous. The occurrence of 3 or more points/m^2 was observed in some areas, while few areas had no points at all. Few outliers were also found sparsely distributed over some areas which were recognised by unreasonably high elevation values in the DSM. High elevation outliers may be caused from the sensor itself. An illustration of non-uniform distribution of LiDAR points/m^2 in the study area is shown in Figure 5.1. The white dots represent the LiDAR point clouds.

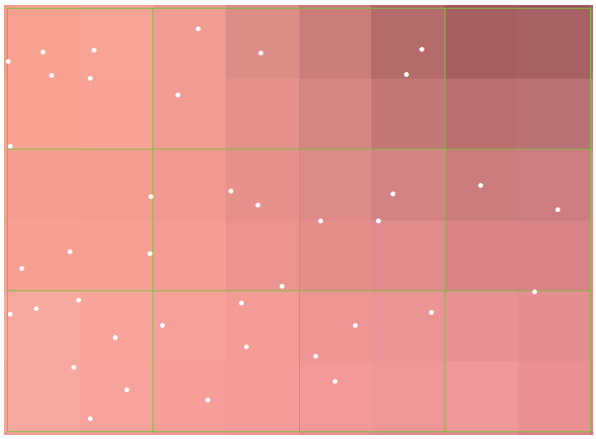

Figure 5.1: LiDAR points from all returns overlaid on 1x1 m grid

Low density point LiDAR can also cause under-estimation of the height by CHM. For instance, Persson et al., (2002) reported that the average tree height underestimation was due to lower LiDAR sampling density. Similarly, Næsset et al., (2002) concluded that tree height estimation can be improved with increased LiDAR sampling density. Holmgren et al., (2008) reported a high correlation coefficient of 0.91 between field measured height and the LiDAR predicted height using high LiDAR return density of 50 returns per m^2. The other reason for under-estimation and over estimation in this study is due to fact that the identification of trees in the field was based on the GeoEye image and the manual delineation of tree crowns were carried out on the co-registered GeoEye image. Although image to image co-registration of CHM raster and the GeoEye image was done with a RMSE of 1.9m, there existed some mis-registration error between the two dataset in some areas. This could have resulted in under estimation and over estimation of the tree heights by CHM due to mismatch between the actual positions of the trees in both datasets.

The time difference between the LiDAR data acquisition and the field work would also cause some cases of over estimation. Personal observation in few plots indicated that some of tree tops were freshly lopped during the field work. The accuracy of the tree height measurement instrument coupled with the human error arising due to undulating terrain and steep slope also led some discrepancies in measuring the actual tree heights. Locating the true treetop under dense canopy was difficult and this led to measuring the wrong treetops because of the obstruction by the branches of neighbouring trees.

5.2. Tree crown delineation

Commercial eCognition software provides various tree crown delineation approaches (i.e. segmentation) such as watershed, multi-resolution and region growing. The individual tree crown delineation in this study was carried out by region growing method using the local maxima approach. The segmentation accuracy was assessed by two methods, D goodness of measure approach and the 1:1 correspondence method. Accuracy assessment of the individual tree crown delineation resulted in an overall accuracy of 70% (D value 0.30) using the D goodness of measure approach and 74 % with the 1:1 correspondence method. The segmentation accuracy of this study is within the range published in other studies using the region growing approach. Many studies have been carried out in pure and mixed forest stands using the local maxima approach of the region growing method (Bunting & Lucas, 2006; Erikson, 2003; Leckie, et al., 2003; Tsendbazar, 2011). For example, Erikson (2003) segmenting individual trees in a mixed forest stand reported an accuracy of 73% with the manual delineated reference tree crowns using colour infrared aerial images. Similarly, Bunting & Lucas (2006) obtained a tree crown delineation accuracy of 72% in a diverse mixed species forest stand and Tsendbazar (2011) reported a tree crown segmentation accuracy of 75% in a heterogeneous mixed forests in Nepal.

The over-segmentation and under-segmentation of individual tree crowns obtained in this study was 0.18 and 0.39 respectively. A reference object is over-segmented if the area of overlap is less than 100 % and under-segmented if the area of overlap is more than 100% (Clinton, et al., 2010). In other words, over-segmentation represents smaller crown delineation compared to the reference crowns and under-segmentation represents bigger crown delineation compared to the reference crowns. The under segmentation was higher than over segmentation because of intermingling tree canopies, irregular tree crown shapes and peculiar branches of broadleaved tree species. When the tree crowns are intermingled, local minima were not detected due to absence of distinct variation within the intermingled canopies. This led to under-segmentation of the individual tree crowns. Commission or omission errors in identifying the local maxima and local minima also led to the under segmentation and over segmentation. Although, Gaussian filters of 3x3 window size were applied to smoothen the images, there still remained some noise in parts of the tree crown. It is because, the varying degree of tree crown size requires different smoothing filter windows (Ke & Quackenbush, 2011b).

The lower segmentation accuracy was also due to identifying the false local maxima (treetops) and local minima. Selection of appropriate search range in detection of local maxima was important, because the local maxima are identified within a user defined search range and the region growing was started in a set of local maxima pixels (treetop). In principle, the number of local maxima should be equal to the actual number of tree crowns. In this study, a search range of 4x4 pixels was used, which is based on the average tree crown diameter measured in the field. The local maxima were searched using the brightness value of CHM layer assuming the lower heights correspond to darker pixels and taller heights to brighter ones. However, the brightest point of the tree does not necessarily always represent the tree top. The reasons are due to difference in the spectral reflectance between the centre and edge of the tree crown which are not always distinct (Wulder & Seemann, 2003). This problem is more pronounced in deciduous trees compared to the coniferous trees. Deciduous trees have ellipsoidal crown shape and causes significant within crown brightness variations in VHR imagery (Ke & Quackenbush, 2011b). Thus, recognising the tree top (peak/maxima) and the crown edge (local minima) was difficult in deciduous forest unlike in coniferous forest with conical crowns. Figure 5.2 shows two or more false treetops identified within one tree crown.

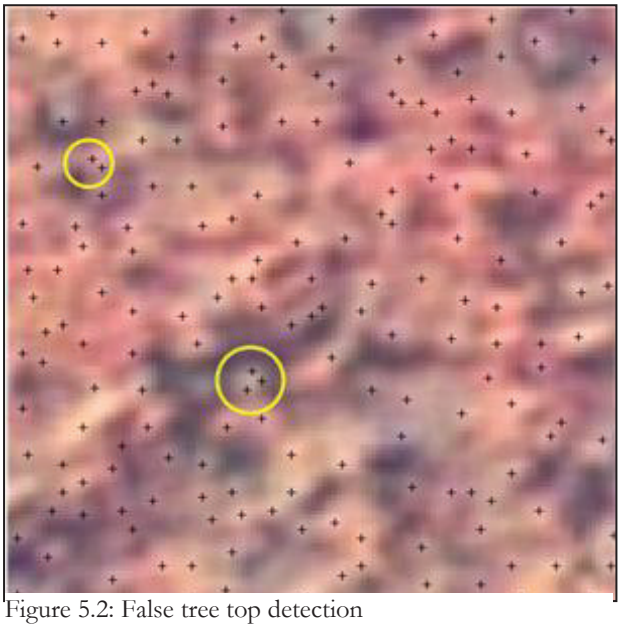

Figure 5.2: False tree top detection

The segmentation accuracy in this study was slightly higher compared to the study carried out by Shah (2011). She obtained a segmentation accuracy of 68% with D goodness measure method and 72% with the 1:1 correspondence method using the region growing algorithm in the same study area, although direct comparison cannot be made due to difference in study area size and the data used. In addition to the VHR imagery used by Shah (2011), low density LiDAR data was also used in this study. Compared to her study, the main reason for obtaining higher segmentation accuracy is because of the fact that height information from the CHM layer was used to mask out low lying vegetation (shrubby vegetation) which had similar reflectance characteristics with the trees on the VHR imagery. The CHM height information was also employed to detect trees (above 2 m) in the shadowed region. The use of LiDAR data in this study also helped to overcome the shadow effects inherent in the VHR images which are common in mountainous terrain. Tree crown delineation using either panchromatic or multispectral imagery was found to have encountered difficulties in dense and intermingled tree canopies because of indistinct intensity pattern (Leckie, et al., 2003).

Although, the segmentation accuracy obtained in this study is comparable with other studies, many studies have reported that the accuracy of tree crown detection and delineation is higher in even-aged and evenly

spaced pure stands than in mixed and heterogeneous forest stands (Gougeon & Leckie, 2006; Leckie, et al., 2003). For instance, Leckie et al., (2003) have obtained segmentation accuracy of 80 % in an even aged Douglas fir stand. They reasoned that higher segmentation accuracy which was obtained in even aged and evenly spaced pure stands to the fact that the trees with similar age and species are more likely to have uniform height and crown structure favourable for image segmentation. However, this study was carried out in a complex heterogeneous forest comprising of un-even aged trees with more than 27 different species as mentioned in Section 4.1. The forest structure consisted of trees with different crown sizes and shapes causing difficulties for the algorithm to produce reasonable segments. Further, the intermingling situation of trees where two or more individual trees overlapped and the close proximity of neighbouring trees also resulted in low segmentation accuracy as shown in Figure 5.3.

Figure 5.3: Intermingled trees

5.3. Classification of species and Accuracy Assessment

Individual tree crown segments were classified into *Shorea robusta* and Other tree species. Only two classes were considered for tree species classification because *Shorea robusta* constitutes about 74% of the total tree species in the study area. Rest of the trees were grouped as Other tree species class for the classification purpose. Moreover, earlier study in the same area has indicated that the class separability between different species was poor (Shah, 2011). The classification of these two classes resulted in an overall accuracy of 81.8% with a kappa value of 0.41. The values of Kappa is interpreted as poor when K<0.4, good when 0.4<K>0.7 and excellent when K>0.75 (Landis & Koch, 1977). It was observed that user accuracy was high for *Shorea robusta* (82.9%) compared to other tree species (75%). The result indicates that *Shorea robusta* was classified more accurately than the Other tree species and it means that the chances for a user to find *Shorea robusta* in the field are high. The producers' accuracy was also higher for *Shorea robusta* than the Other tree species. The reasons for Other tree species not being classified satisfactorily could be due to limited number of training samples assigned to the classifier (i.e. mix of different spectral reflectance from various species). During the classification process, the training samples assigned to the classifier for *Shorea robusta* and Other tree species were not in proportion. The ratio of training samples for *Shorea robusta* and other tree species was 3:1 respectively because the study area is dominated by *Shorea robusta*. Moreover, the difficulty in identifying tree species on the image for other species also led to acquiring limited number of samples for Other tree species. The classification accuracy also depended on the accuracy of the individual tree crown segmentation, because the classification was based on the segmented individual tree crowns (aggregation of pixels) rather than the individual pixels.

The integration of VHR imagery and the low density LiDAR data appeared to improve the tree species classification than using the VHR imagery alone. The overall classification accuracy obtained in this study is 81.8%, an increase in 7.8% higher compared to the earlier study conducted in the same area with similar number of classes by Shah (2011). She obtained an overall accuracy of 74% using the VHR imagery only. However, direct comparisons cannot be made as her study area was only one of the five CFs of this study area. The increase in classification accuracy is because during the feature space optimization during classification, additional information on the vertical structure of individual trees from LiDAR data was used in addition to the spectral information from the VHR imagery. An increase in classification accuracy of 8% was also reported by Holmgren et al., (2008) when integrating high density LiDAR data and high resolution aerial photograph for individual tree based classification. The reason for the increase in the classification accuracy is due to the fact that LiDAR CHM layer mitigates the shadow effect and relief displacement which are inherent in VHR imagery. For instance, Ke et al.,(2010) noted that classification accuracy increases by up to 20% when LiDAR derived topographic information including slope and aspect are used for classification.

Compared to classification results of other studies where species classification was based on two or less classes, the classification accuracy obtained in this study is low. Many studies have reported good classification accuracy when tree species are grouped into three or less number of classes. For instance, Erikson (2004) reported an increase in classification results from 77% for four different species to 91 % when the tree species were grouped into two classes using an aerial image of 3 cm. Likewise, Tsendbazar (2011) also observed an increase in overall classification accuracy from 64.5% to 90.3% when five different tree species were grouped into two broad classes of broadleaved and needle leaved species. However, the higher accuracy obtained in other studies is because of the difference in the type of forest (plantation or mono-species stand and; broadleaved and conifer forests, time of image acquisition, the finer spatial resolution of images, etc). In general, the overall classification accuracy was satisfactory considering the fact that the image was acquired during the leaf shedding season in the month of November.

5.4. Modelling and mapping of carbon stock

Log transformed models were developed in this study by using the log transformed CPA and CHM height as the independent variables and the log transformed carbon as the dependent variable for *Shorea robusta* and Other tree species. Visualization of the scatter plots for dependent variable (carbon) and the single independent variables (CPA and CHM height) exhibited a non-linear relationship. Log transformation of the variables was carried out to correct for non-linearity and heteroscedascity. For trees, in particular, ideal allometry data are strongly heteroscedastic exhibiting increasing variation in biomass with increasing diameter (Chave, et al., 2005). Despite the non-linear relationship between dependent variable of carbon and single independent variables of CPA and CHM height, the multiplicative log transformed models were preferred over multiple non-linear regression in this study. It is because, fitting non-linear biomass allometry models produces systematic biases in estimating biomass from small diameter trees and leads to large errors in landscape biomass estimation from plot level dataset that are dominated by small trees (Mascaro et al., 2011). In this study, a similar characteristic of the forest stand was found with small trees with the mean DBH of 18 cm and mean height of 13 m for *Shorea robusta* and a mean DBH of 18 cm and mean height of 10 m for Other tree species. Moreover, the allometric equation used in this study for estimation of biomass from the field measured DBH and tree height was adapted from Chave et al., (2005), which assumes that log transformed diameter and height are linearly related.

Several studies have used the multiplicative log transformed regression to estimate and biomass and tree volume in different forest types (Chave, et al., 2005; Lim, et al., 2003; Means et al., 2000; Takahashi et al., 2010; Takahashi et al., 2005). For example, Means et al (2000) predicting the wood stem volume used the

regression fitted to natural logarithm of the response variable, since the dependent variable showed heteroscedasticity and an exponentially increasing curve when plotted against the best single independent variable. Similar situation were observed in this study when the dependent variable was plotted against the independent variables of CHM height and CPA, non linear relationship was observed. The reason for this observed relationship is that the study area comprises of both mature forests as well as young naturally regenerating forests. Shimano (1997) found that the relationship between DBH and CPA is non-linear in mature natural forest because the rate of increase in CPA decreases as the tree grows which is influenced by the competition with the neighbouring trees. Similarly, the tree trunk continues to grow at a reduced rate of increment in the later stage but CPA growth stabilises and become constant after diameter has reached certain growth (Shimano, 1997). Therefore, the partially observed non-linear relationship between the CPA and Carbon and; CHM height and Carbon in this study indicates some effect of competition for light, nutrients and space between neighbouring trees. However, linear relationship between DBH and crown diameter is also reported by other studies. For instance, Hemery et al., (2005) reported a strong linear relationship between DBH and crown diameter for trees within DBH range of 20-50 cm and a slight reduction of crown diameter growth for trees exceeding 50cm DBH. In this study, a large portion of the forest stand in the study area is relatively young naturally regenerating forest, while parts of the study area also represents mature forest stand with variations in DBH and crown sizes. In a young forest, the DBH and crown increases follow a linear relationship and as the tree matures, the tree crown increases in decreasing rate after the canopy starts touching each other (Shimano, 1997). Hence, multiplicative log transformed models were developed by log transforming both the dependent and independent variables.

The coefficients of determination (R^2) obtained in this study are 0.74 for *Shorea robusta* and 0.76 for Other tree species for the multiplicative log transformed regression models developed. The adjusted R^2 obtained are 0.74 and 0.75 for *Shorea robusta* and Other tree species respectively for the model development. Validation of the model showed a R^2 of 0.86 for *Shorea robusta* and 0.78 for Other tree species with a RMSE of 43 kg/tree for *Shorea robusta* and 44 kg/tree for Other tree species. The results obtained in this study are in line with the findings of other studies. For instance, Lim et al., (2003) predicting the wood volume and total aboveground biomass have obtained R^2 of 0.86 and 0.78 respectively. Their models were based on the log transformed dependent variables of volume and biomass and the log transformed LiDAR derived height metrics in a temperate deciduous hardwood forests. Similarly, Takahashi et al., (2010) have obtained an Adjusted R^2 of 0.95 and a RMSE percent of 34.3% when predicting stand volume using the multiplicative transformed log model with CPA and height from the combination of QuickBird and low density LiDAR in a Japanese cedar plantation.

The total carbon stock estimated from the multiple regression modelling for the five CF was 36010 MgC in an area of 548 ha. The maximum carbon stock was found in Ludidamgage CF (14014 MgC) and the lowest in Shikhar CF (3543 MgC). Despite the large area in Ludidamgade CF (271 ha), the carbon stock per area was the least amongst the five CFs, because the forests in Ludidamgade CF is relatively young forest recovering from exposure to high deforestation. Baral (2011) have reported an approximate carbon stock of 70 $MgCha^{-1}$ in the tropical forests of Chitwan, Nepal. Similarly, the total carbon stock reported by Shah (2011) was estimated at 31 $MgCha^{-1}$ in Ludidamgade CF. However, the carbon stock obtained in this study for Ludidamgade CF was higher at 51 $MgCha^{-1}$.

5.5. Up-scaling and the relationship between carbon and spectral reflectance of RapidEye imagery

The carbon estimates from the integration of VHR GeoEye imagery and the LiDAR data were up-scaled to the 5 m spatial resolution of the RapidEye imagery as discussed in section 3.12.2. Although the methodology for up-scaling the carbon estimates from the integrated high resolution imagery and LiDAR data to a relatively coarser RapidEye image was developed, weak relationships were observed between the up-scaled carbon and the variables of the RapidEye image. The co-efficient of determination obtained for

NDVI, Red Edge NDVI and PC1 was low. The highest R^2 (0.18) amongst the independent variables was obtained when carbon was regressed with PC1 and the lowest R^2 (0.10) was for NDVI. Similarly, the relationship between the up-scaled carbon stock and the single individual bands of red edge and near infrared (NIR) were also weak. The co-efficient of determination (R^2) obtained for red edge and NIR bands are 0.14 and 0.11 respectively.

Studies on the relationship between the biomass/carbon estimates from the integration of VHR imagery and LiDAR and the spectral reflectance of a relatively coarser imagery have rarely been done. However, studies related to up-scaling forest stand height derived from LiDAR were carried out using mid-resolution imagery such as Landsat-5 TM (Hudak, et al., 2002; Wulder & Seemann, 2003). For instance, Wulder & Seemann (2003) developed an empirical regression between LiDAR estimated height as a dependent variable and the co-georegistered Landsat TM DN values as the independent variable. They found a weak relationship between LiDAR derived heights and Landsat TM image with a R^2 of 0.26. In this study, when the carbon estimates from VHR and LiDAR data as a dependent variable was regressed against the PC1 reflectance as an independent variable, a weak relationship with a R^2 of 0.18 was observed. Similar weak relations were observed between the carbon estimates and the NDVI and Red Edge NDVI. Previous studies have similar findings stating that vegetation indices are not a good predictor of total biomass in uneven aged and mixed broadleaved forests (Hall et al., 1995; Lu, et al., 2004; Sader et al., 1989). Hall, et al (1995) reported that the vegetation indices using the red and near infrared bands were not suitable predictors to study the forest attributes, because of weak correlation with certain vegetation parameters especially biomass. Similarly, Lu et al (2004) found a weak relationship between aboveground biomass and NDVI with a correlation coefficient (r) in the range of 0.15-0.45 in the tropical forests. The main cause of weak relationship between the biomass and vegetation indices as reported in literature is the saturation of biomass in dense forest canopies. Steininger (2000) found that the canopy reflectance saturated when the biomass reached about 15kg/m^2 which makes biomass estimation difficult in mature forests. When saturation occurs, any further increase in biomass does not affect the values of the vegetation indices. Therefore, the vegetation indices derived from red, red edge and the NIR bands from RapidEye image were not suitable to establish a relationship between up-scaled carbon estimates and spectral reflectance for up-scaling to larger areas.

The relationship between the carbon and the single bands of RapidEye image (red edge and NIR bands) in this study were found to be negatively linear with R^2 of 0.14 for red edge and 0.11 for NIR band. Several previous studies have similar findings when assessing the relationship between the biomass and the single bands in the visible and infrared spectrum (Lu, et al., 2004; Ripple et al., 1991; Roy & Ravan, 1996). Roy et al., (1996) found that the biomass was negatively correlated with the single band values in visible and NIR spectrum. They have reported a strong negative relationship between biomass and all the bands of Landsat TM with R^2 ranging from 0.49 to 0.66 except the NIR band (Band 4), which showed a weak negative relationship with a R^2 of 0.09. The study conducted by Lu et al., (2004) also reported similar findings with a weak negative relationship between the aboveground biomass and NIR band. However, the relationship between the carbon and the red edge band was relatively higher with a co-efficient of determination of 0.14. This could be due to that fact that red edge band is more sensitive to vegetation than the NIR band(Wu, et al., 2009).

There are other possible reasons for the low co-efficient of determination (R^2) between the up-scaled carbon and the spectral reflectance of the RapidEye image. The optical sensors can only detect the horizontal (spatial extent) of the forest canopy and cannot detect how much biomass is found in the vertical dimensions (height) or under a canopy. The biomass in the stem that is hidden from the sensor comprises majority of the aboveground biomass. The aboveground biomass beneath the canopy in the woody stem of a tree is estimated to comprise about 40% to 93% of the total biomass (Montagu et al.,

2005). Image co-registration could have also affected the relationship between the carbon and the spectral reflectance. The accuracy for image to image co-registration between the VHR GeoEye image and the RapidEye image was achieved with a RMSE of 1.3m. However, there still existed some unsystematic shifts in the images. This co-registration error could have caused some discrepancies in not comparing the spectral response of the RapidEye with the matching carbon estimates from the integration of GeoEye image and the LiDAR data. Other sources of uncertainties include errors in the generation of the reference carbon map from the integration of VHR imagery and LiDAR data. The temporal difference between the image acquisition dates (GeoEye in November 2009 and RapidEye in April 2011) may have also contributed to weak relationship between the carbon and the spectral reflectance of RapidEye image.

In general, this research attempted to develop a method for up-scaling carbon estimated from the combined VHR satellite imagery and LiDAR data over limited areas to a larger areas using relatively coarser optical satellite imagery as a spatial stratification. The method was developed, however, the relationship between the variables (NDVI, RedEdge NDVI, PC1, Red Edge and NIR bands) and the carbon/biomass was not reasonable to estimate the carbon at a larger scale.

5.6. Sources of Uncertainty: Factors of Error

The success of modeling and estimating aboveground carbon from the extracted tree parameters of the remotely sensed data either at individual tree level or stand level will depend on how the sources of error can be minimized at each level of carbon estimation protocol. There are several potential sources of error such as plot location error, sampling errors, field measurement errors, data processing errors, segmentation and species classification errors, and the errors associated with species and site specific allometric equations. In addition, the co-registration errors in using datasets from multiple sources also amplify uncertainties in modeling and estimating aboveground carbon stock. Errors in each step of the implementation of this research are discussed in the subsequent paragraphs.

Field measurement and data processing errors are common in remote sensing data analysis. In the field, measurement errors include incorrect measurement of the tree parameters and the accuracy of the instruments used i.e. the accuracy of the GPS to locate the centre of plot and the accuracy of vertex hypsometer to measure tree height. The strength of signal received by the handheld GPS depends on the weather conditions and the density of the canopy. During the cloudy days and in the dense canopy forest, weak satellite signals were received posing difficulties to locate the centre of the sampling plots. Human errors can also occur during the field data collection phase. For instance, the difficulty in identifying the actual tree tops in a dense canopy forest obstructed by branches leads to measuring the heights of wrong trees. Further, sampling uncertainties will occur when only a fraction of the population is measured in an inherent natural variability.

In all automatic image segmentation algorithms, the basic assumption is that each tree has a distinct boundary without any overlap between neighbouring tree crowns. However, such situations are rarely found in the naturally regenerating forests. In some cases, the tree crowns are found intertwined and clustered with the neighbouring trees. Therefore, the individual tree crown delineation from remotely sensed data leads to significant errors in the number of crowns delineated and its corresponding crown sizes due to over segmentation and under segmentation (Leckie, et al., 2003; Wulder et al., 2000). The view angle of the sensor during image acquisition also influences the shape of tree crown and its segmentation accuracy (Leckie et al., 2005). For example, due the variation in the position of the sun, the shape of tree crowns looked quite different from what is seen from the images. The tree crown appears circular in shape when the view angle is nearer to nadir and the solar elevation angle is high; and the tree crown displayed crescent shape in off nadir images (Leboeuf, et al., 2007). The time difference between the field data

collection and the image data acquisition can also influence the results of tree crown segmentation. The VHR imagery was acquired in November 2009, while the field work was carried out in October 2011, approximately after a time lag of two years. Although the tree growth during the lag period may not be significant, the crown size on the image looked slight different from the tree crown size measured in the field.

Classification errors can also influence the carbon estimation results, when trees are classified into different species. If a particular tree is classified as other tree species and vice versa, it introduces error in the estimation of biomass as different tree species have different wood specific gravity. The inclusion of wood specific gravity is an important parameter in the allometric equation as it leads to improvement in the AGB estimation model (Chave, et al., 2005). The presence of shadow is another important factor that influences the segmentation results and subsequently leads to the classification error. The shadow effect is more common in mountainous terrain and shadow particularly obscures the canopy area (Gonzalez, et al., 2010; Wulder & Seemann, 2003). Therefore, classification error leads to uncertainties in the estimation of biomass in the subsequent stages such as developing the carbon estimation regression models.

Similarly, the choice of allometric equation is another important factor that influences the carbon estimation models. Since the site and species specific allometric equation for the study area were not available, the allometric equation used in this study was adapted from Chave et al., (2005) which was developed as a general allometric equation for moist mangrove forest stands. Preferably, species specific and site specific models should be used to reduce the errors in biomass/carbon estimation (Cairns et al., 2003). It is because the species composition and stand structure differs significantly between secondary forest and primary forest. As mentioned in section 5.4, the study area comprised of both primary and secondary forests.

Limitations of this study

1. The image to image co-registration between VHR GeoEye image and the LiDAR derived CHM was not satisfactory. If the ground control points are acquired during the fieldwork campaign, the co-registration accuracy can be improved which would reduce the errors.

2. The models were developed for *Shorea robusta* and Other tree species. Other tree species comprises of different tree species, which were grouped into one class due to difficulties in identifying adequate number of samples on the image. Species specific models would enhance better performance of the carbon estimation models.

3. Site specific and species specific allometric equations were not available for biomass estimation in the study area and there are uncertainties from using non site and species specific allometric equation.

6. CONCLUSIONS AND RECOMMENDATIONS

6.1. Conclusion

The overall objective of this study was to model aboveground carbon stock by integration of VHR GeoEye image and airborne LiDAR data and, upscale the results (carbon estimates) to a relatively coarser RapidEye imagery. In conjunction with the specific research objectives and questions, following conclusions were derived from this study.

How accurately can the tree crowns be segmented from the combined GeoEye and LiDAR?
The segmentation results obtained from the combined GeoEye and LiDAR from the D goodness measure method showed an accuracy of 70% (D value=0.30) and the 1:1 correspondence method showed an accuracy of 74%. Therefore, the combination of GeoEye image and LiDAR can be used to obtain accurate tree crown delineation for modelling aboveground carbon. However, the hypothesised accuracy of 75% could not be achieved due to the reasons mentioned in section 5.2.

What is the relationship between CPA, height and carbon in the study area?
There is a significant relationship between CPA, height and carbon at 95% confidence level ($p<=0.05$). The log transformed multiplicative regression models resulted in co-efficient of determination (R^2) of 0.86 and 0.78 for *Shorea robusta* and Other tree species respectively.

How accurate can the aboveground carbon stock be estimated using CPA and height from VHR imagery and LiDAR data in the study area?
Validation of the model showed that the aboveground carbon can be estimated with a reasonable accuracy with a RMSE of 43 kg/tree and a RMSE percent of 32% for *Shorea robusta* and a RMSE of 44kg/tree with a RMSE percent of 34% for Other tree species.

How estimated carbon from the integration of VHR satellite image and airborne LiDAR data can be up-scaled to the RapidEye satellite image of 5 m resolution?
GIS aggregation technique was used to up-scale the amount of carbon mapped in 100 pixels of 0.5 m resolution VHR satellite image and airborne LiDAR to one pixels value of the same grid of RapidEye satellite image of 5 m spatial resolution.

What/how strong is the relationship between up-scaled carbon stock and the spectral reflectance of RapidEye image?
Weak relationships between the up-scaled carbon and the spectral reflectance of the RapidEye image were observed. The co-efficient of determination (R^2) obtained for NDVI, Red Edge NDVI and PC1 are 0.10, 0.12 and 0.18 respectively. Similarly, the co-efficient of determination (R^2) for the individual bands of red edge and NIR are 0.14 and 0.11 respectively. The co-registration error coupled with the biomass saturation problem in broadleaved forest could have influenced the weak relationship.

6.2. Recommendation

In general, the results of this research demonstrated the usefulness of integrating VHR satellite imagery and low density airborne LiDAR data for modelling and estimating the aboveground carbon with an acceptable accuracy. The methodology for up-scaling carbon from the combined VHR imagery and LiDAR data to a relatively coarser RapidEye image was developed, but up-scaling the carbon stock to a larger scale could not be carried out due to weak relationship between up-scaled carbon stock and the spectral reflectance. Nevertheless, the methodologies developed in this research are expected to contribute towards successful implementation of carbon crediting mechanisms such as REDD in the developing countries.

Errors in the development of models for estimation of carbon from VHR and LiDAR data should be reduced. Firstly, the co-registration between the datasets should be improved when using datasets from multiple sources. Secondly, for higher segmentation and classification accuracy, preferably VHR images acquired during tree growing season (summer-early autumn) should be used in order to capture variability in their structure, shape, colour of leaves, etc. The temporal difference between the acquisitions of different datasets should not be long especially when integrating data from multiple sources.

For up-scaling the carbon derived from VHR satellite imagery and airborne LiDAR data to a coarser imagery, cross-polarized L-band radar image of 12.5 m ALOS Pal-SAR images can be used. If a cross-polarized L-band (i.e. ALOS Pal-SAR) of 12.5 meter resolution would have been used instead of RapidEye image, a reasonable relationship could have been established with the forest biomass/carbon. Thus, up-scaling would be done to even relatively coarser pixel size of 12.5 meters. Satellite images with middle infrared (MIR) bands such as Landsat or Aster look promising too. A non-forest mask for the coarser satellite images can be generated to mask out non vegetated areas in the coarser resolution satellite images.

LIST OF REFERENCES

Ali, S. S., Dare, P., & Jones, S. D. (2008). Fusion of remotely sensed multispectral imagery and Lidar data for forest structure assessment at the tree level. *The International Archives of the Photogrammetry, Remote Sensing and Spatial Information Sciences, XXXVII*(Part B7), 93-96.

Asner, G. P. (2009). Tropical forest carbon assessment: integrating satellite and airborne mapping approaches. *Environmental Research Letters, 4*(3).

Baltsavias, E. P. (1999). A comparison between photogrammetry and laser scanning. *ISPRS Journal of Photogrammetry and Remote Sensing, 54*(2-3), 83-94.

Baral, S. (2011). *Mapping carbon stock using high resolution satellite images in sub - tropical forest of Nepal.* MSc Thesis, University of Twente Faculty of Geo-Information and Earth Observation ITC, Enschede.

Basuki, T. M., van Laake, P. E., Skidmore, A. K., & Hussin, Y. A. (2009). Allometric equations for estimating the above-ground biomass in tropical lowland Dipterocarp forests. *Forest Ecology and Management, 257*(8), 1684-1694.

Blaschke, T. (2010). Object based image analysis for remote sensing. *ISPRS Journal of Photogrammetry and Remote Sensing, 65*(1), 2-16.

Blaschke, T., Burnett, C., & Pekkarinen, A. (2006). Image Segmentation Methods for Object-based Analysis and Classification. In S. M. D. Jong & F. D. V. d. Meer (Eds.), *Remote Sensing Image Analysis: Including The Spatial Domain* (Vol. 5, pp. 211-236): Springer Netherlands.

Brown, S. (2002). Measuring carbon in forests: current status and future challenges. *Environmental Pollution, 116*(3), 363-372.

Brown, S., Gillespie, A. J. R., & Lugo, A. E. (1989). Biomass estimation methods for tropical forests with applications to forest inventory data. *Forest Science, 35*(4), 881-902.

Bunting, P., & Lucas, R. (2006). The delineation of tree crowns in Australian mixed species forests using hyperspectral Compact Airborne Spectrographic Imager (CASI) data. *Remote Sensing of Environment, 101*(2), 230-248.

Cairns, M. A., Olmsted, I., Granados, J., & Argaez, J. (2003). Composition and aboveground tree biomass of a dry semi-evergreen forest on Mexico's Yucatan Peninsula. *Forest Ecology and Management, 186*(1–3), 125-132.

Chave, J., Andalo, C., Brown, S., Cairns, M. A., Chambers, J. Q., Eamus, D., et al. (2005). Tree allometry and improved estimation of carbon stocks and balance in tropical forests. *Oecologia, 145*(1), 87-99.

Chen, Q., Baldocchi, D., Gong, P., & Kelly, M. (2006). Isolating individual trees in a savanna woodland using small footprint lidar data. *Photogrammetric Engineering and Remote Sensing, 72*(8), 923-932.

Chubey, M. S., Franklin, S. E., & Wulder, M. A. (2006). Object-based analysis of Ikonos-2 imagery for extraction of forest inventory parameters. *Photogrammetric Engineering and Remote Sensing, 72*(4), 383-394.

Clinton, N., Holt, A., Scarborough, J., Yan, L., & Gong, P. (2010). Accuracy assessment measures for object-based image segmentation goodness. *Photogrammetric Engineering and Remote Sensing, 76*(3), 289-299.

Conchedda, G., Durieux, L., & Mayaux, P. (2008). An object-based method for mapping and change analysis in mangrove ecosystems. *ISPRS Journal of Photogrammetry and Remote Sensing, 63*(5), 578-589.

Culvenor, D. S. (2002). TIDA: an algorithm for the delineation of tree crowns in high spatial resolution remotely sensed imagery. *Computers & Geosciences, 28*(1), 33-44.

Definiens. (2004). *eCognition User Guide 4*.

Definiens. (2009a). *Definiens eCognition Developer 8–Reference Book*. München.

Definiens. (2009b). *Definiens eCognition Developer 8–User guide*. München.

Dhakal, S., & Raut, A. K. (2010). Potential and bottlenecks of the carbon market: The case of a developing country, Nepal. *Energy Policy, 38*(7), 3781-3789.

Dhital, N. (2009). Reducing Emissions from Deforestation and Forest Degradation (REDD) in Nepal: Exploring the Possibilities. *Journal of Forests and Livelihood 8(1)*, 57 - 62.

DOF. (2004). *Community Forestry Inventory Guidelines, Community Forest Division, Department of Forests.* Kathmandu, Nepal.

Dong, J., Kaufmann, R. K., Myneni, R. B., Tucker, C. J., Kauppi, P. E., Liski, J., et al. (2003). Remote sensing estimates of boreal and temperate forest woody biomass: carbon pools, sources, and sinks. *Remote Sensing of Environment, 84*(3), 393-410.

Erikson, M. (2003). Segmentation of individual tree crowns in colour aerial photographs using region growing supported by fuzzy rules. *Canadian Journal of Forest Research, 33*(8), 1557-1563.

Erikson, M. (2004). Species classification of individually segmented tree crowns in high-resolution aerial images using radiometric and morphologic image measures. *Remote Sensing of Environment, 91*(3–4), 469-477.

FAO. (2010). *Global Forest Resources Assessment 2010*. Rome, Italy.

Gasparri, N. I., Parmuchi, M. G., Bono, J., Karszenbaum, H., & Montenegro, C. L. (2010). Assessing multi-temporal Landsat 7 ETM+ images for estimating above-ground biomass in subtropical dry forests of Argentina. *Journal of Arid Environments, 74*(10), 1262-1270.

Gautam, B., Tokola, T., Hamalainen, J., Gunia, M., Peuhkurinen, J., Parviainen, H., et al. (2010). Integration of airborne LiDAR, satellite imagery, and field measurements using a two-phase sampling method for forest biomass estimation in tropical forests.

Gibbs, H. K., Brown, S., Niles, J. O., & Foley, J. A. (2007). Monitoring and estimating tropical forest carbon stocks: making REDD a reality. *Environmental Research Letters, 2*(4), 045023.

Gonzalez, P., Asner, G. P., Battles, J. J., Lefsky, M. A., Waring, K. M., & Palace, M. (2010). Forest carbon densities and uncertainties from Lidar, QuickBird, and field measurements in California. *Remote Sensing of Environment, 114*(7), 1561-1575.

Gougeon, F. A., & Leckie, D. G. (2006). The individual tree crown approach applied to Ikonos images of a coniferous plantation area. *Photogrammetric Engineering and Remote Sensing, 72*(11), 1287-1297.

Hall, F. G., Shimabukuro, Y. E., & Huemmrich, K. F. (1995). Remote Sensing of Forest Biophysical Structure Using Mixture Decomposition and Geometric Reflectance Models. *Ecological Applications, 5*(4), 993-1013.

Hemery, G. E., Savill, P. S., & Pryor, S. N. (2005). Applications of the crown diameter-stem diameter relationship for different species of broadleaved trees. *Forest Ecology and Management, 215*(1-3), 285-294.

Heurich, M., Persson, Å., Holmgren, J., & Kennel, E. (2004). Detecting and measuring individual trees with laser scanning in mixed mountain forest of Central Europe using an algorithm developed for Swedish boreal forest conditions. *International Archives of Photogrammetry, Remote Sensing and Spatial Information Sciences, 36*, 307-312.

Hollaus, M., Wanger, W., Nmaier, B., & Schadauer, K. (2007). Airborne laser scanning of forest stem volume in a mountainous environment. *Sensors, 7*(8), 1559-1577.

Holmgren, J., Persson, A., & Soderman, U. (2008). Species identification of individual trees by combining high resolution LIDAR data with multi-spectral images. *International Journal of Remote Sensing, 29*(5), 1537-1552.

Hudak, A. T., Lefsky, M. A., Cohen, W. B., & Berterretche, M. (2002). Integration of lidar and Landsat ETM+ data for estimating and mapping forest canopy height. *Remote Sensing of Environment, 82*(2-3), 397-416.

Husch, B., Beers, T. W., & Kershaw, J. A. (2003). *Forest mensuration*: Wiley.

ICIMOD. (2010). Forest Carbon Stock in REDD+ Pilot Project Sites: Year One Measurement & Analysis. Retrieved 15/11, 2011, from http://communityredd.net/userfiles/Nepal%20REDD%20CStock%20Year%20One%20Report%202010.pdf

IPCC. (2007). *Climate Change 2007, Synthesis Report*. Geneva, Switzerland.

Jochem, A., Hollaus, M., Rutzinger, M., & Hofle, B. (2011). Estimation of Aboveground Biomass in Alpine Forests: A Semi-Empirical Approach Considering Canopy Transparency Derived from Airborne LiDAR Data. *Sensors, 11*(1), 278-295.

Johansen, K., Coops, N. C., Gergel, S. E., & Stange, Y. (2007). Application of high spatial resolution satellite imagery for riparian and forest ecosystem classification. *Remote Sensing of Environment, 110*(1), 29-44.

Ke, Y. H., & Quackenbush, L. J. (2011a). A comparison of three methods for automatic tree crown detection and delineation from high spatial resolution imagery. *International Journal of Remote Sensing, 32*(13), 3625-3647.

Ke, Y. H., & Quackenbush, L. J. (2011b). A review of methods for automatic individual tree-crown detection and delineation from passive remote sensing. *International Journal of Remote Sensing, 32*(17), 4725-4747.

Ke, Y. H., Quackenbush, L. J., & Im, J. (2010). Synergistic use of QuickBird multispectral imagery and LIDAR data for object-based forest species classification. *Remote Sensing of Environment, 114*(6), 1141-1154.

Keene, O. N. (1995). The log transformation is special. *Statistics in Medicine, 14*(8), 811-819.

Kerkhoff, A. J., & Enquist, B. J. (2009). Multiplicative by nature: Why logarithmic transformation is necessary in allometry. *Journal of Theoretical Biology, 257*(3), 519-521.

Kim, C., & Habib, A. (2009). Object-Based Integration of Photogrammetric and LiDAR Data for Automated Generation of Complex Polyhedral Building Models. *Sensors, 9*(7), 5679-5701.

Kim, S. R., Kwak, D. A., Lee, W. K., Son, Y., Bae, S. W., Kim, C., et al. (2010). Estimation of carbon storage based on individual tree detection in Pinus densiflora stands using a fusion of aerial photography and LiDAR data. *Science China Life Sciences, 53*(7), 885-897.

Kramer, H. J., & Cracknell, A. P. (2008). An overview of small satellites in remote sensing. *International Journal of Remote Sensing, 29*(15), 4285-4337.

Kwak, D. A., Lee, W. K., Lee, J. H., Biging, G. S., & Gong, P. (2007). Detection of individual trees and estimation of tree height using LiDAR data. *Journal of Forest Research, 12*(6), 425-434.

Landis, J. R., & Koch, G. G. (1977). The Measurement of Observer Agreement for Categorical Data. *Biometrics, 33*(1), 159-174.

Larsen, M., Eriksson, M., Descombes, X., Perrin, G., Brandtberg, T., & Gougeon, F. A. (2011). Comparison of six individual tree crown detection algorithms evaluated under varying forest conditions. *International Journal of Remote Sensing*, 1-26.

Le Toan, T., Quegan, S., Woodward, I., Lomas, M., Delbart, N., & Picard, G. (2004). Relating Radar Remote Sensing of Biomass to Modelling of Forest Carbon Budgets. *Climatic Change, 67*(2), 379-402.

Leboeuf, A., Beaudoin, A., Fournier, R. A., Guindon, L., Luther, J. E., & Lambert, M. C. (2007). A shadow fraction method for mapping biomass of northern boreal black spruce forests using QuickBird imagery. *Remote Sensing of Environment, 110*(4), 488-500.

Leckie, D. G., Gougeon, F., Hill, D., Quinn, R., Armstrong, L., & Shreenan, R. (2003). Combined high-density lidar and multispectral imagery for individual tree crown analysis. *Canadian Journal of Remote Sensing, 29*(5), 633-649.

Leckie, D. G., Gougeon, F. A., Tinis, S., Nelson, T., Burnett, C. N., & Paradine, D. (2005). Automated tree recognition in old growth conifer stands with high resolution digital imagery. *Remote Sensing of Environment, 94*(3), 311-326.

Lefsky, M. A., Cohen, W. B., Acker, S. A., Parker, G. G., Spies, T. A., & Harding, D. (1999). Lidar Remote Sensing of the Canopy Structure and Biophysical Properties of Douglas-Fir Western Hemlock Forests. *Remote Sensing of Environment, 70*(3), 339-361.

Lefsky, M. A., Cohen, W. B., & Spies, T. A. (2001). An evaluation of alternate remote sensing products for forest inventory, monitoring, and mapping of Douglas-fir forests in western Oregon. *Canadian Journal of Forest Research-Revue Canadienne De Recherche Forestiere, 31*(1), 78-87.

Lim, K., Treitz, P., Baldwin, K., Morrison, I., & Green, J. (2003). Lidar remote sensing of biophysical properties of tolerant northern hardwood forests. *Canadian Journal of Remote Sensing, 29*(5), 658-678.

Liu, Y., Li, M., Mao, L., Xu, F., & Huang, S. (2006). Review of remotely sensed imagery classification patterns based on object-oriented image analysis. *Chinese Geographical Science, 16*(3), 282-288.

Lu, D. (2006). The potential and challenge of remote sensing-based biomass estimation. *International Journal of Remote Sensing, 27*(7), 1297-1328.

Lu, D., Mausel, P., Brondizio, E., & Moran, E. (2004). Relationships between forest stand parameters and Landsat TM spectral responses in the Brazilian Amazon Basin. *Forest Ecology and Management, 198*(1-3), 149-167.

Maniatis, D., & Mollicone, D. (2010). Options for sampling and stratification for national forest inventories to implement REDD+ under the UNFCCC. *Carbon balance and management, 5*, 9.

Mascaro, J., Litton, C. M., Hughes, R. F., Uowolo, A., & Schnitzer, S. A. (2011). Minimizing Bias in Biomass Allometry: Model Selection and Log-Transformation of Data. *Biotropica, 43*(6), 649-653.

Means, J. E., Acker, S. A., Fitt, B. J., Renslow, M., Emerson, L., & Hendrix, C. J. (2000). Predicting forest stand characteristics with airborne scanning lidar. *Photogrammetric Engineering and Remote Sensing, 66*(11), 1367-1371.

Meng, X., Currit, N., & Zhao, K. (2010). Ground Filtering Algorithms for Airborne LiDAR Data: A Review of Critical Issues. *Remote Sensing, 2*(3), 833-860.

Montagu, K. D., Düttmer, K., Barton, C. V. M., & Cowie, A. L. (2005). Developing general allometric relationships for regional estimates of carbon sequestration—an example using Eucalyptus pilularis from seven contrasting sites. *Forest Ecology and Management, 204*(1), 115-129.

Mora, B., Wulder, M. A., & White, J. C. (2010). Segment-constrained regression tree estimation of forest stand height from very high spatial resolution panchromatic imagery over a boreal environment. *Remote Sensing of Environment, 114*(11), 2474-2484.

Muukkonen, P., & Heiskanen, J. (2007). Biomass estimation over a large area based on standwise forest inventory data and ASTER and MODIS satellite data: A possibility to verify carbon inventories. *Remote Sensing of Environment, 107*(4), 617-624.

Næsset, E., & Økland, T. (2002). Estimating tree height and tree crown properties using airborne scanning laser in a boreal nature reserve. *Remote Sensing of Environment, 79*(1), 105-115.

Omasa, K., Qiu, G. Y., Watanuki, K., Yoshimi, K., & Akiyama, Y. (2003). Accurate estimation of forest carbon stocks by 3-D remote sensing of individual trees. *Environmental Science & Technology, 37*(6), 1198-1201.

Patenaude, G., Hill, R. A., Milne, R., Gaveau, D. L. A., Briggs, B. B. J., & Dawson, T. P. (2004). Quantifying forest above ground carbon content using LiDAR remote sensing. *Remote Sensing of Environment, 93*(3), 368-380.

Patenaude, G., Milne, R., & Dawson, T. P. (2005). Synthesis of remote sensing approaches for forest carbon estimation: reporting to the Kyoto Protocol. *Environmental Science & Policy, 8*(2), 161-178.

Persson, A., Holmgren, J., & Söderman, U. (2002). Detecting and measuring individual trees using an airborne laser scanner. *Photogrammetric Engineering and Remote Sensing, 68*(9), 925-932.

Popescu, S. C. (2007). Estimating biomass of individual pine trees using airborne lidar. *Biomass & Bioenergy, 31*(9), 646-655.

Popescu, S. C., Wynne, R. H., & Scrivani, J. A. (2004). Fusion of small-footprint lidar and multispectral data to estimate plot-level volume and biomass in deciduous and pine forests in Virginia, USA. *Forest Science, 50*(4), 551-565.

Ripple, W. J., Wang, S., Isaacson, D. L., & Paine, D. P. (1991). A preliminary comparison of Landsat Thematic Mapper and SPOT-l HRV multispectral data for estimating coniferous forest volume. *International Journal of Remote Sensing, 12*(9), 1971-1977.

Rosenqvist, Å., Milne, A., Lucas, R., Imhoff, M., & Dobson, C. (2003). A review of remote sensing technology in support of the Kyoto Protocol. *Environmental Science & Policy, 6*(5), 441-455.

Roy, P. S., & Ravan, S. A. (1996). Biomass estimation using satellite remote sensing data - An investigation on possible approaches for natural forest. *Journal of Biosciences, 21*(4), 535-561.

Sader, S. A., Waide, R. B., Lawrence, W. T., & Joyce, A. T. (1989). Tropical forest biomass and successional age class relationships to a vegetation index derived from landsat TM data. *Remote Sensing of Environment, 28*(0), 143-198.

Sexton, J. O., Bax, T., Siqueira, P., Swenson, J. J., & Hensley, S. (2009). A comparison of lidar, radar, and field measurements of canopy height in pine and hardwood forests of southeastern North America. *Forest Ecology and Management, 257*(3), 1136-1147.

Shah, R. (2011). *Comparison of Individual Tree Crown Delineation Methods for Carbon Stock Estimation using Very High Resolution Satellite images.* Unpublished MSc Thesis, University of Twente Faculty of Geo-Information and Earth Observation ITC, Enschede.

Shimano, K. (1997). Analysis of the relationship between DBH and crown projection area using a new model. *Journal of Forest Research, 2*(4), 237-242.

Singh, V., Tewari, A., Kushwaha, S. P. S., & Dadhwal, V. K. (2011). Formulating allometric equations for estimating biomass and carbon stock in small diameter trees. *Forest Ecology and Management, 261*(11), 1945-1949.

Song, C., Dickinson, M. B., Su, L., Zhang, S., & Yaussey, D. (2010). Estimating average tree crown size using spatial information from Ikonos and QuickBird images: Across-sensor and across-site comparisons. *Remote Sensing of Environment, 114*(5), 1099-1107.

Steininger, M. K. (2000). Satellite estimation of tropical secondary forest above-ground biomass: Data from Brazil and Bolivia. *International Journal of Remote Sensing, 21*(6-7), 1139-1157.

Takahashi, T., Awaya, Y., Hirata, Y., Furuya, N., Sakai, T., & Sakai, A. (2010). Stand volume estimation by combining low laser-sampling density LiDAR data with QuickBird panchromatic imagery in closed-canopy Japanese cedar (Cryptomeria japonica) plantations. *International Journal of Remote Sensing, 31*(5), 1281-1301.

Takahashi, T., Yamamoto, K., Senda, Y., & Tsuzuku, M. (2005). Predicting individual stem volumes of sugi (Cryptomeria japonica D. Don) plantations in mountainous areas using small-footprint airborne LiDAR. *Journal of Forest Research, 10*(4), 305-312.

Tsendbazar, N. E. (2011). *Object based image analysis of geo - eye VHR data to model above ground carbon stock in Himalayan mid - hill forests, Nepal.* MSc Thesis, University of Twente, Faculty of Geo-Information and Earth Observation, ITC, Enschede.

UN-REDD. (2008). *UN Collaborative Programme on Reducing Emissions from Deforestation and Forest Degradation in Developing Countries (UN-REDD) :Framework Document.*

UN-REDD. (2010). UN-REDD Programme. Retrieved 26 May, 2011, from http://www.fao.org/climatechange/unredd/53079/en/

UNEP. (2010). UNEP-About the UN-REDD Programme. Retrieved 29 May, 2011, from http://www.unep.org/climatechange/reddplus/Home/tabid/29506/Default.aspx

UNFCCC. (2009). A Brief Introduction to the United Nations Framework Convention on Climate Change (UNFCCC) and Kyoto Protocol. Retrieved 23 May, 2011, from http://www.iisd.ca/process/climate_atm-fcccintro.html

Wang, L., Gong, P., & Biging, G. S. (2004). Individual tree-crown delineation and treetop detection high-spatial-resolution aerial imagery. *Photogrammetric Engineering and Remote Sensing, 70*(3), 351-357.

Weihong, C., Zequn, G., & Zhiyi, Z. (2008). *An Improved Region Growing Algorithm for Image Segmentation.* Paper presented at the 2008 International Conference on Computer Science and Software Engineering.

Wu, C., Niu, Z., Tang, Q., Huang, W., Rivard, B., & Feng, J. (2009). Remote estimation of gross primary production in wheat using chlorophyll-related vegetation indices. *Agricultural and Forest Meteorology, 149*(6-7), 1015-1021.

Wulder, & Seemann, D. (2003). Forest inventory height update through the integration of lidar data with segmented Landsat imagery. *Canadian Journal of Remote Sensing, 29*(5), 536-543.

Wulder, M., Niemann, K. O., & Goodenough, D. G. (2000). Local maximum filtering for the extraction of tree locations and basal area from high spatial resolution imagery. *Remote Sensing of Environment, 73*(1), 103-114.

Wulder, M. A., Han, T., White, J. C., Sweda, T., & Tsuzuki, H. (2007). Integrating profiling LIDAR with Landsat data for regional boreal forest canopy attribute estimation and change characterization. *Remote Sensing of Environment, 110*(1), 123-137.

Zhan, Q., Molenaar, M., Tempfli, K., & Shi, W. (2005). Quality assessment for geo-spatial objects derived from remotely sensed data. *International Journal of Remote Sensing, 26*(14), 2953-2974.

Zhang, Y. (1996). A survey on evaluation methods for image segmentation. *Pattern Recognition, 29*(8), 1335-1346.

Zhang, Y. (2002). Problems in the Fusion of Commercial High-Resolution Satelitte as well as Landsat 7 Images and Initial Solutions. *International Archives of Photogrammetry Remote Sensing and Spatial Information Sciences, 34*(4), 587-592.

Zheng, D., Rademacher, J., Chen, J., Crow, T., Bresee, M., Le Moine, J., et al. (2004). Estimating aboveground biomass using Landsat 7 ETM+ data across a managed landscape in northern Wisconsin, USA. *Remote Sensing of Environment, 93*(3), 402-411.

Zitová, B., & Flusser, J. (2003). Image registration methods: a survey. *Image and Vision Computing, 21*(11), 977-1000.

APPENDICES

Appendix 1: Meta data of RapidEye Imagery

tile Id	latitude	longitude	illumination AzimuthAngle	zenith	acquisitionDateTime	azimuth Angle
4551904	27.74195769	84.3168248	158.142	16.67825	2011-04-22 T05:55:48.259723Z	278.24
4551905	27.74646548	84.5601024	158.9247	16.60403	2011-04-22 T05:55:47.697493Z	278.22
4552005	27.96292758	84.5552488	159.1211	16.8114	2011-04-22 T05:55:44.279129Z	278.24

Appendix 2: List of tree species found in the study area

S.N	Local name	Scientific name
1	Sal	*Shorea robusta*
2	Chilaune	*Schima wallichii*
3	Bhalayo	*Rhus wallichii*
4	Barro	*Terminalia bellirica*
5	Aap	*Mangifera indica*
6	Kyamuna	*Cleistocalyx operculata*
7	Karam	*Adina cordifolia*
8	Saaj	*Terminalia alata*
9	Kumbho	*Cochlospermum religiosum*
10	Januma	*Syzygium cumini*
11	Katus	*Castanopsisindica*
12	sallo	*Pinus roxburghii*
13	Khirro	*Sapium insigne*
14	Bot Dhayaro	*Lagerstroemia parviflora*
15	Mainkanda	*Xeromphis spinosa*
16	Khaniyo	*Ficussemi cordata*
17	Kaiyo	*Wendiandia puberula*
18	Mauwa	*Engelhardia spicata*
19	Amaro	*Spondias pinnata*
20	Chuwa	*Phlogacanthus thyrsiflorus*
21	Putalikath	*Not available*
22	Anger	*Lyonia ovalifolia*
23	Dungre	*Ficus benjamina*
24	Kuhelo	*Litsea polyantha*
25	Panchpate	*Ficus racemosa*
26	Taniyo	*Not available*
27	Khallo	*Albizia lebbek*

Appendix 3: Field data collection sheet

Name of Recorder: Date:

Stratum ID: Sample Plot ID:

Bearing from the road		Bearing for the 1st tree from the centre of the plot		Plot centre	
X		X		X	
Y		Y		Y	
Angle		Angle			

Slope: Plot radius: Aspect: Altitude: Crown density (%):

Sl.No	Tree Species	DBH (cm)	Crown Diameter (m)	Height (m)	Intermingled tree crowns	Remarks
1						
2						
3						
4						
5						
6						
7						

Appendix 4: Results from regression analysis of Field Height Vs CHM Height

Regression statistics	Field Height
Multiple R	0.863451
R Square	0.745548
Adjusted R Square	0.744924
Standard Error	2.345956
Observations	410
Co-efficients	
Intercept	0.570091
Slope (Field Height)	0.896029
p-value	
Intercept	0.198021
Slope (Field Height)	2.5E-123

ANOVA

	df	*SS*	*MS*	*F*	*Sig. F*
Regression	1	6579.135	6579.135	1195.443	2.5E-123
Residual	408	2245.432	5.50351		
Total	409	8824.567			

Relationship: t calculated is 34.57, t critical is 1. 96. Since t calculated > than t critical, the relation is statistically significant at 95% confidence level.

Appendix 5: Histogram for *Shorea robusta*

a. Carbon (kg/tree)

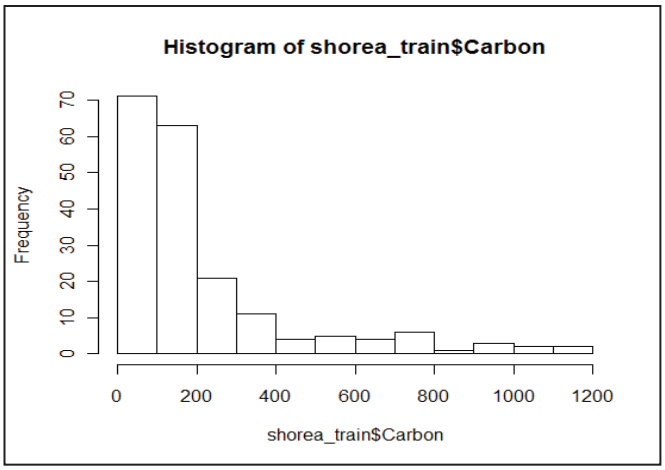

b. CPA (m^2)

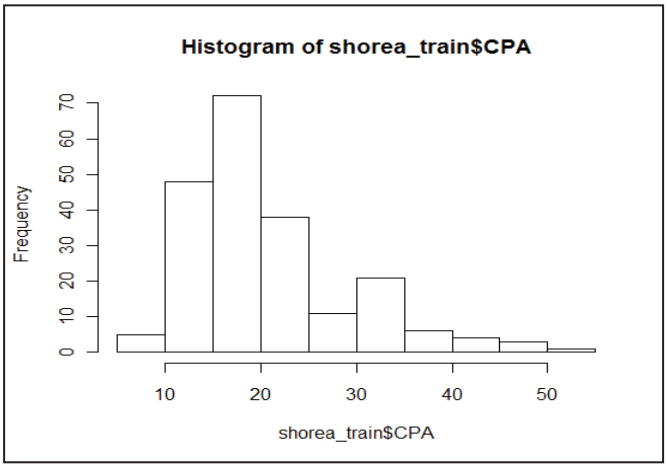

c. CHM height (m)

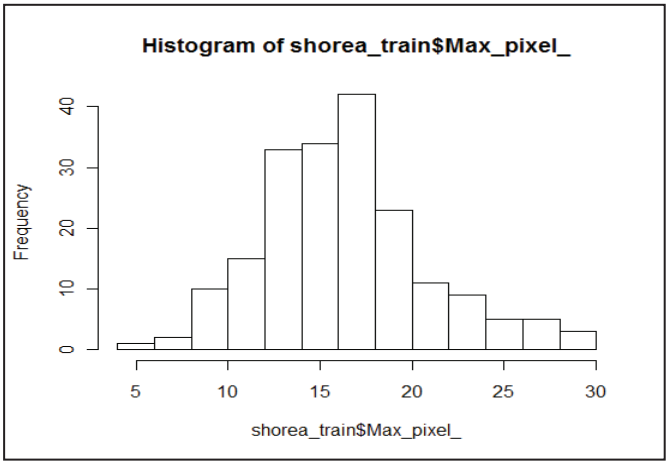

Appendix 6: Histogram for Other tree species

a. Carbon (kg/tree)

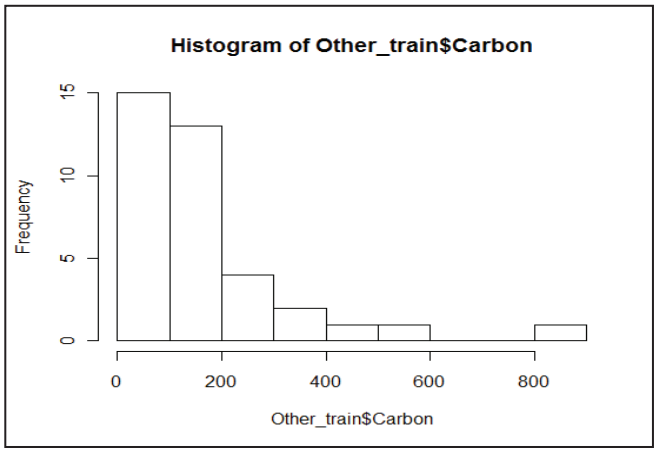

b. CPA (m^2)

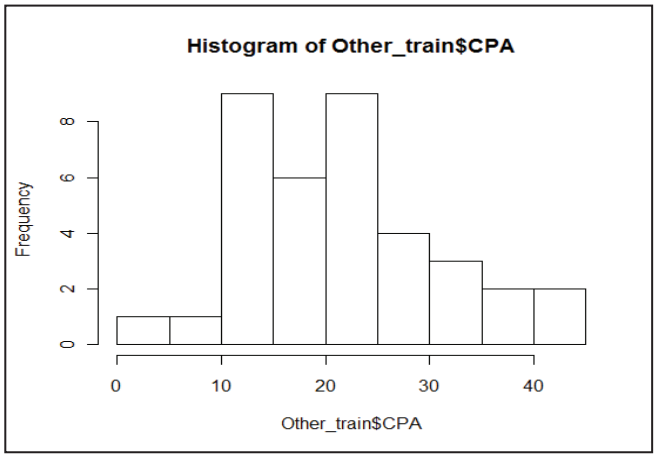

c. CHM height (m)

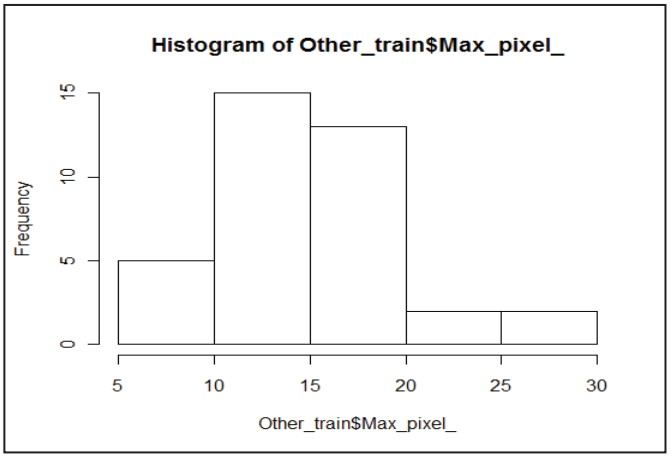

Appendix 7: Test for significance for multiple regression models

Shorea robusta					
	Carbon stock explained by CPA & Height				
	df	*SS*	*MS*	*F*	*Significance F*
Regression	2	110.3806	55.19032	275.6592	6.78E-57
Residual	190	38.04031	0.200212		
Total	192	148.421			
Other tree species					
	Carbon stock explained by CPA & Height				
	df	*SS*	*MS*	*F*	*Significance F*
Regression	2	27.83156	13.91587	55.15583	2.12E-11
Residual	34	8.578179	0.252299		
Total	36	36.40974			

F- test for Shorea robusta

For Shorea robusta, F calculated is 275.6592 and the F critical from the F table is 3.043 at 95% confidence level. Since the F calculated is greater than the F critical, the model was statistically significant at 95 % confidence level.

F- test for Other tree species

For Other tree species, F calculated is 55.15 and the F critical from the F table is 3.259 at 95% confidence level. Since the F calculated is greater than the F critical, the model was statistically significant at 95% confidence level.

Appendix 8: Carbon Stock Map of the individual CF

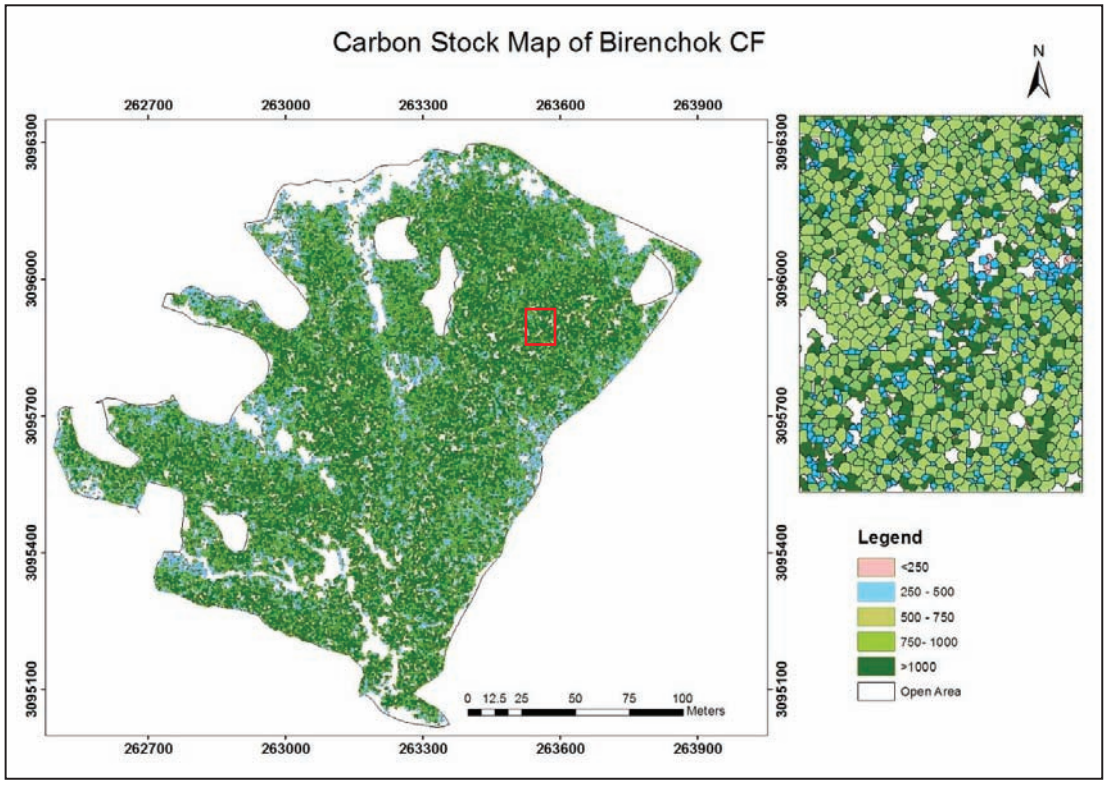

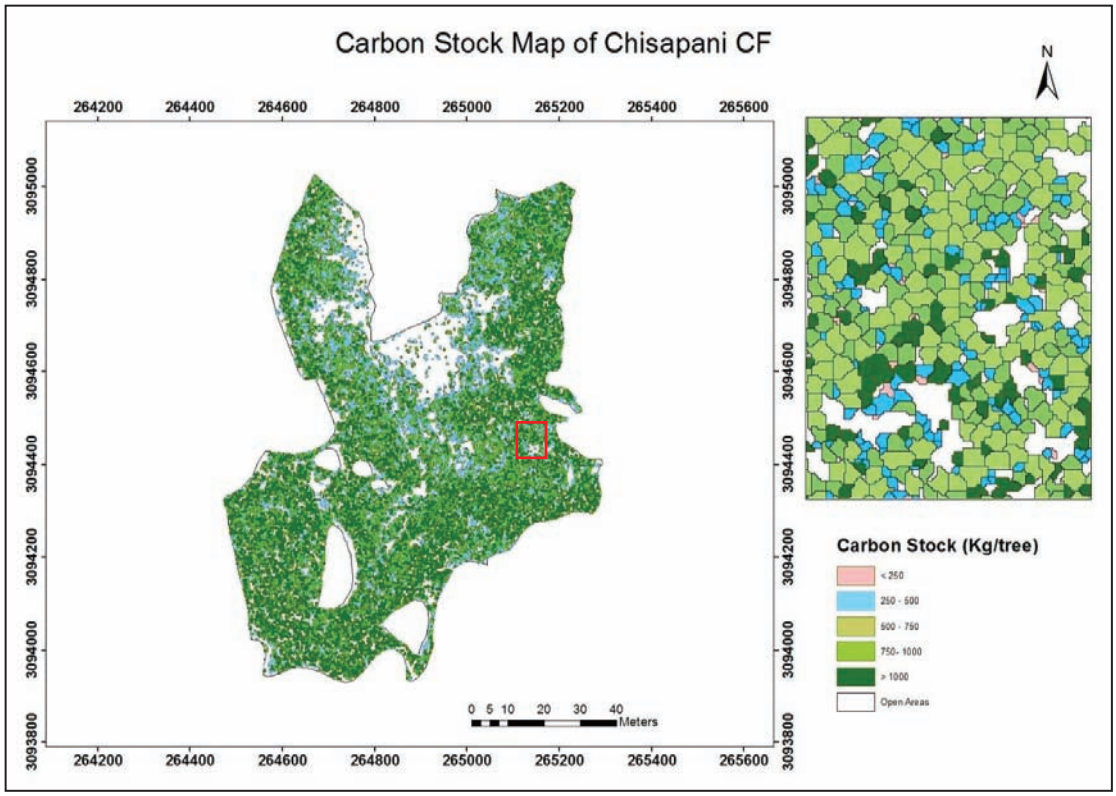

Appendix 8: Carbon Stock Map of the individual CF (contd..)

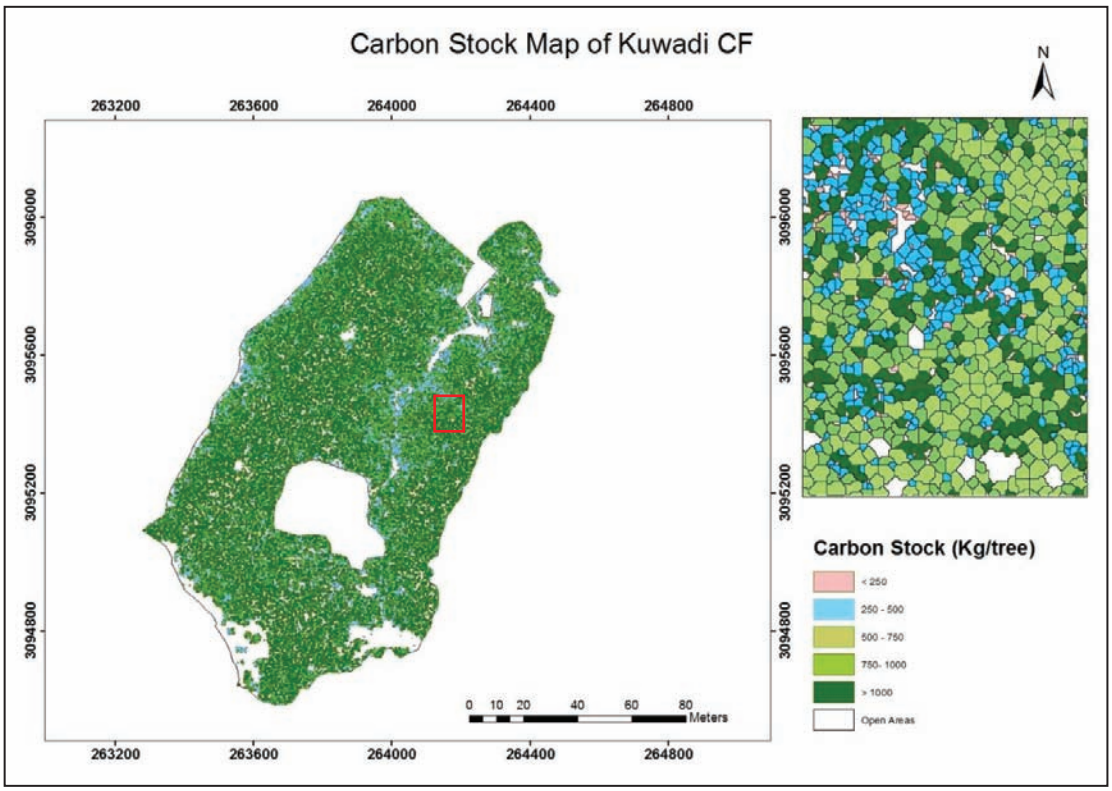

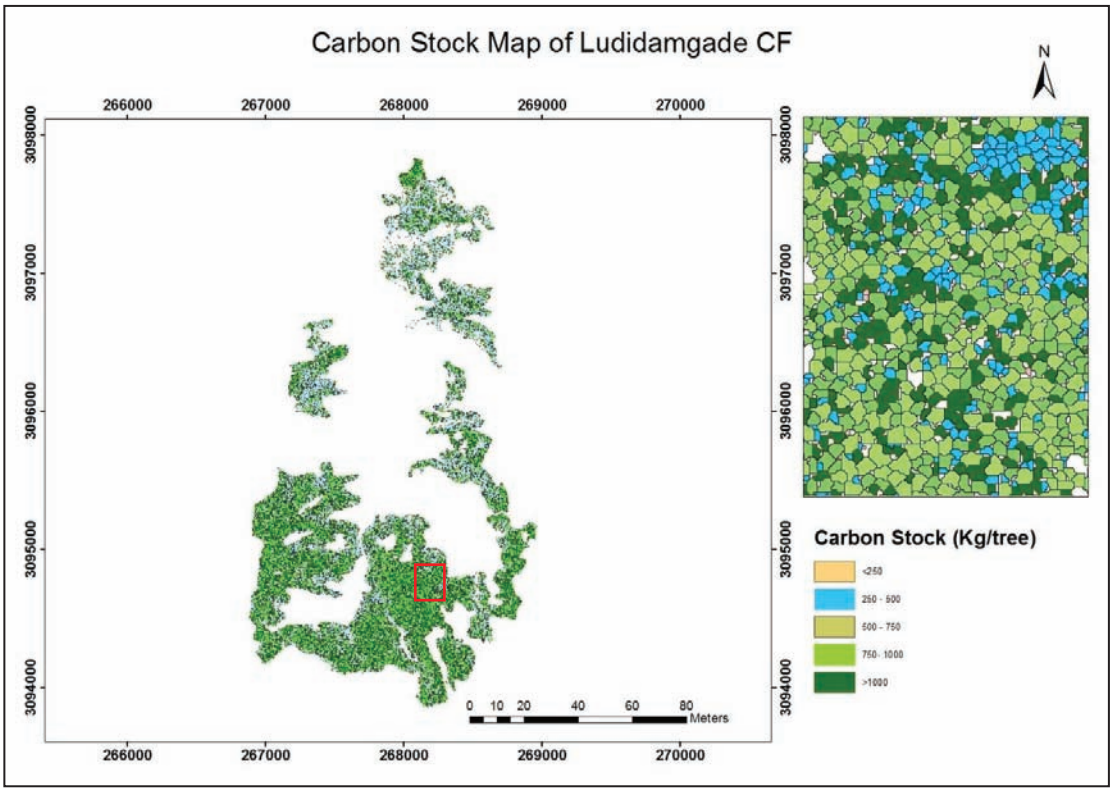

Appendix 8: Carbon Stock Map of the individual CF (contd..)

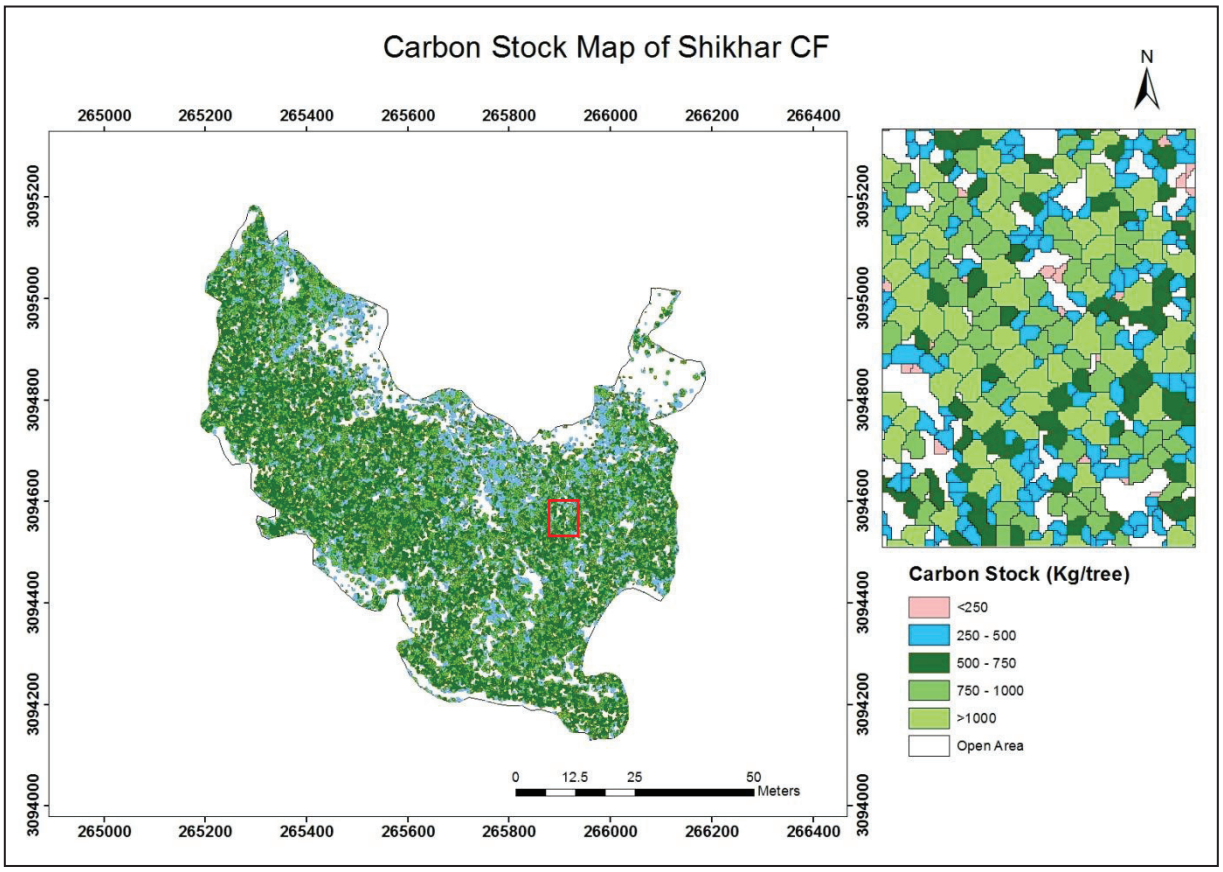

Appendix 9: Test of significance for regression models for up-scaling

Carbon as explained by NDVI					
	df	*SS*	*MS*	*F*	*Significance F*
Regression	1	2832110	2832110	258.7232	5.07E-55
Residual	2124	23250335	10946.49		
Total	2125	26082445			
Carbon as explained by Red Edge NDVI					
	df	*SS*	*MS*	*F*	*Significance F*
Regression	1	2898684	2898684	360.7608	3.36E-75
Residual	2473	19870360	8034.921		
Total	2474	22769045			
Carbon as explained by PC1					
	df	*SS*	*MS*	*F*	*Significance F*
Regression	1	4457199	4457199	443.9465	1.57E-89
Residual	2092	21003567	10039.95		
Total	2093	25460767			
Carbon as explained by Red Edge band					
	df	*SS*	*MS*	*F*	*Significance F*
Regression	1	3867023	3867023	365.47	2.02E-75
Residual	2171	22970960	10580.82		
Total	2172	26837983			
Carbon as explained by NIR Band					
	df	*SS*	*MS*	*F*	*Significance F*
Regression	1	3202908	3202908	274.9525	3.01E-58
Residual	2179	25383069	11648.95		
Total	2180	28585978			

F critical for NDVI = 2.999959
F critical for Rededge NDVI = 2.999363
F critical for PC1 = 2.999845
F critical for red edge band = 2.999872
F critical for NIR band = 2.999908

Since the F calculated is greater than the F critical, all the models were statistically significant at 95% confidence level.